



HAL
open science

LARP6C orchestrates post-transcriptional reprogramming of gene expression during hydration to promote pollen tube guidance

Elodie Billey, Said Hafidh, Isabel Cruz-Gallardo, Celso G Litholdo, Viviane Jean, Marie-Christine Carpentier, Claire Picart, Vinod Kumar, Katarina Kulichova, Eric Maréchal, et al.

► **To cite this version:**

Elodie Billey, Said Hafidh, Isabel Cruz-Gallardo, Celso G Litholdo, Viviane Jean, et al.. LARP6C orchestrates post-transcriptional reprogramming of gene expression during hydration to promote pollen tube guidance. *The Plant cell*, 2021, 33 (8), pp.2637-2661. 10.1093/plcell/koab131 . hal-03275017v2

HAL Id: hal-03275017

<https://univ-perp.hal.science/hal-03275017v2>

Submitted on 30 Jun 2021

HAL is a multi-disciplinary open access archive for the deposit and dissemination of scientific research documents, whether they are published or not. The documents may come from teaching and research institutions in France or abroad, or from public or private research centers.

L'archive ouverte pluridisciplinaire **HAL**, est destinée au dépôt et à la diffusion de documents scientifiques de niveau recherche, publiés ou non, émanant des établissements d'enseignement et de recherche français ou étrangers, des laboratoires publics ou privés.

RESEARCH ARTICLE

LARP6C orchestrates post-transcriptional reprogramming of gene expression during hydration to promote pollen tube guidance

Elodie Billey^{1,2,3*}, Said Hafidh^{4*.@}, Isabel Cruz-Gallardo^{5,6}, Celso G. Litholdo Jr^{1,2}, Viviane Jean^{1,2}, Marie-Christine Carpentier^{1,2}, Claire Picart^{1,2}, Vinod Kumar⁴, Katarina Kulichova⁴, Eric Maréchal⁷, David Honys⁴, Maria R. Conte⁶, Jean-Marc Deragon^{1,2,8@} and Cécile Bousquet-Antonelli^{1,2.@}

¹ CNRS LGDP-UMR5096, 58 Av. Paul Alduy 66860 Perpignan, France.

² Université de Perpignan Via Domitia, LGDP-UMR5096, 58 Av. Paul Alduy 66860 Perpignan, France.

³ Present address: TOTAL RC, 2 place Jean Millier- Arche Nord Coupole/Regnault, 92078 Paris La Défense Cedex, France

⁴ Laboratory of Pollen Biology, Institute of Experimental Botany of the Czech Academy of Sciences, Rozvojová 263, 165 02 Prague 6, Czech Republic.

⁵ Randall Centre for Cell and Molecular Biophysics, King's College London, New Hunt's House, Guy's Campus, London SE1 1UL, UK.

⁶ Present address: Department of Chemistry, King's College London, Britannia House, 7 Trinity St, London SE1 1DB, UK

⁷ Laboratoire de Physiologie Cellulaire et Végétale, UMR 5168 CNRS, CEA, INRAE, Université Grenoble Alpes, IRIG, CEA Grenoble, Grenoble, France.

⁸ Institut Universitaire de France, 1 rue Descartes, 75231 Paris Cedex 5 France

*: These authors contributed equally to the work

Corresponding authors:

cecile.antonelli@univ-perp.fr, hafidh@ueb.cas.cz, jean-marc.deragon@univ-perp.fr

Short title: AtLARP6C in pollen tube guidance

One-sentence summary: The RNA-Binding protein LARP6C is a key player in polarized pollen tube growth in *Arabidopsis* via post-transcriptional regulation of a subset of mRNAs in dry pollen and during the fertilization process.

The authors responsible for distribution of materials integral to the findings presented in this article in accordance with the policy described in the instruction for Authors (www.plantcell.org) are: Dr. C. Bousquet-Antonelli (cecile.antonelli@univ-perp.fr), Dr. Said Hafidh (hafidh@ueb.cas.cz) and Pr. JM Deragon (jean-marc.deragon@univ-perp.fr).

ABSTRACT

Increasing evidence suggests that post-transcriptional regulation is a key player in the transition between mature pollen and the progamic phase (from pollination to fertilization). Nonetheless, the actors in this mRNA-based gene expression reprogramming are poorly understood. We demonstrate that the evolutionarily conserved RNA-binding protein (RBP) LARP6C is necessary for the transition from dry pollen to pollen tubes and the guided growth of pollen tubes towards the ovule in *Arabidopsis thaliana*. In dry pollen, LARP6C binds to transcripts encoding proteins that function in lipid synthesis and homeostasis, vesicular trafficking, and polarized cell growth. LARP6C also forms cytoplasmic granules that contain the poly(A) binding

protein and possibly represent storage sites for translationally silent mRNAs. In pollen tubes, loss of LARP6C negatively affects the quantities and distribution of storage lipids, as well as vesicular trafficking. In *Nicotiana benthamiana* leaf cells and *in planta*, analysis of reporter mRNAs designed from the LARP6C target *MGD2* provided evidence that LARP6C can shift from a repressor to an activator of translation when the pollen grain enters the progamic phase. We propose that LARP6C orchestrates the timely post-transcriptional regulation of a subset of mRNAs in pollen during the transition from the quiescent to active state and along the progamic phase to promote male fertilization in plants.

1 INTRODUCTION

2 In the cytoplasm, mRNAs coated with RNA-binding proteins (RBPs) in the form of
3 ribonucleoprotein particles (mRNPs) are in balance between translation, storage, and
4 decay. Translationally silent mRNPs can be stored and protected from decay in
5 cytosolic aggregates and released when their protein product is needed. In response
6 to developmental or environmental cues, the fine-tuning between mRNA decay rate or
7 storage will have a direct impact on translation and hence gene expression. RBPs play
8 a crucial role in this fine-tuning, enabling gene-specific regulation through binding to
9 their mRNA targets.

10 LA and Related Proteins (LARPs) form a large family of eukaryote RBPs that
11 share the La Motif (LAM), a structured RNA-binding domain. LARPs are classified into
12 five distinct subfamilies, including the LARP6 group (Bousquet-Antonelli and Deragon,
13 2009). In most LARPs, an RNA Recognition Motif (RRM1) is found immediately after
14 the LAM and forms a bipartite RNA-binding unit called the La-module (Maraia et al.,
15 2017). While the LAM is usually very well conserved between subfamilies, the RRM1s
16 are specific to each subgroup (Bousquet-Antonelli and Deragon, 2009; Maraia et al.,
17 2017). Members of the LARP6 subfamily are found in Stramenopiles, Chlorophytes,
18 plants, invertebrates, and vertebrates and are characterized by the La-module and by
19 a short conserved motif known as LSA (LAM and S1 Associated) at the C-terminus
20 (Bousquet-Antonelli and Deragon, 2009) that mediates protein-protein interactions
21 (Cai et al., 2010b; Manojlovic et al., 2017; Vukmirovic et al., 2013; Weng et al., 2009).

22 In mammals, one of the functions of LARP6 is to regulate the synthesis of type
23 I collagen, a heterotrimer composed of two $\alpha 1$ and one $\alpha 2$ subunits whose assembly
24 and correct secretion are dependent upon the coordinate translation of their transcripts
25 at the endoplasmic reticulum (ER) (Zhang and Stefanovic, 2016). The expression of
26 type I collagen is primarily regulated by the binding of LARP6 through its La-module to

27 a stem loop in their 5'-UTRs (Cai et al., 2010a; Martino et al., 2015). LARP6 either
28 stores or stabilizes the collagen mRNA transcripts in a translationally silent form by
29 tethering them to vimentin filaments where they can further be activated for translation
30 or subjected to decay (Challa and Stefanovic, 2011). Alternatively, LARP6 docks the
31 mRNAs to non-muscle myosin filaments (Cai et al., 2010b; Manojlovic et al., 2017) and
32 either recruits STRAP (Serine Threonine kinase Receptor Associated Protein)
33 (Vukmirovic et al., 2013) or RNA helicase A (RHA) via its LSA (Manojlovic et al., 2017),
34 which respectively function as a repressor and activator of translation. Through this
35 mechanism, LARP6 orchestrates the coordinated translation of $\alpha 1$ and $\alpha 2$ collagen
36 transcripts at the ER. More recently, human LARP6 was found to regulate the
37 localisation and translation of ribosomal protein (RP) mRNAs to cell protrusions,
38 enhancing RP synthesis, ribosome biogenesis, and overall protein synthesis in
39 migratory cells (Dermitt et al., 2020). Furthermore, in zebrafish (*Danio rerio*), both
40 *LARP6* paralogs are required for normal oocyte development, chorion formation, and
41 egg activation (Hau et al., 2020).

42 While LARP6 proteins are generally encoded by a single gene, vascular plant
43 proteins are encoded by 3 to 6 genes and are of three evolutionary types named 6A,
44 6B, and 6C (Merret et al., 2013b). Whilst members of the 6A subgroup most closely
45 resemble LARP6 from other eukaryotes, in addition to a reorganized La-module, B-
46 and C-type orthologs carry a PABP-interacting motif 2 (PAM2). *Arabidopsis thaliana*
47 has three *AtLARP6* genes, one of each type, which we will refer to as *LARP6A*, *B* and
48 *C* throughout this manuscript.

49 We previously demonstrated that LARP6C directly associates with the poly(A)
50 binding protein (PABP) in plants, which is consistent with the presence of a PAM2 motif
51 and that the finding that its La-module binds to oligo(U₂₀) homopolymers *in vitro*. In
52 addition, in onion (*Allium cepa*) epidermis, LARP6C accumulates in the cytoplasm, the
53 nucleoplasm, and the nucleolus. Strikingly, LARP6C redistributes to stress granules
54 upon hypoxia, where it associates with mRNP aggregates (Merret et al., 2013b). These
55 data support the view that *Arabidopsis* LARP6C is an RNA-binding protein that is likely
56 involved in mRNA post-transcriptional regulation.

57 In flowering plants, the haploid male gamete (pollen grain) consists of a
58 vegetative cell that encases two sperm cells, which are connected (through a so-called
59 cytoplasmic connexion) with the vegetative cell nucleus to form the male germ unit. A
60 characteristic feature of angiosperm sexual reproduction is that sperm cells are non-

61 motile and must be carried simultaneously to the ovule by a pollen tube (Johnson and
62 Preuss, 2002). Upon adhesion to the stigma, the male vegetative cell hydrates,
63 germinates, and grows into a tube that delivers the two sperm cells to the ovule. The
64 pollen tube is a highly polarized and fast tip-growing cell whose growth directionality is
65 determined by various perceived cues. It is first guided in the gynoeceum by female
66 sporophytic tissue in the pistil (preovular guidance) and then, upon exit from the
67 transmitting tract, it navigates in gametophytic tissues guided by ovule-emitted signals
68 (ovular guidance). Ovular cues guide the pollen tube alongside the funiculus to the
69 micropyle. Upon reaching the ovule, the pollen tube stops growing and bursts to free
70 the sperm cells that will fuse respectively with the egg cell (to form the embryo) and
71 the central cell (to form the endosperm), hence completing the fertilization process
72 (Higashiyama and Takeuchi, 2015).

73 In the pollen tube, upon reception and transduction of extracellular female
74 signals, a complex cellular process targets the cell wall synthesis machinery at the site
75 of perception, hence permitting the delivery of macromolecules at site of extension and
76 the directional growth of the tube. This requires tip-localized receptors, the flow of ions,
77 intracellular trafficking of signalling molecules and proteins, but also vesicular
78 trafficking, cytoskeleton-dependent transport, and novel cell wall formation through
79 exocytosis (Feng et al., 2018; Hafidh et al., 2014; Higashiyama and Takeuchi, 2015).
80 Pollen tube growth also requires changes in the pattern of gene expression that at
81 least in part rely on post-transcriptional mechanisms. Several studies have suggested
82 that all mRNAs required for germination and pollen tube growth are already present in
83 the mature pollen grain and maintained in a translationally silent state until the
84 progamic phase (Hafidh et al., 2018; Honys et al., 2000; Honys and Twell, 2004;
85 Scarpin et al., 2017). Nonetheless, how male gene expression is post-transcriptionally
86 regulated to permit correct pollen guidance is largely unknown, and the mRNA-
87 regulating factors required for proper ovular guidance of pollen are currently unclear.

88 In the present study, we further explored the role of LARP6C and determined
89 that it is a pollen-specific factor required for male fertility during the progamic phase.
90 We provide evidence that loss of LARP6C affects lipid synthesis and homeostasis as
91 well as vesicular trafficking. Moreover, our experimental results support the notion that
92 LARP6C orchestrates the balance between the translation, storage, and decay of its
93 mRNA clients through direct binding, thus intervening in the guided growth of the pollen
94 tube.

95

96 RESULTS

97

98 LARP6C and its RNA-binding domain are required for male fertility at the pollen 99 tube guidance step

100 Immunoblotting and high-throughput transcriptomic analyses (Klepikova et al., 2015)
101 showed that, unlike LARP6A and 6B, LARP6C is almost exclusively expressed in
102 pollen grains and pollen tubes (Figure 1A and Supplemental Figure S1). We therefore
103 investigated its role in male fertility using two Arabidopsis T-DNA insertion mutants,
104 *larp6c-3* and *larp6c-4*. Immunoblotting showed that both alleles are loss-of-function
105 (lof) mutants (Figure 1B). To establish whether *larp6c* is a gametophytic mutation, we
106 monitored the transmission efficiency (TE) through the female (TE^f) and the male (TE^m)
107 gametophytes by reciprocal crosses with wild type and heterozygous *larp6c-3/+* or
108 *larp6c-4/+* mutants (Figure 1C). Both alleles were transmitted normally through the
109 female gametophyte (TE^f *6c-3* = 100% and *6c-4* = 96.7%), whereas their transmission
110 through the male was significantly reduced, with *6c-3* showing TE^m = 74.1% and *6c-4*
111 TE^m = 68.2% (Figure 1C). This suggests that male but not female fertility is
112 compromised by the loss of LARP6C function.

113 There are different stages at which the male gametophyte could be deficient,
114 including pollen development, germination, pollen tube growth or guidance, and sperm
115 delivery (Johnson and Preuss, 2002). We monitored these pollen stages in *larp6c-3*,
116 *6c-4*, and wild-type plants (Figure 1D-F and Supplemental Figure S2A-E). Assessment
117 of male gametophyte maturation by DAPI staining revealed that 10% of the *6c-3* and
118 *6c-4* mutant pollen grains did not complete their maturation and were arrested at the
119 bicellular stage, compared to less than 3% in wild type (Supplemental Figure S2A).

120 We next monitored germination and pollen tube growth during the early and late
121 steps after hydration (*in vitro*) or pollination (*in vivo* and semi *in vivo* [SIV]) (Palanivelu
122 and Preuss, 2006) and Methods) (Figure 1D and Supplemental Figure S2). *In vitro*,
123 *larp6c-3* showed some defects in germination, with over 70% of ungerminated pollen
124 grains after 30 min incubation versus 60% for wild type and an increased frequency of
125 pollen tube burst. Moreover, at 30 min, *larp6c-3* showed less than 5% elongated pollen
126 tubes versus 20% in the wild type, e.g. pollen tubes with lengths over three times that
127 of mature pollen grains. *In vivo*, the situation appeared more dramatic, with a very high
128 levels of ungerminated *larp6c-3* pollen at 15 and 30 min after pollination of over 80 and

129 50%, respectively, compared to wild-type pollen, which showed less than 10%
130 ungerminated pollen after 15 min incubation. Moreover, *in vivo*, at 30 min, *larp6c-3*
131 pollen tubes seemed to be more prone to bursting than wild type (Figure 1D). These
132 germination and pollen tube growth defects were likely due to delays rather than full
133 arrest, since 7 and 24 hours after pollination (Supplemental Figure S2B, C and E) or 4
134 hours after hydration (Supplemental Figure S2D), the density and length of *larp6c*
135 pollen tubes were similar to those of wild type.

136 We next investigated the requirement for LARP6C for pollen tube guidance and
137 ovule targeting competence (Johnson and Preuss, 2002). We set up SIV experiments
138 using pistils from *ms1* plants, a male-sterile mutant with normal pistil function (van der
139 Veen and Wirtz, 1968), to assess the ability of *larp6c*-deficient pollen tubes to be
140 guided through the pistil tissues towards wild-type ovules for fertilization (Figure 1E,
141 top panel and Supplemental Figure S3A). Whereas wild-type pollen targeted 80% to
142 100% of the ovules (with a median value of around 90%), both *larp6c-3* and *6c-4* pollen
143 showed a significant reduction, targeting 50 to 70% of wild-type ovules (with a median
144 value of 60%). This failed pollen tube guidance phenotype was rescued by the N- and
145 C-terminal LARP6C fusion constructs (YFP-LARP6C and LARP6C-tRFP) (Figure 1E
146 and Supplemental Figure S3B-C). In competition assays, irrespective of the order of
147 pollination or the side of the stigma in which the pollen grains were dusted on, *larp6c-*
148 *3* and *6c-4* pollen also showed a clear deficiency in ovule targeting, with a maximum
149 targeting efficiency of 20% compared to the expected 50% rate (Supplemental Figure
150 S3A and D). This further supports the notion that the observed guidance phenotype
151 directly relates to *larp6c* deficiency.

152 We next monitored the ability of the *larp6c* and *larp6c*-complemented pollen to
153 target ovules *in planta* (Figure 1E-F and Supplemental Figure S2E). We hand
154 pollinated *ms1* pistils and following aniline blue staining, scored the number of targeted
155 and non-targeted ovules. Aniline blue stains callose-like polysaccharides contained in
156 pollen tube walls, and after exposure to UV emits yellow-green fluorescence that
157 allows visualization of pollen tubes even after penetration in the ovule. Here again the
158 *larp6c* deficient pollen tubes displayed only 60% ovule targeting efficiency versus the
159 80% average observed in wild-type pollinated pistils (Figure 1E, bottom panel). The
160 targeting efficiency by the (*larp6c-3*; LARP6C-tRFP) and (*larp6c-3*; YFP-LARP6C)
161 complemented lines recovered to a wild-type frequency (Figure 1E). Considering that
162 4 hours after pollination, the density and length of mutant pollen tubes were similar to

163 those of wild type (Supplemental Figure S2E), it appears unlikely that the ovule
164 targeting deficiency of *larp6c* pollen was due to delays in germination or pollen tube
165 elongation. Nonetheless, to completely rule out this possibility, we monitored the type
166 of ovule targeting defects at 4, 8, and 24 hours after pollination (HAP) *in vivo*. We
167 observed and scored two types of behaviour: type I: if pollen tube attraction and
168 reception were normal and type II: if pollen tube attraction was defective. We did not
169 observe a situation where attraction was normal but reception defective. Consistent
170 with previous experiments, we found that *larp6c*-deficient pollen tubes showed a
171 significant increase in type II behaviour compared to wild type (Figure 1F). At 24 HAP,
172 while some 40% of the ovules remain unfertilized in pistils pollinated with *larp6c-3* or *4*
173 mutant pollen due to attraction defects, only 5% of the ovules were not fertilized when
174 pollination was conducted with wild-type pollen (Figure 1F).

175 Considering that *LARP6A* mRNA is highly expressed in pollen (3 to 4 times
176 more than *LARP6C* mRNA in mature pollen grain, Supplemental Figure S1A), we
177 wondered whether *LARP6A* and *LARP6C* could at least partially act redundantly. In
178 backcross experiments, *larp6a-1* loss-of-function pollen (Supplemental Figure S3F)
179 displayed over 95% transmission efficiency, and the transmission efficiency of (*larp6c-3*;
180 *larp6a-1*) was not significantly different from that of single *larp6c-3* mutant pollen
181 (82.7%) (Supplemental Figure S3F). We also ran *in vivo* pollination assays with wild-
182 type, *larp6c-3*, or (*larp6c-3*; *larp6a-1*) pollen and scored fertilization behaviours
183 (Supplemental Figure S3G). Consistent with the results of backcross experiments, the
184 absence of *LARP6A* did not affect fertilization in the wild-type or *larp6c* null
185 background.

186 Finally, to confirm that *larp6c* loss of function specifically affects male fertility,
187 we examined the capability of *larp6c-3* and *6c-4* mutant ovules to attract wild-type
188 pollen tubes by SIV and *in vivo* assays and found no significant difference from wild
189 type (Supplemental Figure S4). A detailed description of these experiments can be
190 found in the legend of Supplemental Figure S4.

191 We previously demonstrated that *LARP6C* is an RNA-binding protein and that
192 its La-module is sufficient to bind RNA homopolymers *in vitro* (Merret et al., 2013b).
193 We hence wondered whether the RNA-binding function of *LARP6C* is necessary for
194 its role in pollen tube guidance. Since for LARPs, including human *LARP6*, which carry
195 a bipartite La-Module, the LAM is absolutely necessary to bind RNA both *in vitro* and
196 *in vivo* (Martino et al., 2015; Cai et al., 2010a), we constructed a truncated *LARP6C*

197 deleted of its La Motif (*LARP6CΔ-LAM*). We then stably expressed this deletion mutant
198 construct in the *larp6c-3* and *larp6c-4* backgrounds under the control of the *LARP6C*
199 native promoter (Supplemental Figure S3C). *In vivo* fertilization assays showed that
200 pollen expressing *LARP6CΔ-LAM* had the same pollen tube guidance defects as *larp6c*
201 loss-of-function pollen, suggesting that *LARP6CΔ-LAM* cannot complement the *larp6c-*
202 3 lof phenotype and that the La-Module RNA-binding motif is essential for *LARP6C*
203 function in pollen tube guidance (Figure 1F).

204 In summary, our results support the notion that *LARP6C* is required for male
205 fertility at least in part at the progamic phase through its function in pollen germination
206 and during pollen tube guidance and does not appear to act redundantly with *LARP6A*.
207 Moreover, *LARP6C* function in pollen tube guidance requires an intact La-Module,
208 supporting the notion that this physiological role involves the RNA-binding activity of
209 *LARP6C*.

210

211 ***LARP6C* forms dynamic cytoplasmic granules in mature pollen grains and in** 212 **pollen tubes**

213 To better understand the cellular roles of *LARP6C*, we monitored its subcellular
214 distribution across pollen maturation and during pollen tube growth (Figure 2A and
215 Supplemental Figure S5). In microspores, *LARP6C* was only detected in the nucleolus.
216 At the bicellular stage, *LARP6C* was much more generally distributed in the cytoplasm
217 of the vegetative cell, as well as in the vegetative and generative cell nuclei. At the
218 tricellular stage, the subcellular distribution of *LARP6C* was similar to that at the
219 bicellular stage, with possibly reduced amounts of *LARP6C* in the sperm cell nucleus
220 compared to other subcellular compartments. In mature pollen grain, *LARP6C*
221 displayed a complex localization pattern. It was clearly present in vegetative cell
222 cytoplasm but transitioned from a diffuse pattern to a granular, aggregate-like pattern
223 (Figure 2A and Supplemental Figure S5). In addition to this granular distribution,
224 *LARP6C* appeared to concentrate around the membrane surrounding the vegetative
225 cell nucleus, the sperm cells and the cytoplasmic connection linking the sperm cell 1
226 to the vegetative cell nucleus.

227 To determine more precisely the distribution of *LARP6C* in mature pollen grains,
228 we performed colocalization experiments between *LARP6C*-tRFP and various markers
229 (Figure 2B). The histone H2B-GFP fusion protein, expressed under the control of the
230 tomato (*Solanum lycopersicum*) pollen-specific *LAT52* promoter (Twell et al., 1989),

231 was used to label the vegetative cell nucleus, thereby demonstrating the absence of
232 LARP6C in this compartment. GEX2 is a sperm cell-expressed transmembrane protein
233 (Mori et al., 2014) that labels the sperm cell membranes and the cytoplasmic
234 connection between sperm cell 1 and the vegetative cell nucleus (Brownfield et al.,
235 2009; McCue et al., 2011; Mori et al., 2014). Confocal analyses showed that LARP6C
236 and GEX2 displayed distinct distributions (Figure 2B). The tRFP signal surrounded the
237 GFP-GEX2 signal decorating the outer membrane of the male germ unit but not the
238 membrane connecting the two sperm cells (the inner membrane), supporting the notion
239 that LARP6C is excluded from the sperm cells and therefore only resides in the
240 vegetative cell cytoplasm in mature pollen.

241 We next inquired on the nature of LARP6C cytoplasmic foci (Figure 2B).
242 Eukaryotic cells contain many types of membrane-less cytoplasmic aggregates
243 composed of translationally silent mRNAs and RBPs (Buchan, 2014). So far, only two
244 types of mRNP granules have been identified in plant cells: processing bodies (p-
245 bodies) and stress granules (Weber et al., 2008). Plant p-bodies are - as in other
246 eukaryotes - characterized by the presence of actors of the general mRNA turnover
247 process, such as the DCP1/DCP2 decapping holoenzyme, the XRN4 exoribonuclease,
248 or the deadenylation complex. Stress granules, on the contrary, contain factors
249 belonging to the translational machinery, including the poly(A) binding protein (Weber
250 et al., 2008). First clues on the nature of LARP6C aggregates observed in mature
251 pollen were derived by colocalization experiments with specific markers of p-bodies
252 and stress granules, namely DCP1 and PABP, respectively. We used a YFP-tagged
253 DCP1 protein expressed from its own upstream genomic sequences (Merret et al.,
254 2013a). Although YFP-DCP1 displayed a punctuate distribution in the vegetative cell
255 cytoplasm, similar to LARP6C, no obvious colocalization of DCP1 and LARP6C was
256 observed. Of note, DCP1 accumulation appeared to be restricted to the vegetative cell
257 cytoplasm, at least in mature pollen, and contrary to LARP6C, it did not localize at the
258 periphery of the sperm cells or the vegetative nucleus (Figure 2B).

259 The Arabidopsis genome contains seven genes (*PAB2* to *8*) encoding canonical
260 PABPs, including *PAB3*, *5*, *6* and *7* (Belostotsky and Meagher, 1996; Belostotsky,
261 2003; Honys and Twell, 2004), whose transcripts accumulation is restricted to pollen.
262 We fused the genomic sequence of the *PAB5* gene (the most highly expressed of the
263 pollen specific *PABP* genes) to a YFP tag under the control of its own upstream
264 sequences. In the vegetative cell cytoplasm, the YFP-PAB5 protein displayed a pattern

265 identical to that of the LARP6C protein in that it accumulated in foci surrounding the
266 sperm cells and was excluded from the vegetative nucleus, but contrary to LARP6C, it
267 was also present in the cytoplasm of sperm cells.

268 Finally, in pollen tubes, LARP6C was clearly excluded from the sperm cells and
269 restricted to vegetative cell cytoplasm. In the cytoplasm, LARP6C signals showed
270 various degrees of aggregate patterns, with foci appearing to be organized along a
271 longitudinal string-like structure (Figure 2A and Supplemental Figure S5C). To explore
272 the possibility that LARP6C foci could bind to the cytoskeleton structure, we co-
273 expressed LARP6C-tRFP with GFP-AtTUB6 (which labels microtubules) in *Nicotiana*
274 *benthamiana* epidermis cells (Ambrose and Cyr, 2007), GFP-FABD2 (Voigt et al.,
275 2005), or LifeACT-GFP (Cvrčková and Oulehlová, 2017) (which label actin
276 microfilaments; Figure 2C and Supplemental Movie S1). While LARP6C did not
277 significantly co-localize with actin microfilament markers, it co-localized with GFP-
278 tubulin (Figure 2C and Supplemental Movie S1). Not only did the strings formed by
279 LARP6C foci overlap with tubulin filaments, but LARP6C foci also appeared to move
280 along microtubules, as revealed by time series observations (Supplemental Movie S1).

281 Finally, as an additional exploration of possible redundancy, we ran
282 colocalization experiments between LARP6C and LARP6A (Supplemental Figure S5B,
283 C). We previously showed that, when transiently expressed in onion epidermis cells,
284 LARP6C localized to stress granules (together with PABP), while LARP6A did not.
285 Consistently, in mature pollen grain, we observed that LARP6C formed foci, while
286 LARP6A did not (Supplemental Figure S5C). Additionally, LARP6A and 6C showed
287 distinct subcellular distributions in pollen tubes, with 6A mainly accumulating in sperm
288 cell cytoplasm while 6C was excluded from the sperm cells (Supplemental Figure
289 S5C).

290 In summary, our data indicate that LARP6C shows a dynamic subcellular
291 distribution across pollen maturation. We found that in mature pollen and pollen tubes,
292 LARP6C is restricted to the vegetative cell cytoplasm and is present in aggregates that
293 could possibly associate with microtubules.

294

295 **RIP-seq pulldown reveals LARP6C mRNA targets in mature pollen grain**

296 The presence of LARP6C in cytoplasmic aggregates, which contain the poly(A) binding
297 protein, together with our previously published data (Merret et al., 2013b), strongly
298 support the notion that at the cellular level, LARP6C likely acts to control mRNA fate

299 in pollen. In addition, since its RNA-binding domain is necessary to fulfil its role in
300 pollen tube guidance, we reasoned that the identification of its mRNA clients would
301 help reveal how LARP6C controls male fertilization at the molecular level. We hence
302 sought to identify its mRNA targets using an unbiased RNA immunoprecipitation and
303 sequencing (RIP-seq) strategy. We conducted the RNA immunoprecipitation
304 procedure from complemented *larp6c-3* lof mature pollen grains expressing a
305 PRO_{6C}:LARP6C-FlagHA tagged version (6C-FH hereafter) (Supplemental Figure S3B,
306 C) and from wild-type pollen grains as a negative control. After assessing the efficiency
307 of the immunoprecipitation through immunoblotting (Supplemental Figure S6A), RNAs
308 were extracted from the input and eluate fractions and subjected to RNA-seq. After
309 mapping and filtering of the dataset (see Supplemental Methods), a RPKM (read per
310 kilobase per million mapped reads) value was calculated for each protein-coding gene.
311 The replicates were found to be reproducible (Supplemental Figure S6B), enabling us
312 to build a table with a mean normalized value per gene and filter out those with less
313 than 1 RPKM value in one of the four samples (input or eluate from wild type or 6C-
314 FH) (Supplemental Data Set S1). Using such criteria, we retained a list of 7356
315 expressed transcripts.

316 We first filtered out transcripts based on input fraction values, retaining mRNAs
317 that are not differentially expressed (DE) and show a fold change between 6C-FH and
318 wild-type < 1.2 in order to select for transcripts whose levels did not vary between
319 control and 6C-FH inputs. Then, from this trimmed list, we selected mRNAs that are
320 DE (FDR 0.01) and accumulated to a higher extent in the eluate fraction of 6C-FH
321 compared to wild type (Figure 3A). Next, we selected mRNAs that were enriched by
322 the immunoprecipitation procedure, by selecting those with a RE_{6C-FH} (RE is the eluate
323 over input ratio) value > 1 . To further increase stringency and reveal mRNAs that are
324 most likely to be direct targets of LARP6C, we compared the RE_{WT} to the RE_{6C-FH} and,
325 based on the repartition of the values (Supplemental Figure S6C and D) selected
326 transcripts with an (RE_{6C-FH}/RE_{WT}) value of 3 or more (Figure 3B). Through the above
327 series of filters, we identified a high-confidence list of 115 genes encoding direct or
328 indirect mRNA targets of LARP6C (Supplemental Data Set S1).

329 No gene ontology (GO) term was found to be significantly enriched amongst the
330 115 mRNAs identified as potential LARP6C targets. Nonetheless, a gene-to-gene
331 analysis shows that the majority of LARP6C targets encode factors likely to be involved
332 in polarized cell growth and male fertilization. This includes protein involved in

333 endomembrane system trafficking and synthesis, signalling factors and kinases
334 (Grebnev et al., 2017; Samaj et al., 2006) and most strikingly proteins involved in lipid
335 metabolism and homeostasis control (Ischebeck, 2016) (Figure 3C, Supplemental
336 Data Set S1). Also, we found that some LARP6C targets are known actors of pollen
337 gametogenesis, pollen germination, pollen tube growth and guidance, or tip-polarized
338 growth, such as the growth of roots or neurons (Supplemental Data Set S1).

339

340 **Loss of LARP6C affects lipid metabolism and the endomembrane system during** 341 **pollen tube growth**

342 In angiosperms, lipids are crucial for male fertilization. Pollen tube elongation depends
343 on lipids synthesized and stored in pollen grain before desiccation or produced on the
344 way from pistil to ovule (Ischebeck, 2016). Amongst the list of LARP6C targets are
345 actors involved in fatty acid synthesis, di- and triacylglycerol (TAG) synthesis and
346 homeostasis, whose control were previously found to be necessary for correct pollen
347 tube growth (Botté et al., 2011; Pleskot et al., 2012; Zheng et al., 2018). This includes
348 genes encoding fatty acid synthesis factors (FAD2 (Botella et al., 2016), ACX4 (Khan
349 et al., 2012) and AtLPEAT2 (Stålberg et al., 2009)); DGAT1, which catalyzes the first
350 step of TAG synthesis (Zhang et al., 2009); DYRKP-2A (Schulz-Raffelt et al., 2016)
351 and MPK6 kinases, which regulate TAG production (Zheng et al., 2018); SDP1, a TAG
352 lipase involved in membrane lipid homeostasis control (Kelly et al., 2013); and MGD2,
353 which catalyzes the synthesis of monogalactosyldiacylglycerol (MGDG) (Botté et al.,
354 2011).

355 Considering that LARP6C might control the expression of genes encoding
356 proteins involved in glycerolipid metabolism and homeostasis at the post-
357 transcriptional level, we tested lipid accumulation and synthesis in the absence of
358 LARP6C in mature pollen grains and pollen tubes (Figure 4). First, we visualized lipid
359 droplets (LDs), which consist of a phospholipid monolayer surrounding a core of
360 neutral lipids such as TAG and fatty acid steryl esters, by staining with Bodipy 505/515
361 (which stains neutral lipids) and Nile Red (which stains non-polar and neutral lipids)
362 (Figure 4A-B). In *larp6c-3* mature pollen grain, we did not detect any significant
363 difference in staining compared to wild-type grains (Figure 4A). We then germinated
364 and grew wild-type and *larp6c-3* pollen tubes *in vitro* and visualized LD accumulation
365 at 2 and 4 h post germination (Figure 4B). At 2h after germination, 77 out 132 (58%)
366 observed pollen tubes showed fewer LDs compared to wild type, and at 4h, 84% (n

367 =100/119) of pollen tubes showed an abnormal distribution of LDs. In 72% of the
368 cases, LDs were absent from apical and sub-apical regions and were only detected in
369 the shank, and 12% showed an overaccumulation and aggregation of lipids at the tip.
370 Such aberrant distribution was never observed amongst the wild-type pollen tubes (n
371 = 109). This phenomenon was even more pronounced when pollen tubes were grown
372 through a pistil explant, with 100% of *larp6c-3* pollen tubes showing an atypical
373 distribution of LDs (Figure 4C, SIV). These results support the notion that lipid
374 synthesis and/or distribution in pollen tubes is perturbed in the absence of LARP6C.

375 We next explored the impact of the downregulation of lipid synthesis on pollen
376 tube guidance in the absence of LARP6C. Amongst the LARP6C mRNA targets,
377 *MGD2* encodes a pollen specific (our data and (Qin et al., 2009)) MGDG synthase
378 (Botté et al., 2011). *In situ* labelling of Arabidopsis pollen tube membranes previously
379 showed the presence of digalactosyldiacylglycerol (DGDG) (which are synthesized
380 from MGDG), and the chemical inhibition of the MGD enzymatic pathway with
381 galvestine-1 reduces MGDG content and downregulates pollen tube elongation rates
382 (Botté et al., 2011), supporting a role for MGD in male fertilization.

383 We reasoned that if one of the molecular bases of the guidance defect of *larp6c*
384 relates to the misregulation of *MGD2* mRNA fate and expression, the specific inhibition
385 of its enzymatic activity and downregulation of MGDG/DGDG production with
386 galvestine-1 should alleviate or aggravate the *larp6c* lof phenotype. We hence
387 monitored pollen tube elongation rates and pollen tube guidance in the presence of
388 galvestine-1 by SIV assays (Figure 4D, E). Consistent with a previous report (Botté et
389 al., 2011), we observed that galvestine-1 application reduced pollen tube elongation in
390 wild-type pollen as well as *larp6c-3* mutant pollen (Figure 4D). However, when we
391 monitored pollen tube guidance efficiency, wild-type pollen tubes were only slightly or
392 not affected at all, whereas pollen tubes of *larp6c* mutants showed a considerable
393 decrease in ovule targeting in the presence of galvestine-1 (Figure 4E). Under these
394 conditions, only 30 to 60% of ovules were targeted by *larp6c*-pollen tubes, whereas
395 the mock-treated samples showed 60 to 70% targeting. In some pistil explants, *larp6c*
396 pollen tubes showed no ovule targeting at all in the presence of the MGD inhibitor, a
397 situation that was never observed with *larp6c-3* pollen tubes in the absence of the
398 MGD inhibitor (Figures 1E-F and 4E). Collectively, these results support a synergic
399 effect between the loss-of-function of LARP6C and the pharmacological inhibition of
400 MGD2 synthase activity on pollen tube guidance but not on pollen tube elongation.

401 LARP6C also binds mRNA encoding factors involved in endosome functioning
402 and vesicular trafficking. Brefeldin A (BFA) is a fungal toxin known to perturb
403 endomembrane system trafficking, particularly at the level of retrograde Golgi to ER
404 trafficking and to induce ectopic ER-Golgi fusions known as BFA bodies (Tse et al.,
405 2006). We therefore monitored *larp6c-3* pollen tube sensitivity to BFA compared to wild
406 type (Figure 5). After 1h activation on germination medium, the pollen tubes were
407 exposed to BFA and the number and size of BFA bodies scored over time through FM
408 4-64 staining. As soon as 10 min after exposure to BFA, *6c-3* pollen tubes showed
409 increased number of BFA bodies and a dramatic increase in size compared to wild-
410 type 17 min after treatment. At this time point, ectopic BFA-particles were also bigger
411 in the mutant than in wild type. These results indicate that pollen tubes deprived of
412 LARP6C are hypersensitive to pharmacological perturbation of endosomal trafficking.
413

414 **LARP6C directly binds to the 5'-UTRs of its mRNA targets**

415 We next sought to understand how LARP6C recognises and influences the fate of its
416 mRNA targets through binding. RNA-binding proteins often bind to primary sequence
417 motifs shared between their mRNA targets to regulate their fate. Considering that *cis*
418 regulatory elements are mostly located in the 5' and/or 3' untranslated regions (UTRs)
419 of transcripts, we looked for primary sequence motif(s) shared between the UTRs of
420 the putative LARP6C targets. Using the Araport database, we found and retrieved the
421 5'- and 3'-UTRs for 112 mRNAs and ran a discriminative motif search using a MEME
422 search (at the MEME suite portal (<https://meme-suite.org/>)). Whereas no significant
423 motif could be detected in the 3'-UTRs of LARP6C mRNA targets, we identified two
424 regions we named A-box ($E^{\text{value}}: 5.5E^{-99}$) and B-box ($E^{\text{value}}: 9.3E^{-91}$) motifs that are
425 highly enriched in the 5'-UTRs of LARP6C mRNA targets (Figure 6A). As a control, we
426 ran an identical motif search using a set of 112 randomly chosen 5'- and 3'-UTRs from
427 genes expressed in pollen according to our transcriptomic analyses. We found no
428 significant enrichment for an A- or a B-type region, supporting the idea that these
429 sequence motifs are specific for mRNAs that are in a complex with LARP6C.

430 The A motif is a purine-rich 21 nt sequence with a clear dominance of A over G
431 nucleotides, while the B motif is a pyrimidine-rich 21 nt sequence with a majority of U
432 (T in DNA) over C repeats (Figure 6A, Supplemental Data Set S1). A closer
433 examination of sequences that contain the A and/or B consensus sequence revealed
434 two major categories for each box type. In particular, sequences harbouring the A motif

435 are mainly composed of either A or AG/AAG repeats, whilst sequences sharing the B
436 consensus motif contain either U or UC/UUC repeats (Supplemental Data Set S1).
437 Amongst the 112 identified 5'-UTRs, 70 (62.5%) bear the A motif, 74 (66%) the B motif,
438 and 49 (43.7%) carry both (Supplemental Figure S6E).

439 The presence of motifs shared by transcripts that co-immunoprecipitated with
440 LARP6C *in vivo* suggests that one or both of these boxes mediate the direct binding
441 of LARP6C. To explore this hypothesis, we tested the RNA-binding unit of LARP6C,
442 the La-module, for its ability to interact with these boxes *in vitro* (Figure 6B-E and
443 Supplemental Figure S7). We designed two oligonucleotide sequences for the A motifs
444 called A1 and A2, representing the “A-rich” and the “AG/AAG-rich” types, respectively
445 (Supplemental Figure S7A). Analogously, B1 and B2 were designed for the B motifs
446 exemplifying the “U-rich” and “UC/UUC-rich” types, respectively (Figure 6B). As a
447 control, we designed oligos B3 and B4, representing C- or CU/CCU-rich sequences,
448 respectively. A recombinant version of the LARP6C La-module, identical to the one
449 used in Merret *et al.* (Merret et al., 2013b), was expressed in *E. coli* as previously
450 described and its ability to bind the A and B type oligo RNAs was quantified by
451 isothermal titration calorimetry (ITC) and electrophoretic mobility shift assay (EMSA)
452 (Figure 6B-E and Supplemental Figure S7). In the ITC experiments, serial titration of
453 LARP6C La-module with RNA oligos B1 and B2 generated (in both cases) a profile
454 that could be fitted to a sigmoid-shaped binding curve centred around a 1:1
455 stoichiometry, with a dissociation constant in the low micromolar range (Kds of 2.8 μ M
456 and 3.7 μ M, respectively, indicating direct binding of LARP6C La-module to B1 and B2
457 type motifs (Figure 6B and Supplemental Table S1). The binding mode of LARP6C La-
458 module for the B1 and B2 oligos is similar (but with higher affinity) to that previously
459 observed for an U20 homopolymer (Supplemental Table S1 and (Merret et al., 2013b)).
460 On the contrary, no binding of oligos B3, B4, A1, or A2 to the recombinant LARP6C
461 domain was detected by ITC under the same experimental conditions (Figure 6D,
462 Supplemental Figure S7A and Supplemental Table S1).

463 To confirm the ITC results, parallel EMSAs were performed using RNA oligos
464 labelled at the 5' end with γ -³²P to monitor RNA-protein complex formation by native
465 gel electrophoresis. Experiments were conducted in the presence or absence of tRNA
466 competitor. For oligos showing the ability to form a complex with La-module, the
467 fraction of bound RNA was plotted against the protein concentration and the

468 dissociation constant determined (Figure 6C). In agreement with the ITC results,
469 EMSA confirmed that B1 and B2 oligos associate with the LARP6C La-module, with
470 estimated dissociation constants in the low micromolar range (Kds of 0.8 μ M and 1.9
471 μ M, respectively), again suggesting a high affinity of LARP6C La-module towards B1
472 and B2 oligos (Figure 6C). The binding behaviour of B2 oligo was very similar to what
473 we observed for an oligo(U₂₀) (Merret et al., 2013b), whereas B1 showed a slightly
474 higher binding affinity. Assays with oligos A1, A2, B3, oligo(C₂₀) and to a lesser extent
475 with B4 were hindered by samples being retained in the wells of the gel at high protein
476 concentration (Figure 6E and Supplemental Figure S7B), an issue most likely linked to
477 protein and/or protein/RNA non-specific aggregation (Hellman and Fried, 2007).
478 Despite changing various experimental conditions, this issue could not be overcome.
479 The presence of a tRNA competitor marginally helped in the case of B4, albeit
480 association with LARP6C was observable only at high protein concentrations and a Kd
481 could not be calculated, as the binding curve did not reach a plateau (Figure 6E).

482 Collectively, these experiments demonstrate that LARP6C La-module binds to
483 oligos B1 and B2 with high affinity and with a similar association mechanism observed
484 with oligo(U₂₀). B1, which contains three stretches of U residues, one of which is 6
485 uridines long, appeared to bind slightly more tightly than B2 and U₂₀. Altogether, these
486 results indicate that the LARP6C La-module strongly binds to B type motifs and does
487 not associate with A type motifs, at least *in vitro*, and that it displays low affinity for B4.
488 We hence propose that *in vivo*, LARP6C directly binds (at least) to mRNAs that carry
489 a B1 or B2-type box in their 5'-UTRs to execute post-transcriptional regulation on its
490 mRNA targets.

491

492 **LARP6C is not required for the accumulation of its mRNA targets in mature** 493 **pollen grain**

494 To gain a global view of the role of LARP6C in the accumulation of its mRNA targets,
495 we monitored the polyadenylated transcriptome of mature pollen grains in the absence
496 of LARP6C. Pollen grains were collected from wild-type and *larp6c-3* plants grown
497 together in a greenhouse (see Supplemental Methods), total RNAs were extracted
498 from the pollen, and the polyadenylated fraction was subjected to next generation
499 sequencing. Following mapping and filtering of the reads (see Supplemental Methods),
500 we retained a list of 7399 transcripts with at least 1 RPKM as reliably expressed from
501 both Col-0 and *larp6c-3* (Supplemental Figure S8, Supplemental Data Set S2). We

502 then used a DE-seq pipeline (FDR 0.05) to find genes whose transcripts differentially
503 accumulate in the mutant background and retained those with a fold change of at least
504 1.5 between wild type and *larp6c-3*. We found 2174 genes that were up- or
505 downregulated in *larp6c-3* pollen compared to the wild type (Figure 7A). Monitoring the
506 fold changes of these transcripts between wild type and (*larp6c-3*; 6C-FH) in the input
507 fraction of the RIP-seq samples, we observed that they are centred around 1 (Figure
508 7B). This suggests that the expression of the *LARP6C-FlagHA* transgene in the *larp6c-*
509 *3* background fully complemented the *larp6c-3* mutation and restored a wild-type
510 expression level, demonstrating that the LARP6C-FlagHA translational fusion is
511 functional and that the mis-regulation of the *larp6c-3* pollen transcriptome is biologically
512 significant and a direct consequence of the loss of LARP6C function. We then asked
513 if the steady-state levels of LARP6C-bound mRNAs are affected in *larp6c-3* pollen
514 grains. Of the 115 targets, 96 were detected in the RNA-seq data, and only 15 of these
515 differentially accumulated in the *larp6c-3* background (Figure 7C, Supplemental Data
516 Set S2). Of these, ten were downregulated by 1.5- to 2.8-fold and five were
517 upregulated by 1.5- to 1.7-folds in *larp6c-3* (Figure 7D). These observations suggest
518 that, at least in dry pollen, LARP6C is not required for maintaining steady-state levels
519 of its mRNA targets.

520

521 **LARP6C controls the expression of a reporter transcript containing a functional** 522 **5'-UTR B-box motif**

523 To gain a mechanistic insight into the impact of LARP6C binding to its mRNA targets,
524 we performed transient assays to monitor the expression of a *YFP* reporter gene under
525 the control of a modified 5'-UTR belonging to *MGD2*, a LARP6C mRNA target that
526 carries a potential *bona fide* B-box and no A-box motif (Supplemental Data Set S1).
527 We then respectively replaced the native B-box by two sequences that we
528 demonstrated *in vitro* are strongly bound (B1-box) or not bound at all (B3-box) by the
529 LARP6C La-module (Figure 6). We inserted the modified 5'-UTR sequences
530 downstream of the CaMV35S promoter and fused to coding sequence of YFP (*B1-YFP*
531 and *B3-YFP*) in a plant binary vector (Figure 8A). These YFP-containing plasmids were
532 transiently expressed in *Nicotiana benthamiana* leaves individually or co-infiltrated with
533 a plant binary vector expressing a tRFP-tagged LARP6C also under the control of the
534 CaMV35S promoter. Three days post infiltration, leaves were collected and YFP
535 mRNA and protein levels assessed (Figure 8B and C). Quantitative analyses showed

536 that when the LARP6C protein was present, *B1-YFP* transcript levels increased by
537 two-fold (Figure 8B). Conversely, co-expression of LARP6C with the *B3-YFP* construct
538 did not significantly affect *B3-YFP* mRNA levels (Figure 8B). Remarkably, the presence
539 of LARP6C significantly reduced YFP protein accumulation when expressed from the
540 B1 but not the B3 construct (Figure 8C). We also monitored the subcellular distribution
541 of the tRFP-LARP6C fusion protein following agroinfiltration. Similar to findings for
542 mature pollen grains (Figure 2) and onion epidermis cells following stress exposure,
543 LARP6C formed foci in the cytoplasm of *N. benthamiana* leaves (Figure 8D). Since in
544 pollen grains and onion epidermis cells, LARP6C foci contained the poly(A) binding
545 protein, we reason that LARP6C also likely aggregates into mRNP granules in *N.*
546 *benthamiana*.

547

548 **LARP6C controls native MGD2 protein levels and distribution in pollen tubes**

549 We next asked whether LARP6C controls the mRNA and proteins levels of their target
550 genes using *MGD2* mRNA as an example. We cloned the *MGD2* genomic locus
551 (starting at position - 579 from ATG) including its native B-box motif in fusion with the
552 YFP coding region that we placed at the C-terminus and transformed this chimeric
553 gene into the wild-type background. We then screened pollen and pollen tubes from
554 22 primary transformants and selected line 6, which we crossed to *larp6c-3*
555 homozygous plants. In the F2 generation, we selected plant homozygous for the
556 *larp6c-3* allele that expressed heterozygous *MGD2-YFP*. We then performed
557 microscopic observations of wild type and *larp6c-3* pollen that was heterozygous for
558 the *MGD2-YFP* transgene. Pollen grains were placed on *in vitro* pollen germination
559 agarose pad medium and YFP signals monitored in mature pollen grain (dry pollen),
560 pollen at 15 and 30 minutes after hydration (Figure 9A), and pollen tubes at the 4 hour
561 time point (Figure 9B). Strikingly, both in wild type and *larp6c-3*, mature pollen grains
562 show very low levels of YFP signal, which intensified over time upon hydration and in
563 pollen tubes.

564 To confirm this finding and to assess the role of LARP6C in MGD2 protein
565 accumulation, we quantified fluorescence intensity in dry pollen and at 1h and 4h after
566 activation. As shown in Figure 9C, MGD2-YFP levels drastically increased in pollen
567 tubes 1h after activation in both the wild type and mutant. Nonetheless, compared to
568 wild type, *larp6c-3* dry pollen showed higher levels of fluorescence, a situation opposite
569 that observed in 1h pollen tubes, which showed reduced MGD2-YFP signals in the

570 absence of LARP6C. Using specific antibodies (Awai et al., 2001), we made similar
571 observations for endogenous MGD2 accumulation, finding significantly more protein in
572 pollen tubes than in dry pollen. Moreover, the loss of LARP6C function induced
573 overaccumulation of MGD2 in mature pollen and underaccumulation in pollen tubes
574 compared to wild type (Figure 9C right panel). Next, RT-qPCR assays revealed that
575 the mRNA levels of *MGD2-YFP* and endogenous *MGD2* did not significantly vary
576 before and after pollen hydration and that loss-of-function of LARP6C did not affect
577 mRNA levels (Figure 9D). This is consistent with previously published transcriptomic
578 data showing that endogenous *MGD2* mRNA levels did not significantly vary between
579 dry pollen and pollen tubes after 30 min or at 4h activation *in vitro* (Qin et al., 2009).

580 Beyond an impact on protein levels, the loss of LARP6C function also appeared
581 to affect MGD2-YFP distribution along the pollen tube (Figure 9B). In wild type, MGD2-
582 YFP signal showed a diffuse cytosolic pattern, with the signal intensity distributed along
583 a gradient decreasing from the shank toward the tip in almost 94% (n = 124) of the
584 pollen tubes. In the absence of LARP6C, the gradient distribution of MGD2-YFP was
585 lost in 59% (n = 109) of the observed pollen tubes, which showed a uniform distribution
586 of the signal that also reached the pollen tube tip.

587

588 **DISCUSSION**

589 We report here that LARP6C, an evolutionarily conserved RNA-binding protein, is
590 essential for male fertility, acting during gametogenesis and germination and especially
591 during the progamic phase, during which it is necessary for the directional growth of
592 pollen tubes.

593

594 **The role of LARP6C in vesicular trafficking during male fertilization**

595 The anisotropic growth of the pollen tube, which takes place exclusively at the apical
596 dome, requires vast amounts of secretory vesicles delivered at the tip via cytoplasmic
597 streaming. Golgi-derived secretory vesicles supply cell wall material as well as material
598 for plasma membrane extension at the site of growth. Vesicles also deliver
599 transmembrane proteins, such as receptor kinases, which are inserted into the apical
600 plasma membrane through exocytosis (Grebnev et al., 2017). Indeed, the exocyst
601 secretory complex was found to be essential for the specification of plasma membrane
602 nanodomains that define sites for the directional growth of pollen tubes (Li et al., 2010;
603 Synek et al., 2017, 2006; Vukašinović and Žárský, 2016). We found that *larp6c*-pollen

604 tubes are hypersensitive to Brefeldin-A and identified several transcripts encoding
605 components of the vesicular system as LARP6C mRNA clients, including factors
606 involved in the trafficking of ER vesicles, constituents of the vacuolar trafficking system
607 HOPS (Takemoto et al., 2018), components and regulators of the ESCRT (Endosomal
608 Sorting Complex Required for Transport) (Reyes et al., 2014), and a subunit of the
609 exocyst complex (Supplemental Data Set S1). We hence propose that the pollen tube
610 guidance defects of *larp6c* mutants are in part the consequence of abnormal vesicular
611 trafficking.

612

613 **LARP6C is necessary for lipid homeostasis during male fertilization**

614 To optimize polar tip growth, pollen has evolved a unique lipid composition. In
615 particular, pollen grains produce extra-plastidial glycerolipids and store fatty acids and
616 TAGs in LDs (Ischebeck, 2016). LDs are necessary for gametogenesis, pollen grain
617 maturation, viability, and germination. They also might be required for pollen tube
618 guided growth, as supported by the finding that MPK6 is a regulator of their synthesis
619 involved in pollen tube guidance (Zhang et al., 2009; Zheng et al., 2018). The exact
620 role of LDs in pollen tubes is not currently clear, but it has been proposed that TAGs
621 could be synthesized in the shank of the pollen tube and transported to the tip in the
622 form of LDs to deliver membrane components (Ischebeck, 2016). In line with this idea,
623 we report that LDs are distributed from shank to tip in wild-type pollen tubes (Figure
624 4). Hence, the role of LARP6C in pollen tube guidance could also involve maintaining
625 adequate LD levels, distribution, and possibly composition, as it can specifically bind
626 mRNAs encoding fatty acid, TAG, phospho-, and glycerolipid synthases (FAD2, ACX4,
627 TAG1, LPEAT2, MGD2) for lipases such as SDP1, which is involved in storage lipid
628 breakdown (Kelly et al., 2013), and for regulators of their synthesis, such as DYRKP-
629 2A (Schulz-Raffelt et al., 2016) and MPK6 kinases (Zheng et al., 2018).

630 MGD2 is one of the three Arabidopsis synthases that catalyse the last step of
631 MGDG synthesis. Consistent with the finding that galactolipids are unique and major
632 constituents of plastid membranes, MGD1 and MGD3 were previously found to localize
633 inside chloroplasts and at the periphery of plastids, respectively, which are consistent
634 with a protein embedded in the outer envelope membrane. The subcellular distribution
635 of MGD2 was more difficult to interpret than that of its two counterparts, as it was
636 detected in the cytosol (Awai et al., 2001). Here, in the absence of any plastid, we also
637 report that MGD2 is present in the cytosol of the pollen tube and that it is distributed

638 from shank to tip along a decreasing gradient that is lost in the absence of LARP6C.
639 These observations uncover an unsuspected role for cytosolic MGD2, which could
640 have the ability to produce MGDG outside plastids and possibly transport its substrate
641 DAG to the site of MGDG synthesis. Since MGDG is the substrate for DGDG, which
642 was detected at the periphery of pollen tubes (Botté et al., 2011), MGD2 could
643 participate to pollen tube membrane expansion. Alternatively, as DAG is also a
644 substrate for TAG production, MGD2 may also transport this substrate to the sites of
645 LD production and therefore participate to the guidance process. The changes in
646 MGD2 protein levels and distribution along pollen tubes could hence be another reason
647 for the observed guidance defect of the *larp6c* mutants.

648 On top of vesicular trafficking and lipid dynamics, LARP6C likely controls other
649 cellular processes required for the directed growth of pollen tubes. Indeed, several
650 LARP6C targets encode actors in processes involved in pollen tube elongation and
651 guidance, such as signalling factors and kinases, cell wall modification players, or ion
652 transporters. Moreover, some LARP6C clients were experimentally found to be
653 involved in anisotropic cell elongation. These include, the transcription factor TFIIIB1,
654 which controls guided pollen tube growth (Zhou et al., 2013); TUB4, a structural
655 microtubule component required for normal hypocotyl guidance and elongation (Yu et
656 al., 2015); or the α/β hydrolase-domain protein WAV2, which is involved in directional
657 root growth (Mochizuki et al., 2005) (Supplemental Data Set S1).

658

659 **Molecular functions of LARP6C during male fertilization**

660 LARP6C is an RNA-binding protein that physically interacts with PABP, a master
661 regulator of mRNA translation and decay (Merret et al., 2013b). Here we demonstrated
662 that LARP6C at least in part co-localizes with PABP in mature pollen grain.
663 Furthermore, a LARP6C protein deficient in its RNA-binding domain (La-module) was
664 unable to restore LARP6C's function in pollen tube guidance. We hence propose that
665 LARP6C acts at the molecular level to control gene expression by regulating mRNA
666 fate in the cytoplasm.

667 We provided strong evidence that LARP6C directly interacts with mRNAs
668 harbouring B-boxes of the B1 or B2 type in their 5'-UTRs (*i.e.* at least 52 of the 115
669 transcripts identified by RIP-seq (Supplemental Data Set S1)). For some transcripts,
670 only A-boxes were identified in the 5'-UTR. This might have occurred because we were
671 only able to retrieve a partial 5'-UTR sequence, and inadvertently missed sequence

672 regions that could contain the B-box, but it is also possible that some LARP6C RIP
673 targets are in complex with this RBP but not through direct binding.

674 In *N. benthamiana* leaf epidermis, LARP6C appeared to control the levels of its
675 mRNA targets as well as the amount of the corresponding translated proteins. LARP6C
676 promoted the overaccumulation of *YFP* mRNA that carried its recognition sequence,
677 specifically a B1 type B-box motif (Figure 6). We propose that at least in somatic cells,
678 this overaccumulation is the result of LARP6C-mediated protection from cytoplasmic
679 decay, rather than an action at the transcriptional level. Surprisingly, our results also
680 show that this increase in mRNA levels is associated with a decrease in the
681 corresponding YFP protein levels (Figure 8). This suggests that LARP6C could, while
682 protecting its mRNA targets, dampen their translation. Alternatively, LARP6C could
683 control protein stability, but since it is unlikely to interact with the reporter YFP protein
684 (the only protein encoded by the reporter gene we designed), we deem this hypothesis
685 unlikely. In eukaryotic cells, one common feature of mRNP granules is that they contain
686 translationally silent mRNAs that are capable of (re)-entering translation in response
687 to the appropriate signals and protect these mRNAs from decay (Buchan, 2014).
688 Hence, the presence of LARP6C in foci that we propose are mRNP storage granules
689 also rather favours the first hypothesis.

690 The mRNA stabilization effect of LARP6C binding observed in transient *N.*
691 *benthamiana* assays is in contrast with the observation that in pollen grains, LARP6C
692 does not seem to control its targets' steady-state levels. In pollen, as in animal
693 gametes, mRNAs are highly stable, suggesting that in the male gametophyte, the
694 mRNA decay machineries, as well as the translational apparatus, have poor activity
695 (Ylstra and McCormick, 1999; Hafidh et al., 2018). This assumption is consistent with
696 our observation that DCP1, a core constituent of the mRNA decapping complex,
697 localises to foci in mature pollen grains and that this localisation is thought to be linked
698 to quenched DCP1 activities. Indeed, work conducted in animal cells proposed that
699 when components of the mRNA decay machineries are present in p-bodies, they are
700 catalytically inactive (Hubstenberger et al., 2017). The discrepancies between the
701 results from transient assays in *N. benthamiana* leaf cells and RNA-seq of pollen
702 grains could hence be the consequence of differences in how the mRNA decay
703 complex operates between sporophytic and reproductive cells.

704 *In vivo*, we propose that LARP6C plays a dual role in controlling of the levels of
705 translated proteins encoded by its targets' transcripts. Using *MGD2* mRNA as a model,

706 we indeed showed that whilst antagonizing MGD2 protein accumulation in mature
707 pollen grains, LARP6C promotes its translation after germination without affecting
708 *MGD2* mRNA levels (Figure 9). Although the possibility that LARP6C regulates the
709 amount of MGD2 protein post-translationally cannot be ruled out at this stage, we
710 believe that it is unlikely, as discussed for the YFP reporter protein. This implies that
711 LARP6C shifts from a repressor to an activator role in translation. This could be the
712 result of a differential pattern of post-translation modifications that might allow LARP6C
713 to recruit different sets of accessory proteins to its target mRNAs before and after
714 pollen hydration, resulting in a mode switch from repression to activation.

715 In 2017, Scarpin *et al.* reported that like *MGD2* mRNA, *SK14* mRNA is
716 translationally silent in mature pollen grain and reactivated at germination. They also
717 found that *SK14* mRNA aggregates in sub-cytoplasmic bodies that also contain the p-
718 body component DCP1 (Scarpin *et al.*, 2017). Here, we also demonstrated the
719 existence of foci in mature pollen grain containing proteins that function in mRNA
720 regulation (LARP6C and PAB5), which we believe also contain mRNAs. mRNP
721 granules exist in most eukaryotes and in many cell types and are of different types
722 based on their protein content. However, a common feature is that they store and
723 protect translationally silent mRNPs until their protein product is needed. We therefore
724 propose that a large portion of mRNAs whose expression is necessary for male
725 fertilization are stored in mature pollen grains in the form of mRNP aggregates until
726 their protein products are required during the progamic phase, as supported by
727 previous findings (Hafidh *et al.*, 2018), and that LARP6C is one of the *trans*-acting
728 factors that orchestrate this process (see Supplemental Figure S9 for a summary
729 model).

730 An intriguing observation from the current study is that LARP6C appears to be
731 required for the distribution of the protein encoded by one of its client mRNAs, *MGD2*,
732 along the pollen tube. We presently have no conclusive proof that LARP6C does not
733 act at the protein level to participate in this gradient distribution. Nonetheless,
734 considering that LARP6C is an mRNA-binding protein, we hypothesize that the
735 defective distribution of MGD2 in *larp6c* is the consequence of the aberrant regulation
736 of its mRNA. We propose that LARP6C transports the translationally silent mRNAs
737 present in mRNP granules to the appropriate cytoplasmic location where the protein is
738 then translated and required. The existence of such localized translation events
739 following the transport of silent mRNAs is a conserved and widespread feature of

740 eukaryotes, including plants, where few examples of mRNAs targeted to the surface
741 of the ER, chloroplasts, or mitochondria have been reported (Tian et al., 2020). In the
742 vast majority of cases, mRNAs are transported by cytoskeletal motors in the form of
743 silent mRNPs (Bullock, 2011; Eliscovich and Singer, 2017). Consistent with a possible
744 role in mRNA delivery, our data support the notion that LARP6C, in association with
745 mRNP granules, likely navigates along microtubules in growing pollen tubes.
746 Considering the phenotypes of *larp6c*-pollen, we propose that mRNA movement and
747 localized translation are necessary for the polarized growth of pollen tubes and hence
748 plant reproduction.

749

750 **The role of LARP6 proteins in mRNA control might be evolutionarily conserved**

751 Interestingly, a recent study by Dermit *et al.* demonstrated that human LARP6 acts in
752 migrating cells to navigate mRNAs encoding ribosomal proteins (RPs) along
753 microtubules to transport them from the cell body to protrusions; these cellular
754 migrating fronts act as translation hotspots. This function of human LARP6 in the
755 spatiotemporal control of RP mRNA translation is necessary for cell proliferation and
756 migration (Dermit et al., 2020). The physiological roles of zebrafish LARP6 differ from
757 that of *Arabidopsis* LARP6C, as it participates in oocyte development, chorion
758 formation, and egg activation whilst it is not involved in male fertilization. Nevertheless,
759 the authors suggest that zebrafish LARP6 could function in chorion formation by
760 regulating mRNA metabolism in microvilli, i.e., fine cell protrusions extending from both
761 the developing oocytes and granulosa cells (Hau et al., 2020). It is interesting that
762 LARP6 proteins, which are highly conserved eukaryotic RBPs, seem to have acquired
763 distinct physiological roles during eukaryote evolution but could have retained their
764 molecular mode of action in mRNA transport and translational control.

765

766 **METHODS**

767

768 **Plant material and growth conditions**

769 *Arabidopsis thaliana* ecotype Columbia-0 (Col-0) was used as the wild-type reference.
770 The *larp6c-3* (SAIL_268E02) (McElver et al., 2001) and *larp6c-4* (WiscDsLox293-
771 296invG4) (Woody et al., 2007) lines were respectively ordered from the NASC and
772 ABRC stock centres. Genotyping primers are shown in Supplemental Data Set S3.
773 Stable transgenic lines were obtained using the *Agrobacterium tumefaciens*-based

774 floral dip technique (Clough and Bent, 1998). For *in vitro* culture, surface sterilized
775 seeds were sown on synthetic Murashige & Skoog (MS) medium at 2.20 g/L (1/2 MS)
776 with 0.8% agar and stored for 48 h at 4°C in the dark before being grown under
777 continuous light (50-60 $\mu\text{E}\cdot\text{m}^{-2}\cdot\text{s}^{-1}$) at 20°C. Plants in soil cultures were grown in growth
778 chambers under a 16 h light (100 $\mu\text{E}\cdot\text{m}^{-2}\cdot\text{s}^{-1}$) / 8 h dark cycle at 20°C with approximately
779 75% humidity. See Supplemental Methods for growth conditions used to collect mature
780 pollen for RNA-seq and RIP-seq experiments.

781

782 **Cloning and plasmids**

783 All LARP6C-containing fusion proteins (YFP, TagRFP, and FLAGHA) were expressed
784 under the control of the upstream genomic sequences (spanning region -1181 to -1
785 from ATG) of the *LARP6C* gene (*AT3G19090* locus). To obtain the LARP6C-tRFP and
786 LARP6C-FLAGHA fusions, we isolated total genomic DNA from Col-0 and PCR
787 amplified the *LARP6C* genomic region starting from nucleotide -1181 from the ATG to
788 the last nucleotide before the stop codon using primers 543 and 544 (Supplemental
789 Data Set S3). The PCR product was inserted at sites *KpnI* and *NheI* upstream of either
790 the tagRFP or FLAG-HA tag into a pCAMBIA1300-based plant binary vector
791 expressing the *HPTII* (hygromycin) resistance gene, giving rise to vectors pEB16 and
792 pEB13. To obtain the YFP-LARP6C expressing binary vector, the genomic region
793 spanning nucleotides -1181 to -1 from the ATG of the *LARP6C* gene was PCR
794 amplified with primers 974 and 975 from vector pEB13 and cloned at sites *SacI* and
795 *KpnI* upstream of a Gateway entry cassette into a pPZP221 (Hajdukiewicz et al., 1994)
796 based plant binary vector carrying the *AAC1* (gentamycin) resistance gene, giving rise
797 to vector p788. The *LARP6C* coding genomic region was PCR amplified from total
798 genomic DNA with primers 976-977 and cloned at sites *SpeI-EcoRV* downstream of
799 the YFP tag located between the AttL1 and L2 Gateway donor sites, giving rise to
800 plasmid p793. The plant binary vector p795 was obtained through a Gateway cloning
801 reaction between p788 and 793. The *PAB5* genomic sequence (-1966 from the ATG
802 to the last nucleotide before the stop codon) was PCR amplified from total genomic
803 DNA with primers eb3 and eb4 and cloned using the restriction endonucleases *XbaI*
804 and *BamHI* into vector CTL579 (pCAMBIA-1300) upstream of the GFP tag, giving rise
805 to plasmid pEB3. To prepare transgenic lines expressing the YFP-LARP6C Δ LAM
806 protein, we transformed *larp6c-3* or *larp6c-4* plants with plasmid p844. The

807 *LARP6C*Δ*LAM* CDS codes for a LARP6C protein deleted of the region spanning amino
808 acids 137-227 and was obtained as follow. We PCR amplified the regions of the coding
809 sequence from +1 to + 411 from ATG (primers 1197 and 1198) with primer 1198, which
810 also adds a 3'-tail extension of 20 nt complementary to region 684-704 of the CDS
811 (located just downstream to the LAM). A second PCR product was generated with
812 primers 1199-1200, starting from position 684 to the stop codon. To fuse both products,
813 we ran a third PCR amplification with primers 1201-1200 and an equimolar mixture of
814 products 1 and 2 as a matrix. The resulting fragment corresponds to the full-length
815 *LARP6C* CDS deleted of its LAM and carrying *Xba*I and *Eco*RV restriction sites at its
816 5' and 3' ends, respectively. This fragment was inserted downstream of the *YFP*
817 sequence into a Gateway donor vector through enzymatic restriction and ligation
818 (p843). The *YFP-LARP6C*Δ*LAM* fusion construct was transferred into a plant binary
819 vector under the control of the *LARP6C* native promoter through Gateway cloning
820 between p843 and p788 (p844).

821 The binary vector pGEX2-GEX2GFP was obtained from (Mori et al., 2014).
822 Binary plasmids for transient assays were prepared as follow. DNA fragments
823 encompassing a basal CaMV35S promoter without enhancer sequences (Töpfer et al.,
824 1987), modified *MGD2* 5'-UTRs, and the *YFP* CDS were ordered from GeneCust
825 (<http://www.genecust.com/fr>) and subcloned into a Gateway donor vector. DNA
826 cassettes were then introduced into a plant binary vector containing the *HPTII*
827 (hygromycin) resistance gene (vector CTL575, a derivative of pCAMBIA-1300). The
828 *LARP6C* coding sequence was fused downstream of the tagRFP fluorescent reporter
829 and placed under the control of a strong CaMV35S promoter by Gateway
830 recombination with the plant binary entry vector p-SITE-6C1 (Martin et al., 2009).

831 To prepare a translational *MGD2*-*YFP* fusion, we amplified the *MGD2* genomic
832 region starting from nucleotide -579 from the ATG to the last nucleotide before the stop
833 codon using primers 31 and 32 (Supplemental Data Set S3). The complete PCR
834 product was cloned into pDONR221 via the TOPOisomerase cloning technique to
835 generate entry vector pDONR221-*MGD2*no-stop. To generate the plant expression
836 vector, LR Clonase was used to recombine pDONR221-*MGD2*no-stop into the
837 pB7FWG,0 Gateway binary vector in frame with C-terminal *YFP*. Primary
838 transformants were selected using BASTA selection.

839

840 **Pollen phenotyping**

841 Pollen transmission tests were conducted through hand pollination of wild-type pistils
842 with pollen from mutant and complemented homozygous plants. The number of off-
843 spring carrying the mutation was scored either by PCR-based genotyping or by
844 selection of antibiotic/herbicide-resistant seedlings. The number of mutant seedlings
845 was expressed as a percentage over the total number of seedlings and transmission
846 efficiency of the mutant gametophyte calculated as $TE = ((No\ of\ mutant /$
847 $No\ of\ WT) \times 100)$. Experiments were conducted in triplicate. Pollen tube guidance
848 efficiency was scored either by semi *in vivo* (Palanivelu and Preuss, 2006) or *in vivo*
849 assays by observing pistils hand pollinated with the mutant pollen of interest and
850 stained with aniline blue (Mori et al., 2006). Emasculated pistils were from *ms1* (male
851 sterility 1) heterozygous plants. This guaranteed that the pistils were not contaminated
852 with wild-type pollen, as the *ms1-1* mutant is male sterile (van der Veen and Wirtz,
853 1968; Ito et al., 2007). Monitoring of pollen tube guidance in the presence of galvestine-
854 1 was conducted through semi *in vivo* assays on plates containing 1% DMSO for mock
855 treatment or 5 or 10 μ M of galvestine-1 with a final concentration of 1% DMSO. For all
856 pollen tube guidance assays, *in vivo* aniline blue staining and semi *in vivo* as well as
857 *in vivo* blue dot assays were performed according to (Kulichová et al., 2020).

858

859 **Pollen and pollen tube collection for total RNA and protein extraction**

860 Approximately 250 μ L equivalent of open flowers were collected in 1.5 mL Eppendorf
861 tubes for each respective genotype. To collect mature pollen, flowers were vigorously
862 and briefly vortexed with 500 μ L of RIPA extraction buffer for protein extraction or with
863 pollen germination medium for RNA extraction and spun in a benchtop centrifuge for
864 1 minute. Media were removed and pellets stored at -80°C until extraction. For pollen
865 activation/germination, the pollen pellet was resuspended in liquid pollen germination
866 medium and incubated for 1h at 22°C . One biological replicate corresponds to one
867 sample of 250 μ L equivalent of open flowers.

868

869 **Microscopy**

870 Subcellular localization experiments in pollen grain and pollen tubes were conducted
871 with an LSM700 confocal microscope (Zeiss) using emission/excitation wavelengths:
872 405 nM / 420-480 nM for DAPI, 555 nM / 600-700 nM for tRFP and 488 nM / 490-555
873 nM for YFP and GFP. Mature pollen grains were collected by dipping open flowers into

874 a drop of DAPI solution (1X PBS pH 7, 0.5% Triton-X100, 1 μ g/mL 4',6-diamino-2-
875 phenylindole) on a glass slide. To collect immature pollen grains at the microspore, bi-
876 and tricellular stages, anthers were collected from unopened buds, placed in a drop of
877 DAPI solution on a glass slide, and gently crushed to free the pollen grains from pollen
878 sacs. Pollen tubes germinated and grown as described in the Supplemental Methods
879 were directly observed from the germination slide. For cytoskeleton co-localization,
880 PRO_{LARP6C}-tRFP:LARP6C was co-infiltrated in *Nicotiana benthamiana* leaves with
881 either p35S:GFP-AtTUB6, p35S:GFP-FABD2, or pUBQ-LifeAct:GFP. Confocal
882 images were taken under a Nikon Eclipse Ti confocal microscope equipped with a
883 CSU-X1 spinning disk module and Andor iXon3 EMCCD camera, as well as with a
884 Zeiss LSM880 confocal microscope, and captured with ZEN 2.3v software. Images
885 were analyzed and assembled with ImageJ/ Fiji (<http://imagej.net/http://fiji.sc/Fiji>),
886 Adobe Photoshop CS6 (www.adobe.com), Ink-scape (www.inkscape.org), and NIS
887 Elements (LIM) software. For YFP quantification in pollen tubes, MGD2-YFP signals
888 in the respective genotypes were captured under a Zeiss LSM880 confocal microscope
889 using an Argon 488 laser and detected with GasP detector with fixed configurations.
890 Zen (blue edition) software was used to quantify pixel intensity, and data were
891 processed in Excel.

892

893 **Pharmacological treatment**

894 For the galvestine-1 inhibition assay, pollen tubes were grown on solid pollen
895 germination medium containing 1% DMSO for mock treatment or 5 or 10 μ M of
896 galvestine-1 at a final concentration of 1% DMSO. For Brefeldin A treatment,
897 Arabidopsis pollen tubes were grown for 1h *in vitro* and stained by incubating with 1
898 μ M FM4-64 (Thermo Fisher Scientific, <https://www.thermofisher.com>) concomitantly
899 with Brefeldin A at 25 μ M (BFA, Sigma, www.sigmaaldrich.com, BFA stock solution at
900 50 mM in DMSO) in liquid pollen germination medium for 5 and 10 min. To visualize
901 lipid droplets, Bodipy stain (505/515) at a final concentration of 2 μ M and Nile red stain
902 (552/636) at a final concentration of (0.1 μ g/mL) were simultaneously added to
903 germinated pollen tubes and incubated for 3 min prior to imaging.

904

905 **Total RNA extraction and RT-qPCR**

906 For RNA-sequencing purpose, total RNA was purified from mature pollen grain as
907 follow. 0.5 to 3 mg of dry pollen was ground with a Silamat S6 mixing device (Ivolcar
908 Vivadent, Schaan, Liechtenstein) in 500 μ L of GuHCl buffer (8 M GuHCl, 20 mM MES,
909 20 mM EDTA, at pH 7, 50 mM β -mercaptoethanol) and with 5 glass beads. Following
910 1 min vortexing at full speed and 10 min incubation on ice, RNAs were separated from
911 proteins via two consecutive phenol-chloroform-IsoAmylAlcool (IAA) (25:24:1)
912 extractions, followed by one extraction with chloroform-IAA (24:1), consisting of 1 min
913 vortexing at full speed and 10 min centrifugation at 16°C, 14,000 g. RNAs are then
914 precipitated in the presence of 0.7 vol isopropanol, 1/20th CH₃COOH at 1 M for 20 min
915 at -20°C. Following 20 min centrifugation at 4°C, 14,000 g, the RNA pellet was washed
916 in 90% EtOH and resuspended in RNase free water. The average efficiency of pollen
917 RNA extraction was 5-6 μ g of RNA per mg of dry pollen. To measure *MGD2* (*YFP-*
918 *MGD2* and endogenous *MGD2*) mRNA levels, total RNA was extracted from 5 mg of
919 dry pollen and 250 μ l equivalent of flowers used to grow pollen tubes for 4h *in vitro*
920 from (*MGD2-YFP; LARP6C*) and (*MGD2-YFP; larp6c-3*) homozygous lines. One
921 biological replicate corresponds to 5 mg of dry pollen and 250 μ L equivalent flowers
922 for pollen tubes. A total of three biological and six technical replicates were generated.
923 *MGD2* native primers and *TUB8* were used for measurement and normalization,
924 respectively. Relative expression was computed as above.

925 To quantify *YFP* mRNA levels in *N. benthamiana* transient assays, total RNA
926 was isolated from the samples using a Monarch Total RNA Miniprep Kit (New England
927 Biolabs), and genomic DNA was eliminated using gDNA removal columns and on-
928 column DNaseI-treated (New England Biolabs). 5 μ g of total RNA was reverse
929 transcribed with a SuperScript IV kit (Life Technology) using an oligodT₁₈ primer. qPCR
930 was conducted on a LightCycler 480 Multiwell Plates 384-well themocycler (Roche
931 Applied Sciences) with the following amplification program: 5 min 95°C, 40 cycles of
932 15 s at 95°C, and 1 min at 60°C. After amplification, melting curve analysis was
933 performed with a temperature gradient of 0.1°C/s from 60°C to 95°C. The PCR mixture
934 contained Takyon qPCR master mix (Eurogentec), 500 nM gene-specific primers, and
935 1 μ L cDNA in a total reaction volume of 10 μ L. Primer efficiencies were determined
936 using standard curves, with 10-fold serial dilution series ranging from 1 \times 10¹ to
937 1 \times 10⁶ of the cDNA samples. Relative quantification was performed by the $\Delta\Delta C_T$
938 method (Livak and Schmittgen, 2001), with *YFP* and *HPTII* used as the target and

939 reference gene, respectively. The sequences of the primers used for RT- and qPCR
940 are shown in Supplemental Table S2.

941

942 **RNA-seq, RIP-seq, bioinformatics**

943 Techniques related to large scale analyses (RNA-seq and RIP-seq), as well as the
944 bioinformatic analyses, are detailed in the Supplemental Methods.

945

946 **Protein-related techniques**

947 Total protein extracts were separated by SDS PAGE on an acrylamide gel before being
948 electrotransferred onto a PVDF membrane (0.45 μ M, Merck Millipore). After saturation
949 in a (1X TBS - 0.1% tween - 5% fat-free dry milk) solution, the membranes were
950 incubated with the appropriate primary then secondary antibodies, washed three times
951 with a 1X TBS - 0.1% Tween solution, and chemiluminescence revealed with an EMD
952 Millipore Immobilon Western Chemiluminescent HRP Substrate kit. Antibodies against
953 the LARP6C protein were custom made (at Agro-Bio, La Ferté St Aubin, France)
954 through immunization of rabbits with the peptide "KRTSQFTDRDREELGQ" (amino
955 acids 220-235). Anti-LARP6C antibodies are utilized at 1/1000 dilution in a (1X TBS -
956 0.1% Tween - 5% fat-free dry milk) solution and incubated overnight at 4°C with gentle
957 shaking. Secondary antibodies were anti-rabbit HRP (Bio-Rad) and used at a 1/5,000
958 dilution. Anti-ACTIN antibodies were from Affinity Bio Reagents (Golden, CO, USA)
959 and used at 1/15,000 dilution. Secondary antibodies were anti-mouse HRP (Bio-Rad)
960 used at a 1/10,000 dilution. For transient assays, the YFP protein was detected using
961 the GFP antibody (Clontech) at 1/5,000 and the UGPase antibody (Agrisera) at 1/7,500
962 dilution, both incubated overnight at 4°C. Secondary antibodies anti-mouse HRP (Bio-
963 Rad) used at a 1/2,000 dilution and anti-rabbit HRP (Bio-Rad) used at a 1/5,000 dilution
964 were incubated for YFP and UGPase detection, respectively, for 1h at room
965 temperature. To detect endogenous MGD2, proteins were extracted from 5 mg of dry
966 pollen and 250 μ l equivalent of flowers used to germinate pollen tubes *in vitro* for 1h
967 or 4h from (MGD2-YFP; LARP6C) and (MGD2-YFP; *larp6c-3*) homozygous lines. One
968 biological replicate corresponds to 5 mg of pollen grain, and 250 μ L equivalent open
969 flowers for pollen tubes. A total of three replicates for dry pollen and 1h activated pollen,
970 and two replicates for 4h pollen tubes were generated. After SDS-PAGE separation,
971 membrane blocking was performed with 5% milk for 30 min at room temperature. The

972 membrane was incubated with antibodies against MGD2 (a gift from Eric Maréchal
973 (LPCV, Grenoble) (Awai et al., 2001), at 1/500 dilution, overnight at 4°C. Secondary
974 anti-Rabbit HRP (Agrisera) was used at 1/10,000 dilution and incubated for 1h at room
975 temperature prior to membrane development.

976 For RNA-protein binding *in vitro* assays, the LARP6C La-module (amino acids
977 137-223) was recombinantly expressed as in (Merret et al., 2013b). The hexahistidine
978 tag (His-tag) was removed by proteolysis via incubation at 4°C overnight with HRV 3C
979 Protease in a buffer containing 50 mM Tris-HCl pH 7.25, 100 mM KCl, 0.2 mM EDTA,
980 1 mM DTT, 10% glycerol. The cleaved His-Tag and the protease were separated from
981 the La-module through retention onto a Ni-NTA column. The protein was then
982 subjected to heparin column purification and dialysis in a final buffer as in (Merret et
983 al., 2013b).

984

985 **ITC and EMSA**

986 RNA oligos were custom made from IBA-Lifescience GmbH (Göttingen, Germany) at
987 a 1 μ Molar scale and HPLC purified. The lyophilized RNAs were resuspended in
988 RNase free water (DEPC treated) at concentrations ranging from 2.5 to 3 mM. The
989 ITC experiments were performed as in (Merret et al., 2013b) on an iTC200
990 microcalorimeter (Malvern). Here, 20 injections of 2 μ L RNA solutions at 200-320 μ M
991 concentration were added to protein solutions (LARP6C La-module) at 20-30 μ M with
992 a computer-controlled 40 μ L syringe. Control titrations of RNA into buffer alone and
993 into protein solution without the His-tag were performed. The heat per injection
994 normalized per mole of injectant versus molecular ratio was analyzed with the
995 MicroCal-Origin 7.0 software package and fitted using a nonlinear least-square
996 minimization algorithm using a theoretical single-site binding model. ΔH (reaction
997 enthalpy change in kcal/mol), K_b (binding constant equal to $1/K_d$), and n (molar ratio
998 between the two proteins in the complex) were the fitting parameters. The reaction
999 entropy was calculated using the equations $\Delta G = -RT \ln K_b$ ($R = 1.986$ cal/mol K; $T =$
1000 298 K) and $\Delta G = \Delta H - T\Delta S$. All ITC experiments were repeated at least three times,
1001 and a detailed analysis of the thermodynamic parameters and errors calculated as the
1002 standard deviation from the mean value are reported in Supplemental Table S1. For
1003 EMSA (Electrophoretic Mobility Shift Assay), RNAs were 5'-labelled with γ - 32 P-ATP
1004 using T4 polynucleotide kinase. Recombinant protein and RNA were mixed and

1005 incubated for 15 minutes at room temperature in 20 mM Tris pH 7.25, 200 mM KCl,
1006 5% of glycerol, 1 mM DTT, 0.1 mg/mL of BSA and 0.7 units of RNase inhibitors
1007 (RNaseOUT, Invitrogen). Each reaction mixture (22 μ L) contained 3 nM of labelled
1008 RNA oligo and varying amounts of LARP6C La-module (3-fold serial dilutions from an
1009 88 μ M sample). The experiments were performed in the absence or presence of
1010 unlabelled mixed tRNAs from *E. coli* MRE 600 (0.01 mg/mL). After the addition of 2 μ L
1011 of 30% Ficoll, the samples were loaded on a 9% native polyacrylamide gel prerun at
1012 100 mV for 1 hour at 4°C in 0.5x TBE (Tris-borate-EDTA buffer). A typical EMSA
1013 experiment was run at 4°C for 1 hour at 125 mV. Gels were dried onto 3MM
1014 chromatography paper, exposed to a phosphoimaging plate overnight, analysed on a
1015 Typhoon Trio phosphoimager, and quantified with Image Quant TL software. The
1016 fraction of bound RNA was plotted versus the protein concentrations. To determine the
1017 dissociation constants, the data were fitted with Origin 8.0 to a modified Hill equation
1018 (Ryder et al., 2008) using non-linear least squares methods and assuming a 1:1
1019 stoichiometry.

1020

1021 ***Nicotiana benthamiana* transient assays**

1022 Plasmids B1-YFP, B3-YFP and RFP-LARP6C were respectively transformed into
1023 *Agrobacterium tumefaciens* strain LB4404. Transformed bacteria were cultivated until
1024 they reached OD 0.8 and used to infiltrate fully expanded leaves from eight-week-old
1025 *N. benthamiana* plants using a needleless syringe as described in (Ruiz et al., 1998).
1026 When double transformations were performed (B1-YFP and RFP-LARP6C or B3-YFP
1027 and RFP-LARP6C), an equimolar mixture of *Agrobacterium* cultures (OD 0.4) was
1028 used for transformation. For each transformation, we also used an *Agrobacterium*
1029 culture carrying a plasmid (OD 0.2) allowing the expression of the P19 suppressor of
1030 RNA silencing (Lasierra and Prat, 2018). Three days post-infiltration (3 dpi),
1031 transformed leaf segments were collected, flash frozen, and total RNA or protein
1032 extracted. Alternatively, at 3 dpi transformed leaves were observed by confocal
1033 microscopy to monitor YFP and tRFP signals.

1034

1035 **Accession Numbers**

1036 Sequence data in this study can be found under the following accession numbers:
1037 Bioproject PRJNA557669. RNA-Seq-Col0-Rep 1: SRR9887494; RNA-Seq-Col0-Rep

1038 1: SRR9887493; RNA-Seq-*larp6c-3*-Rep 1; SRR9887496; RNA-Seq-*larp6c-3*-Rep 2
1039 SRR9887495; RIP-Col0-Input-Rep 1: SRR9887498; RIP-Col0-Eluate-Rep 1:
1040 SRR9887500; RIP-Col0-Input-Rep 2: SRR9887497; RIP-Col0-Eluate-Rep 2:
1041 SRR9887499; RIP-LARP6C-Input-Rep 1: SRR9887490; RIP-LARP6C-Eluate-Rep 1:
1042 SRR9887492; RIP-LARP6C-Input-Rep 2: SRR9887489; RIP-LARP6C-Eluate-Rep 2 :
1043 SRR9887491.

1044

1045 **Supplemental Data**

1046

1047 **Supplemental Figure S1:** Expression profiles of *LARP6A*, *6B* and *6C* mRNAs across
1048 development.

1049 **Supplemental Figure S2:** Pollen maturation, germination, and pollen tube growth of
1050 *larp6c* loss-of function mutants.

1051 **Supplemental Figure S3:** Schematic representation of *LARP6C* transgenes and
1052 immunoblotting analyses of their accumulation. Semi *in vivo* pollen tube guidance
1053 competition assays. Analysis of *LARP6A* function in male fertilization.

1054 **Supplemental Figure S4:** Pollen attraction competence of *larp6c-3* and *6c4* ovules.

1055 **Supplemental Figure S5:** Confocal analyses of *LARP6C*-tRFP and/ *LARP6A*-GFP in
1056 pollen.

1057 **Supplemental Figure S6:** Reproducibility of the RIP-seq data, RIP-seq filtering
1058 workflow, representation of the position of A and/or B boxes on the 5'-UTRs of *LARP6C*
1059 targets.

1060 **Supplemental Figure S7:** ITC and EMSA assessment of *LARP6C* La-module binding
1061 to A type oligos.

1062 **Supplemental Figure S8:** Reproducibility of the RNA-seq data.

1063 **Supplemental Figure S9:** Model of the molecular functions of *LARP6C* in male
1064 fertilization.

1065 **Supplemental Table S1:** Thermodynamic parameters of the calorimetric analyses
1066 shown in Figure 4B, 4D and Supplemental Figure 6A.

1067 **Supplemental Table S2:** List and sequences of primers used for q-PCR, genotyping
1068 and cloning.

1069 **Supplemental Methods**

1070 **Supplemental Data Set S1: Results of RIP-seq experiment.**

1071 **Supplemental Data Set S2: Results of RNA-Seq experiment.**

1072 **Supplemental Movie S1:** LARP6C foci move along microtubules.

1073

1074 **ACKNOWLEDGEMENTS**

1075 This work was supported by the CNRS, the University of Perpignan (UPVD), the Institut
1076 Universitaire de France (IUF) and the Bio-Environnement platform through utilization
1077 of the confocal microscope. This study is set within the framework of the "Laboratoires
1078 d'Excellence (LABEX)" TULIP (ANR-10-LABX-41). EB was the recipient of a PhD grant
1079 from the UPVD, Doctoral School ED305. CGL jr. is the recipient of a short-term contract
1080 supported by the ANR Heat-EpiRNA (ANR-17-CE20-007-01). SH, KK and DH are
1081 supported by GACR grant numbers 17-23203S and 18-02448S. SH is also supported
1082 by European Regional Development Fund-Project "Centre for Experimental Plant
1083 Biology" (No. CZ.02.1.01/0.0/0.0/16_019/0000738). ICG was supported by a Royal
1084 Society Newton International fellowship (ref. NF140482). IGC and MRC thank the
1085 Centre for Biomolecular Spectroscopy at King's College London funded by a capital
1086 award from the Wellcome Trust. We thank David Twell group (Leicester University) for
1087 sharing LAT52:H2B-GFP marker, Martin Potoský (Cell Biology, IEB Prague), Eva
1088 Kollárová and Fatima Cvrčková (Faculty of Science, Charles University, Prague) for
1089 the cytoskeleton constructs. The authors would like to thank Eric Maréchal (LPCV,
1090 Grenoble) for sharing MGD2 antibodies and galvestine-1, as well as for fruitful
1091 discussions on LARP6C targets' functions, in particular those involved in lipid biology.

1092 This work was funded by the CNRS, The University of Perpignan (UPVD), the
1093 Agence Nationale pour la Recherche (ANR) grant Heat-EpiRNA (n°: ANR-17-CE20-
1094 007-01); a Bonus Quality Research (BQR) funded by the University of Perpignan ; a
1095 Collaborative PICS Project (LARP&STRESS, n° 6170) funded by CNRS; Grantová
1096 agentura České republiky (GACR) grants (n°: 17-23203S and 18-02448S), European
1097 Regional Development Fund-Project "Centre for Experimental Plant Biology" (No.
1098 CZ.02.1.01/0.0/0.0/16_019/0000738) and the Royal Society Newton International
1099 fellowship (ref. NF140482).

1100

1101 **AUTHOR CONTRIBUTIONS**

1102 EB and SH performed experiments and analyzed the data. CP helped EB with confocal
1103 microscopy analyses. VJ helped EB with plant maintenance and reciprocal crossed. MCC
1104 performed RNA-seq and RIP-seq bioinformatics. VK and KK assisted SH with *in vitro* pollen
1105 tube assays and VK assisted SH with experiments presented in Figure 9. ICG and MRC

1106 designed and analyzed EMSA and ITCs; ICG performed the experiments. CGL Jr. ran
1107 experiments from Figure 8. EM contributed his knowledge on lipid metabolism and suggested
1108 a role for MGD2 as cargo for TAGs. CBA coordinated the work, designed the research,
1109 analyzed data and wrote the paper. JMD helped with data analysis. EB, SH, MRC, JMD and
1110 DH revised the manuscript.

1111

1112 REFERENCES

1113 **Ambrose, J.C. and Cyr, R.** (2007). The Kinesin ATK5 Functions in Early Spindle
1114 Assembly in Arabidopsis. *Plant Cell* **19**: 226–236.

1115 **Awai, K., Maréchal, E., Block, M.A., Brun, D., Masuda, T., Shimada, H., Takamiya,
1116 K., Ohta, H., and Joyard, J.** (2001). Two types of MGDG synthase genes, found
1117 widely in both 16:3 and 18:3 plants, differentially mediate galactolipid syntheses
1118 in photosynthetic and nonphotosynthetic tissues in *Arabidopsis thaliana*. *Proc.*
1119 *Natl. Acad. Sci. U. S. A.* **98**: 10960–5.

1120 **Belostotsky, D.A.** (2003). Unexpected complexity of poly(A)-binding protein gene
1121 families in flowering plants: three conserved lineages that are at least 200 million
1122 years old and possible auto- and cross-regulation. *Genetics* **163**: 311–9.

1123 **Belostotsky, D.A. and Meagher, R.B.** (1996). A pollen-, ovule-, and early embryo-
1124 specific poly(A) binding protein from *Arabidopsis* complements essential functions
1125 in yeast. *Plant Cell* **8**: 1261–75.

1126 **Botella, C., Sautron, E., Boudiere, L., Michaud, M., Dubots, E., Yamaryo-Botté, Y.,
1127 Albrieux, C., Marechal, E., Block, M.A., and Jouhet, J.** (2016). ALA10, a
1128 Phospholipid Flippase, Controls FAD2/FAD3 Desaturation of Phosphatidylcholine
1129 in the ER and Affects Chloroplast Lipid Composition in *Arabidopsis thaliana*. *Plant*
1130 *Physiol.* **170**: 1300–14.

1131 **Botté, C.Y. et al.** (2011). Chemical inhibitors of monogalactosyldiacylglycerol
1132 synthases in *Arabidopsis thaliana*. *Nat. Chem. Biol.* **7**: 834–842.

1133 **Bousquet-Antonelli, C. and Deragon, J.-M.** (2009). A comprehensive analysis of the
1134 La-motif protein superfamily. *RNA* **15**.

1135 **Brownfield, L., Hafidh, S., Borg, M., Sidorova, A., Mori, T., and Twell, D.** (2009). A
1136 plant germline-specific integrator of sperm specification and cell cycle
1137 progression. *PLoS Genet.* **5**: e1000430.

1138 **Buchan, J.R.** (2014). mRNP granules. Assembly, function, and connections with
1139 disease. *RNA Biol.* **11**: 1019–30.

1140 **Bullock, S.L.** (2011). Messengers, motors and mysteries: sorting of eukaryotic
1141 mRNAs by cytoskeletal transport. *Biochem. Soc. Trans.* **39**: 1161–5.

1142 **Cai, L., Fritz, D., Stefanovic, L., and Stefanovic, B.** (2010a). Binding of LARP6 to
1143 the conserved 5' stem-loop regulates translation of mRNAs encoding type I
1144 collagen. *J. Mol. Biol.* **395**: 309–26.

1145 **Cai, L., Fritz, D., Stefanovic, L., and Stefanovic, B.** (2010b). Nonmuscle myosin-
1146 dependent synthesis of type I collagen. *J. Mol. Biol.* **401**: 564–78.

1147 **Challa, A.A. and Stefanovic, B.** (2011). A novel role of vimentin filaments: binding
1148 and stabilization of collagen mRNAs. *Mol. Cell. Biol.* **31**: 3773–89.

1149 **Clough, S.J. and Bent, A.F.** (1998). Floral dip: a simplified method for *Agrobacterium*-
1150 mediated transformation of *Arabidopsis thaliana*. *Plant J.* **16**: 735–43.

1151 **Cvrčková, F. and Oulehlová, D.** (2017). A new kymogram-based method reveals
1152 unexpected effects of marker protein expression and spatial anisotropy of
1153 cytoskeletal dynamics in plant cell cortex. *Plant Methods* **13**: 19.

1154 **Dermit, M., Dodel, M., Lee, F.C.Y., Azman, M.S., Schwenzer, H., Jones, J.L.,**
1155 **Blagden, S.P., Ule, J., and Mardakheh, F.K.** (2020). Subcellular mRNA
1156 Localization Regulates Ribosome Biogenesis in Migrating Cells. *Dev. Cell* **55**:
1157 298-313.e10.

1158 **Eliscovich, C. and Singer, R.H.** (2017). RNP transport in cell biology: the long and
1159 winding road. *Curr. Opin. Cell Biol.* **45**: 38–46.

1160 **Feng, Q.-N., Liang, X., Li, S., and Zhang, Y.** (2018). The ADAPTOR PROTEIN-3
1161 Complex Mediates Pollen Tube Growth by Coordinating Vacuolar Targeting and
1162 Organization. *Plant Physiol.* **177**: 216–225.

1163 **Grebnev, G., Ntefidou, M., and Kost, B.** (2017). Secretion and Endocytosis in Pollen
1164 Tubes: Models of Tip Growth in the Spot Light. *Front. Plant Sci.* **8**: 154.

1165 **Hafidh, S., Potěšil, D., Fíla, J., Feciková, J., Čapková, V., Zdráhal, Z., and Honys,**
1166 **D.** (2014). In search of ligands and receptors of the pollen tube: the missing link
1167 in pollen tube perception. *Biochem. Soc. Trans.* **42**: 388–94.

1168 **Hafidh, S., Potěšil, D., Müller, K., Fíla, J., Michailidis, C., Herrmannová, A.,**
1169 **Feciková, J., Ischebeck, T., Valášek, L.S., Zdráhal, Z., and Honys, D.** (2018).
1170 Dynamics of the Pollen Sequestrome Defined by Subcellular Coupled Omics.
1171 *Plant Physiol.* **178**: 258–282.

1172 **Hajdukiewicz, P., Svab, Z., and Maliga, P.** (1994). The small, versatile pPZP family
1173 of *Agrobacterium* binary vectors for plant transformation. *Plant Mol. Biol.* **25**: 989–

1174 94.

1175 **Hau, H.T.A. et al.** (2020). Maternal *Larp6* controls oocyte development, chorion
1176 formation and elevation. *Development* **147**.

1177 **Hellman, L.M. and Fried, M.G.** (2007). Electrophoretic mobility shift assay (EMSA) for
1178 detecting protein–nucleic acid interactions. *Nat. Protoc.* **2**: 1849–1861.

1179 **Higashiyama, T. and Takeuchi, H.** (2015). The mechanism and key molecules
1180 involved in pollen tube guidance. *Annu. Rev. Plant Biol.* **66**: 393–413.

1181 **Honys, D., Combe, J.P., Twell, D., and Capková, V.** (2000). The translationally
1182 repressed pollen-specific *ntp303* mRNA is stored in non-polysomal mRNPs during
1183 pollen maturation. *Sex. Plant Reprod.* **13**: 135–144.

1184 **Honys, D. and Twell, D.** (2004). Transcriptome analysis of haploid male gametophyte
1185 development in *Arabidopsis*. *Genome Biol.* **5**: R85.

1186 **Hubstenberger, A. et al.** (2017). P-Body Purification Reveals the Condensation of
1187 Repressed mRNA Regulons. *Mol. Cell* **68**: 144-157.e5.

1188 **Ischebeck, T.** (2016). Lipids in pollen - They are different. *Biochim. Biophys. Acta*
1189 **1861**: 1315–1328.

1190 **Ito, T., Nagata, N., Yoshida, Y., Ohme-Takagi, M., Ma, H., and Shinozaki, K.** (2007).
1191 *Arabidopsis* MALE STERILITY1 Encodes a PHD-Type Transcription Factor and
1192 Regulates Pollen and Tapetum Development. *Plant Cell* **19**: 3549–3562.

1193 **Johnson, M.A. and Preuss, D.** (2002). Plotting a course: multiple signals guide pollen
1194 tubes to their targets. *Dev. Cell* **2**: 273–81.

1195 **Kelly, A.A., van Erp, H., Quettier, A.-L., Shaw, E., Menard, G., Kurup, S., and**
1196 **Eastmond, P.J.** (2013). The SUGAR-DEPENDENT1 Lipase Limits
1197 Triacylglycerol Accumulation in Vegetative Tissues of *Arabidopsis*. *PLANT*
1198 *Physiol.* **162**: 1282–1289.

1199 **Khan, B.R., Adham, A.R., and Zolman, B.K.** (2012). Peroxisomal Acyl-CoA oxidase
1200 4 activity differs between *Arabidopsis* accessions. *Plant Mol. Biol.* **78**: 45–58.

1201 **Klepikova, A. V, Logacheva, M.D., Dmitriev, S.E., and Penin, A.A.** (2015). RNA-
1202 seq analysis of an apical meristem time series reveals a critical point in
1203 *Arabidopsis thaliana* flower initiation. *BMC Genomics* **16**: 466.

1204 **Kulichová, K., Kumar, V., Steinbachová, L., Klodová, B., Timofejeva, L., Juříček,**
1205 **M., Honys, D., and Hafidh, S.S.** (2020). PRP8A and PRP8B spliceosome
1206 subunits act coordinately to control pollen tube attraction in *Arabidopsis thaliana*.
1207 *Development* **147**.

1208 **Lasierra, P. and Prat, S.** (2018). Transient Transactivation Studies in *Nicotiana*
1209 *benthamiana* Leaves. *Methods Mol. Biol.* **1794**: 311–322.

1210 **Li, S., van Os, G.M.A., Ren, S., Yu, D., Ketelaar, T., Emons, A.M.C., and Liu, C.-M.**
1211 (2010). Expression and functional analyses of EXO70 genes in *Arabidopsis*
1212 implicate their roles in regulating cell type-specific exocytosis. *Plant Physiol.* **154**:
1213 1819–30.

1214 **Livak, K.J. and Schmittgen, T.D.** (2001). Analysis of Relative Gene Expression Data
1215 Using Real-Time Quantitative PCR and the $2^{-\Delta\Delta CT}$ Method. *Methods* **25**: 402–
1216 408.

1217 **Manojlovic, Z., Earwood, R., Kato, A., Perez, D., Cabrera, O.A., Didier, R., Megraw,**
1218 **T.L., Stefanovic, B., and Kato, Y.** (2017). La-related protein 6 controls ciliated
1219 cell differentiation. *Cilia* **6**: 4.

1220 **Maraia, R.J., Mattijssen, S., Cruz-Gallardo, I., and Conte, M.R.** (2017). The La and
1221 related RNA-binding proteins (LARPs): structures, functions, and evolving
1222 perspectives. *Wiley Interdiscip. Rev. RNA* **8**.

1223 **Martin, K., Kopperud, K., Chakrabarty, R., Banerjee, R., Brooks, R., and Goodin,**
1224 **M.M.** (2009). Transient expression in *Nicotiana benthamiana* fluorescent marker
1225 lines provides enhanced definition of protein localization, movement and
1226 interactions in planta. *Plant J.* **59**: 150–62.

1227 **Martino, L. et al.** (2015). Synergic interplay of the La motif, RRM1 and the interdomain
1228 linker of LARP6 in the recognition of collagen mRNA expands the RNA binding
1229 repertoire of the La module. *Nucleic Acids Res.* **43**: 645–60.

1230 **McCue, A.D., Cresti, M., Feijó, J.A., and Slotkin, R.K.** (2011). Cytoplasmic
1231 connection of sperm cells to the pollen vegetative cell nucleus: potential roles of
1232 the male germ unit revisited. *J. Exp. Bot.* **62**: 1621–31.

1233 **McElver, J. et al.** (2001). Insertional mutagenesis of genes required for seed
1234 development in *Arabidopsis thaliana*. *Genetics* **159**: 1751–63.

1235 **Merret, R., Descombin, J., Juan, Y.-T., Favory, J.-J., Carpentier, M.-C., Chaparro,**
1236 **C., Charng, Y.-Y., Deragon, J.-M., and Bousquet-Antonelli, C.** (2013a). XRN4
1237 and LARP1 are required for a heat-triggered mRNA decay pathway involved in
1238 plant acclimation and survival during thermal stress. *Cell Rep.* **5**.

1239 **Merret, R., Martino, L., Bousquet-Antonelli, C., Fneich, S., Descombin, J., Billey,**
1240 **É., Conte, M.R., and Deragon, J.-M.** (2013b). The association of a La module
1241 with the PABP-interacting motif PAM2 is a recurrent evolutionary process that led

1242 to the neofunctionalization of la-related proteins. *RNA* **19**.

1243 **Mochizuki, S., Harada, A., Inada, S., Sugimoto-Shirasu, K., Stacey, N., Wada, T.,**
1244 **Ishiguro, S., Okada, K., and Sakai, T.** (2005). The Arabidopsis WAVY GROWTH
1245 2 protein modulates root bending in response to environmental stimuli. *Plant Cell*
1246 **17**: 537–47.

1247 **Mori, T., Igawa, T., Tamiya, G., Miyagishima, S.-Y., and Berger, F.** (2014). Gamete
1248 attachment requires GEX2 for successful fertilization in Arabidopsis. *Curr. Biol.*
1249 **24**: 170–175.

1250 **Mori, T., Kuroiwa, H., Higashiyama, T., and Kuroiwa, T.** (2006). GENERATIVE
1251 CELL SPECIFIC 1 is essential for angiosperm fertilization. *Nat. Cell Biol.* **8**: 64–
1252 71.

1253 **Palanivelu, R. and Preuss, D.** (2006). Distinct short-range ovule signals attract or
1254 repel Arabidopsis thaliana pollen tubes in vitro. *BMC Plant Biol.* **6**: 7.

1255 **Pleskot, R., Pejchar, P., Bezvoda, R., Lichtscheidl, I.K., Wolters-Arts, M., Marc,**
1256 **J., Zárský, V., and Potocký, M.** (2012). Turnover of Phosphatidic Acid through
1257 Distinct Signaling Pathways Affects Multiple Aspects of Pollen Tube Growth in
1258 Tobacco. *Front. Plant Sci.* **3**: 54.

1259 **Qin, Y., Leydon, A.R., Manziello, A., Pandey, R., Mount, D., Denic, S., Vasic, B.,**
1260 **Johnson, M.A., and Palanivelu, R.** (2009). Penetration of the stigma and style
1261 elicits a novel transcriptome in pollen tubes, pointing to genes critical for growth in
1262 a pistil. *PLoS Genet.* **5**: e1000621.

1263 **Reyes, F.C., Buono, R.A., Roschztardt, H., Di Rubbo, S., Yeun, L.H., Russinova,**
1264 **E., and Otegui, M.S.** (2014). A novel endosomal sorting complex required for
1265 transport (ESCRT) component in Arabidopsis thaliana controls cell expansion and
1266 development. *J. Biol. Chem.* **289**: 4980–8.

1267 **Ruiz, M.T., Voinnet, O., and Baulcombe, D.C.** (1998). Initiation and Maintenance of
1268 Virus-Induced Gene Silencing. *Plant Cell* **10**: 937–946.

1269 **Ryder, S.P., Recht, M.I., and Williamson, J.R.** (2008). Quantitative analysis of
1270 protein-RNA interactions by gel mobility shift. *Methods Mol. Biol.* **488**: 99–115.

1271 **Samaj, J., Müller, J., Beck, M., Böhm, N., and Menzel, D.** (2006). Vesicular
1272 trafficking, cytoskeleton and signalling in root hairs and pollen tubes. *Trends Plant*
1273 *Sci.* **11**: 594–600.

1274 **Scarpin, M.R., Sigaut, L., Temprana, S.G., Boccaccio, G.L., Pietrasanta, L.I., and**
1275 **Muschietti, J.P.** (2017). Two Arabidopsis late pollen transcripts are detected in

1276 cytoplasmic granules. *Plant direct* **1**: e00012.

1277 **Schulz-Raffelt, M., Chochois, V., Auroy, P., Cuiné, S., Billon, E., Dauvillée, D., Li-**
1278 **Beisson, Y., and Peltier, G.** (2016). Hyper-accumulation of starch and oil in a
1279 *Chlamydomonas* mutant affected in a plant-specific DYRK kinase. *Biotechnol.*
1280 *Biofuels* **9**: 55.

1281 **Stålberg, K., Ståhl, U., Stymne, S., and Ohlrogge, J.** (2009). Characterization of two
1282 *Arabidopsis thaliana* acyltransferases with preference for
1283 lysophosphatidylethanolamine. *BMC Plant Biol.* **9**: 60.

1284 **Synek, L., Schlager, N., Eliáš, M., Quentin, M., Hauser, M.-T., and Žárský, V.**
1285 (2006). AtEXO70A1, a member of a family of putative exocyst subunits specifically
1286 expanded in land plants, is important for polar growth and plant development.
1287 *Plant J.* **48**: 54–72.

1288 **Synek, L., Vukašinović, N., Kulich, I., Hála, M., Aldorfová, K., Fendrych, M., and**
1289 **Žárský, V.** (2017). EXO70C2 Is a Key Regulatory Factor for Optimal Tip Growth
1290 of Pollen. *Plant Physiol.* **174**: 223–240.

1291 **Takemoto, K., Ebine, K., Askani, J.C., Krüger, F., Gonzalez, Z.A., Ito, E., Goh, T.,**
1292 **Schumacher, K., Nakano, A., and Ueda, T.** (2018). Distinct sets of tethering
1293 complexes, SNARE complexes, and Rab GTPases mediate membrane fusion at
1294 the vacuole in *Arabidopsis*. *Proc. Natl. Acad. Sci. U. S. A.* **115**: E2457–E2466.

1295 **Tian, L., Chou, H.-L., Fukuda, M., Kumamaru, T., and Okita, T.W.** (2020). mRNA
1296 Localization in Plant Cells. *Plant Physiol.* **182**: 97–109.

1297 **Töpfer, R., Matzeit, V., Gronenborn, B., Schell, J., and Steinbiss, H.H.** (1987). A
1298 set of plant expression vectors for transcriptional and translational fusions. *Nucleic*
1299 *Acids Res.* **15**: 5890.

1300 **Tse, Y.C., Lo, S.W., Hillmer, S., Dupree, P., and Jiang, L.** (2006). Dynamic response
1301 of prevacuolar compartments to brefeldin a in plant cells. *Plant Physiol.* **142**:
1302 1442–59.

1303 **Twell, D., Wing, R., Yamaguchi, J., and McCormick, S.** (1989). Isolation and
1304 expression of an anther-specific gene from tomato. *Mol. Gen. Genet.* **217**: 240–5.

1305 **van der Veen, J.H. and Wirtz, P.** (1968). EMS-induced genic male sterility in
1306 *Arabidopsis thaliana*: A model selection experiment. *Euphytica* **17**: 371–377.

1307 **Voigt, B., Timmers, A.C.J., Samaj, J., Müller, J., Baluska, F., and Menzel, D.**
1308 (2005). GFP-FABD2 fusion construct allows in vivo visualization of the dynamic
1309 actin cytoskeleton in all cells of *Arabidopsis* seedlings. *Eur. J. Cell Biol.* **84**: 595–

1310 608.

1311 **Vukašinić, N. and Žárský, V.** (2016). Tethering Complexes in the Arabidopsis
1312 Endomembrane System. *Front. cell Dev. Biol.* **4**: 46.

1313 **Vukmirovic, M., Manojlovic, Z., and Stefanovic, B.** (2013). Serine-threonine kinase
1314 receptor-associated protein (STRAP) regulates translation of type I collagen
1315 mRNAs. *Mol. Cell. Biol.* **33**: 3893–906.

1316 **Weber, C., Nover, L., and Fauth, M.** (2008). Plant stress granules and mRNA
1317 processing bodies are distinct from heat stress granules. *Plant J.* **56**: 517–30.

1318 **Weng, H., Kim, C., Valavanis, C., Wang, Z., and Schwartz, L.M.** (2009). Acheron,
1319 an novel LA antigen family member, binds to CASK and forms a complex with Id
1320 transcription factors. *Cell. Mol. Biol. Lett.* **14**: 273–87.

1321 **Woody, S.T., Austin-Phillips, S., Amasino, R.M., and Krysan, P.J.** (2007). The
1322 WiscDsLox T-DNA collection: an arabidopsis community resource generated by
1323 using an improved high-throughput T-DNA sequencing pipeline. *J. Plant Res.* **120**:
1324 157–65.

1325 **Ylstra and McCormick** (1999). Analysis of mRNA stabilities during pollen
1326 development and in BY2 cells. *Plant J.* **20**: 101–8.

1327 **Yu, J., Qiu, H., Liu, X., Wang, M., Gao, Y., Chory, J., and Tao, Y.** (2015).
1328 Characterization of tub4(P287L), a β -tubulin mutant, revealed new aspects of
1329 microtubule regulation in shade. *J. Integr. Plant Biol.* **57**: 757–69.

1330 **Zhang, M., Fan, J., Taylor, D.C., and Ohlrogge, J.B.** (2009). DGAT1 and PDAT1
1331 Acyltransferases Have Overlapping Functions in Arabidopsis Triacylglycerol
1332 Biosynthesis and Are Essential for Normal Pollen and Seed Development. *Plant*
1333 *Cell* **21**: 3885–3901.

1334 **Zhang, Y. and Stefanovic, B.** (2016). LARP6 Meets Collagen mRNA: Specific
1335 Regulation of Type I Collagen Expression. *Int. J. Mol. Sci.* **17**: 419.

1336 **Zheng, Y., Deng, X., Qu, A., Zhang, M., Tao, Y., Yang, L., Liu, Y., Xu, J., and Zhang,**
1337 **S.** (2018). Regulation of pollen lipid body biogenesis by MAP kinases and
1338 downstream WRKY transcription factors in Arabidopsis. *PLoS Genet.* **14**:
1339 e1007880.

1340 **Zhou, J.-J., Liang, Y., Niu, Q.-K., Chen, L.-Q., Zhang, X.-Q., and Ye, D.** (2013). The
1341 Arabidopsis general transcription factor TFIIIB1 (AtTFIIIB1) is required for pollen
1342 tube growth and endosperm development. *J. Exp. Bot.* **64**: 2205–18.

1343

1344 **FIGURE LEGENDS**

1345

1346 **Figure 1: LARP6C is required for pollen tube guidance. (A)**, Immunoblot analysis
1347 of steady-state LARP6C protein accumulation. The same blot was probed with
1348 antibodies against LARP6C or ACTIN as a loading control. **(B)**, *larp6c-3* and *larp6c-4*
1349 alleles are loss-of-function mutants. Top panel: schematic representation of the
1350 *LARP6C* gene and LARP6C protein. Plain boxes represent exons and lines represent
1351 introns. The colour code for exons is identical to that for the conserved protein
1352 domains. The insertion sites of the T-DNAs in *larp6c-3* and *6c-4* mutants are reported.
1353 Bottom panel: immunoblot analysis of LARP6C accumulation in flowers from wild-type,
1354 *larp6c-3* and *6c-4* lines. ACTIN was used as a loading control. **(C)**, Transmission
1355 efficiencies of *larp6c-3* and *6c-4* mutant alleles. Transmission Efficiency (TE) was
1356 calculated as: $(([\text{No of mutant}] / [\text{No of wild type}]) \times 100)$. ns: the number of mutant
1357 seedlings in the progeny is not significantly different from the expected number of
1358 mutant seedlings. **(D)** Scoring of germination rate, pollen tube bursting, and elongation
1359 *in vitro* and *in vivo*. Left panels show representative images of *in vivo* (upper part) and
1360 *in vitro* (lower part) experiments. On the right, graphs report the frequency of
1361 ungerminated pollen (1), PT emergence (2), PT burst (3), and PT longer than three
1362 lengths of the pollen grain (PT>3) 15 or 30 minutes after pollination. n represents the
1363 number of scored pollen grains. **(E)**, Semi *in vivo* (SIV) (upper panel) and *in vivo*
1364 (bottom panel) pollen tube guidance assays. For SIV assays, wild-type ovules were
1365 arranged around homozygous *ms1* pistil explants pollinated with pollen from various
1366 homozygous backgrounds. For *in vivo* assays, homozygous *ms1* pistils were pollinated
1367 *in planta* with pollen from various homozygous genotypes. For each type of
1368 experiment, the numbers of targeted (blue boxes) and non-targeted (white boxes)
1369 ovules were scored and results represented as whisker notched boxplots. The
1370 genotypes of the pollen used for fertilization are recorded below the graphs and n is
1371 the total number of ovules scored in each experiment. The dotted lines respectively
1372 show the wild type mean values of targeted (blue) and non-targeted (dark red) ovules
1373 by wild-type pollen. **(F)** *In vivo* scoring of pollen tube behaviours. Wild-type pistils were
1374 pollinated *in planta* with pollen from various homozygous genotypes (recorded below
1375 the graph) and the behaviour of pollen tubes monitored and scored over a time course:
1376 4h, 8h and 24h after pollination (HAP). Type-I (blue bars): targeting and reception are
1377 normal, Type-II (white bars): attraction (targeting) is defective. Below the graph are

1378 representative images of the type of behaviours observed. Scale bars correspond to
1379 10 μm . The table below the graphs report the numbers of scored ovules (n). p-values
1380 were calculated with an unpaired Student t-test. ns: not significant, *: p-value \leq 0.05, **:
1381 p-value \leq 0.01, **: p-value \leq 0.001.

1382

1383 **Figure 2: Subcellular distribution of LARP6C across pollen development and**
1384 **pollen tubes. (A)** Subcellular localization of fluorescently tagged YFP-LARP6C by
1385 confocal microscopy at different stages of pollen maturation: UNM: uninucleate
1386 microspore, BCP: bicellular pollen, TCP: tricellular pollen, MPG: mature pollen grain
1387 and Pollen tube. Scale bars correspond to 5 μm for pollen and 10 μm for pollen tube
1388 images. Representative images of LARP6C fused at its C-terminus with a tagRFP
1389 reporter are shown in Supplemental Figure S5A. **(B)** Confocal observation of mature
1390 pollen grains that stably co-express the LARP6C-tRFP fusion and the H2B-GFP fusion,
1391 the GFP-GEX2 fusion, the YFP-DCP1 fusion or the PAB5-GFP fusion. Except for the
1392 H2B-GFP marker, which is expressed from the tomato *LAT52* promoter, all marker
1393 genes are expressed from their own upstream genomic sequences. Scale bars
1394 correspond to 5 μm . In (A) and (B), arrows indicate the position of the Nucleolus (No),
1395 Generative Cell Nucleus (GCN), Vegetative Nucleus (VCN), Sperm Cell Nucleus
1396 (SCN) and Cytoplasmic Connection (CC). **(C)** Confocal observation of *N. benthamiana*
1397 epidermis cells transiently expressing the LARP6C-tRFP fusion co-expressed with
1398 microtubule-binding GFP-AtTUB6 and two actin-binding GFP-FABD2 or LifeAct-GFP
1399 reporters. n = 20 cells from three independent infiltration repeats.

1400

1401 **Figure 3: RIP-Seq identification of LARP6C mRNA targets. (A)** Volcano plot
1402 repartition of the log₂ of fold changes between values in the eluate fractions of
1403 LARP6C-FH and wildtype for mRNAs found in the LARP6C-FH eluate fraction,
1404 according to their p-values obtained through the DESeq2 pipeline. Red dots represent
1405 mRNAs that are significantly more represented in LARP6C-FH eluates. A p-value
1406 \leq 0.01 and FC \geq 1 was used as significance criteria. **(B)** Plotting the RE (Eluate-
1407 RPM/Input-RPM) values in LARP6C-FH against the RE values in wild type for the 635
1408 mRNAs highlighted in graph A. mRNAs with a RE_{6c-FH} \geq 3RE-WT are labelled as
1409 blue dots. See Supplemental Figure S6C for a detailed description of the RIP-seq

1410 pipeline. (C) Pie chart representation of the number of LARP6C targets within the
1411 various functional categories identified.

1412

1413 **Figure 4: Loss of LARP6C function affects lipid homeostasis in pollen tubes.**

1414 Wild-type and *larp6c-3* pollen grains were stained with Bodipy 505/515 and Nile red at
1415 the Mature Pollen Stage (MPG) (A) or in pollen tubes (PTs) (B, C). In (B) PTs were
1416 germinated and grown *in vitro*. PTs were collected at 2 h and 4 h after activation for
1417 staining. Representative images are shown. In (C) PTs grown semi *in vivo* were
1418 collected 7h following pollination (4 hap, pistils are cut at shoulder, placed on plate with
1419 ovules and further incubated 3 hours before scoring). n represents the number of
1420 pollen tubes with LDs distributed as on the presented image over the total number of
1421 observed pollen grains. Scale bars correspond to 10 μm in (A) and to 5 μm in (B, C).
1422 (D), Monitoring of pollen tube growth in the presence of galvestine-1. Whisker boxplot
1423 representation of the length of wild-type or *larp6c-3* pollen tubes grown *in vitro* for 4
1424 hours in the presence or absence of galvestine-1. 1: untreated, 2: mock (1% DMSO),
1425 3 and 4: 5 μM and 10 μM galvestine-1. (E) Semi *in vivo* pollen tube guidance assays.
1426 Assays were conducted either in the presence of 1% DMSO (untreated) or in the
1427 presence of 10 μM of galvestine-1. Results are represented as whisker boxplots. p-
1428 values were obtained through an unpaired Student t-test, ns: not significant, ***: p-
1429 value ≤ 0.001 .

1430

1431 **Figure 5: Pollen tubes deprived of LARP6C are hypersensitive to Brefeldin A**

1432 (BFA). Pollen grains were germinated *in vitro* and after 1h activation on germination
1433 medium, pollen tubes were incubated with mock (DMSO) or 25 μM BFA. (A)
1434 Representative images of FM4-64 staining captured at the respective times or wild
1435 type (WT) and *larp6c-3* PTs treated with mock or BFA. Sketched outline of the PTs
1436 with red dots (counts) describing the appearance of the particle frequency and size, as
1437 detected by the ImageJ particle analysis plug in. (B) Following FM 4-64 staining, the
1438 number (top panel) and size (bottom panel) of BFA bodies was scored over a time
1439 course and represented as violin plots. Number of PTs observed to score particle
1440 number: WT: mock: 23, 10 min: 14, 17 min: 30; *larp6c-3*: mock: 32, 10 min: 35, 17 min:
1441 25. Number of PTs observed to score particle size: WT: mock: 59, 10 min: 62, 17 min:

1442 95; *larp6c-3*: mock: 61, 10 min: 115, 17 min: 189. p-values were obtained with an
1443 unpaired Student t-test, ns: not significant, **: p-value \leq 0.01, ***: p-value \leq 0.001.

1444

1445 **Figure 6: The LARP6C La-module binds to B-type RNA boxes. (A)**, Consensus
1446 sequences of the conserved motifs within the 5'-UTRs of LARP6C-bound
1447 mRNAs. Calorimetric **(B, D)** and EMSA **(C, E)** analyses of the interaction between the
1448 LARP6C La-module (encompassing residues 137-332) and oligos B1, B2 **(B, C)**, U₂₀
1449 **(C)**, B3 and B4 **(D, E)**. In **(B)** and **(D)**: for each graph, the upper panel corresponds to
1450 the raw titration data showing the thermal effect of injecting an RNA oligo solution into
1451 a calorimetric cell containing the recombinant LARP6C La-module. The lower panels
1452 show the normalized heat per injection values obtained by integrating the raw data and
1453 subtracting the heat value of the RNA dilution. The red lines in the graphs for oligos
1454 B1 and B2 **(B)** represent the best fit derived by a non-linear best-square procedure
1455 based on an independent binding site model. The dissociation constants (K_d) are
1456 indicated for the B1 and B2 oligos; the thermodynamic parameters are shown in
1457 Supplemental Table S1. **(C, E)**, EMSAs of LARP6C La-module binding to: B1, B2 or
1458 oligo U₂₀ **(C)**, B3 or B4 **(E)**. Decreasing concentrations (μ M) (88 (lane 1), 29.3 (lane 2),
1459 9.8 (lane 3), 3.3 (lane 4), 1.1 (lane 5), 0.4 (lane 6), 0.12 (lane 7), 0.04 (lane 8) and 0
1460 (lane 9)) of the recombinant LARP6C La-module were mixed with 3nM of 5'-labelled
1461 oligos. B stands for Bound, F for Free, red asterisks mark the RNA-protein complex,
1462 and the red arrows on panels E shows samples retained into the gel wells. Experiments
1463 were conducted in the absence (-tRNA) or presence (+tRNA) of unlabelled competitor
1464 (tRNA_{mix} of *E. coli* MRE 600 at 0.01 mg/mL concentration). Graphs in panel C show
1465 the quantification of the bound RNA fraction versus the protein concentration in the
1466 absence (black lines) or presence (red lines) of tRNA competitor. The values of the
1467 dissociation constants are reported. K_d values reported for the EMSA experiments
1468 were calculated out of three independent replicates with the following standard
1469 deviations: LARP6C-B1 (-tRNA): 0.8 +/- 0.1; LARP6C-B1 (+tRNA): 3.5 +/- 0.3;
1470 LARP6C-B2 (-tRNA): 1.9 +/- 0.3; LARP6C-B2 (+tRNA): 5.6 +/- 0.2.

1471

1472 **Figure 7: *larp6c* loss-of-function does not affect the steady-state transcript**
1473 **levels of its target in dry pollen. (A)**, Heat map representation of the log₂(RPKM)
1474 values of genes that are differentially expressed between wild type (WT) and *larp6c-3*
1475 plants. The heat map was built from the list of DE genes with log₂(RPKM) values

1476 between -2 and +10 (2142 genes: 98.5% of the DE genes). **(B)**, Plot representation of
1477 the log₂ values of the ratios: (*larp6c-3*/wild type) (upper panel) and log₂(6C-FH/wild
1478 type) (lower panel) for the 2174 genes found to be differentially expressed in *larp6c-3*
1479 mutant pollen. Red lines mark the cut off value (log₂(1.5) and log₂(1/1.5)). **(C)** Venn
1480 diagram representation of the number of transcripts that are DE in *larp6c-3* and/or
1481 immunoprecipitated by 6C-FH. Note that of the 115 RIP targets, 19 were not present
1482 in the transcriptomic data from RNA-seq. **(D)** plot representation of the log₂(*larp6c-*
1483 *3*/WT) for mRNAs identified by RIP-seq. Red lines mark the cut off value (log₂(1.5)
1484 and log₂(1/1.5)).

1485

1486 **Figure 8: LARP6C binding at the 5'UTR of a reporter construct reduces protein**
1487 **and increases mRNA levels.** **(A)** Schematic representation of the YFP reporter
1488 constructs, **(B)** RT-qPCR monitoring of YFP mRNA levels. To normalize YFP mRNA
1489 levels to transformation efficiency, we used the levels of *HPTII* mRNA encoded by the
1490 *HPTII* gene carried by the YFP binary plasmid but not the tRFP-LARP6C one. SDs
1491 were calculated from three biological replicates. p-value were obtained using a
1492 Student-t test. **P < 0.005, ns: not significant. **(C)** Immunoblot analysis of tRFP-
1493 LARP6C and YFP protein levels. Two immunoblots were prepared and respectively
1494 hybridized with anti-LARP6C or GFP antibodies. Levels of UGPase were used as a
1495 loading control. Representative images of three replicates are shown. **(D)** Confocal
1496 imaging of YFP from leaves not transformed with tRFP-LARP6C (left panels) and of
1497 YFP and tRFP-LARP6C distribution (right panels). Scale bars represent 20 μm.
1498 Leaves that were observed are different from those used to prepare total RNA and
1499 protein extracts. Representative images of three biological replicates are shown.

1500

1501 **Figure 9: LARP6C is involved in the dynamic fine-tuning of MGD2 protein**
1502 **accumulation *in vivo*.** Monitoring of the levels of MGD2-YFP fusion protein expressed
1503 from the *MGD2* native promoter (*PROMGD2:MGD2-YFP*) and endogenous MGD2 in
1504 wild type (WT) and *larp6c-3* plants. **(A)** Representative images of YFP signal in
1505 heterozygous mature pollen grains at activation: 0, 15 and 30 min after incubation on
1506 *in vitro* germination medium. Bottom panels show images in pseudo colour with the
1507 associated scale bar representing the intensity of the YFP signal. White arrows and
1508 asterisks respectively point to segregation pollen grains expressing or not expressing
1509 the translational fusion. **(B)** Live cell imaging of MGD2-YFP distribution in pollen tubes.

1510 The numbers of pollen tubes with gradient MGD2 distribution toward the tip, uniform
1511 (lost gradient), or no expression of MGD2-YFP are reported in the table below. Scale
1512 bars correspond to 10 μ m. **(C)** Left panel: fluorescence quantification of MGD2-YFP in
1513 wild type (WT) and *larp6c-3* (*6c-3*) pollen and during the progamic phase (1 and 4h).
1514 n=3 biological replicates at each time point, a Student t-test for two independent
1515 samples/two-tailed test was conducted, with ns: not significant, **** p-value \leq 0.0001.
1516 Right panel: immunoblot analysis of endogenous levels of MGD2 in pollen and during
1517 progamic phase in wild type and *larp6c-3*. Experiments were conducted in two or three
1518 independent replicates labelled R1, R2, and R3. **(D)** RT-qPCR analysis of *MGD2*
1519 mRNA levels originating from the *MGD2-YFP* transgene and endogenous *MGD2* gene
1520 in dry pollen and 4h pollen tubes. Experiments were conducted in three independent
1521 replicates, and *TUBULIN8* mRNA was used as a control. An unpaired Student t-test
1522 was conducted, with n.s.: not significant. Both wild type and *larp6c-3* express MGD2-
1523 YFP from the same primary transformant (line 6). In A and B, the MGD2-YFP
1524 transgene is in the heterozygous state and the *larp6c-3* allele is homozygous. In C and
1525 D, wild type and *larp6c-3* carry the MGD2-YFP transgene in the homozygous state.
1526

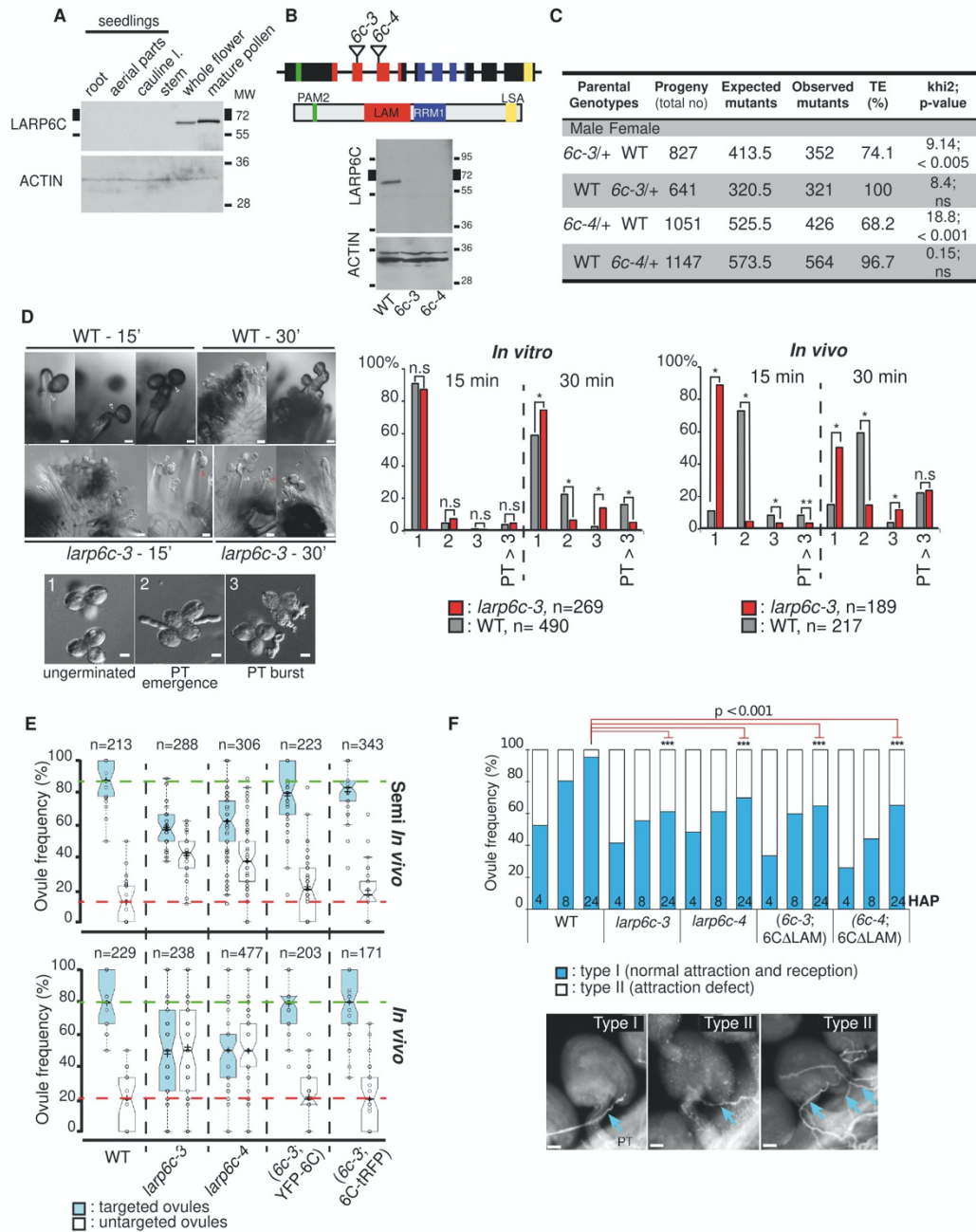


Figure 1: LARP6C is required for pollen tube guidance. (A), Immunoblot analysis of steady-state LARP6C protein accumulation. The same blot was probed with antibodies against LARP6C or ACTIN as a loading control. (B), *larp6c-3* and *larp6c-4* alleles are loss-of-function mutants. Top panel: schematic representation of the *LARP6C* gene and LARP6C protein. Plain boxes represent exons and lines represent introns. The colour code for exons is identical to that for the conserved protein domains. The insertion sites of the T-DNAs in *larp6c-3* and *6c-4* mutants are reported. Bottom panel: immunoblot analysis of LARP6C accumulation in flowers from wild-type, *larp6c-3* and *6c-4* lines. ACTIN was used as a loading control. (C), Transmission efficiencies of *larp6c-3* and *6c-4* mutant alleles. Transmission Efficiency (TE) was calculated as: $(([\text{No of mutant}] / [\text{No of wild type}]) \times 100)$. ns: the number of mutant seedlings in the progeny is not significantly different from the expected number of mutant seedlings. (D) Scoring of germination rate, pollen tube bursting, and elongation *in vitro* and *in vivo*. Left panels show representative images of *in vivo* (upper part) and *in vitro* (lower part) experiments. On the right, graphs report the frequency of ungerminated pollen (1), PT emergence (2), PT burst (3), and PT longer than three lengths of the pollen grain (PT>3) 15 or 30 minutes after pollination. n represents the number of scored pollen grains. (E), Semi *in vivo* (SIV) (upper panel) and *in vivo* (bottom panel) pollen tube guidance assays. For SIV assays, wild-type ovules were arranged around homozygous *ms1* pistil explants pollinated with pollen from various homozygous backgrounds. For *in vivo* assays, homozygous *ms1* pistils were pollinated *in planta* with pollen from various homozygous genotypes. For each type of experiment, the numbers of targeted (blue boxes) and non-targeted (white boxes) ovules were scored and results represented as whisker notched boxplots. The genotypes of the pollen used for fertilization are recorded below the graphs and n is the total number of ovules scored in each experiment. The dotted lines respectively show the wild type mean values of targeted (blue) and non-targeted (dark red) ovules by wild-type pollen. (F) *In vivo* scoring of pollen tube behaviours. Wild-type pistils were pollinated *in planta* with pollen from various homozygous genotypes (recorded below the graph) and the behaviour of pollen tubes monitored and scored over a time course: 4h, 8h and 24h after pollination (HAP). Type-I (blue bars): targeting and reception are normal, Type-II (white bars): attraction (targeting) is defective. Below the graph are representative images of the type of behaviours observed. Scale bars correspond to 10 μm . The table below the graphs report the numbers of scored ovules (n). p-values were calculated with an unpaired Student t-test. ns: not significant, *: p-value ≤ 0.05 , **: p-value ≤ 0.01 , ***: p-value ≤ 0.001 .

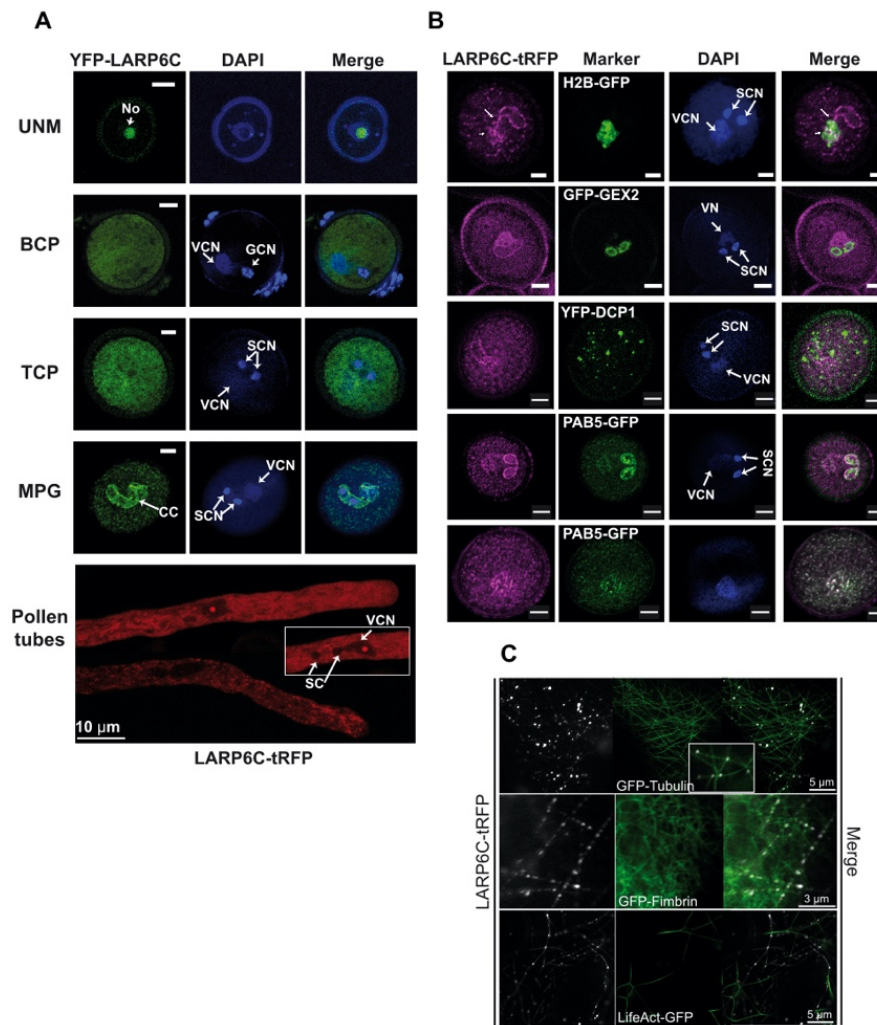


Figure 2: Subcellular distribution of LARP6C across pollen development and pollen tubes. (A) Subcellular localization of fluorescently tagged YFP-LARP6C by confocal microscopy at different stages of pollen maturation: UNM: uninucleate microspore, BCP: bicellular pollen, TCP: tricellular pollen, MPG: mature pollen grain and Pollen tube. Scale bars correspond to 5 μ m for pollen and 10 μ m for pollen tube images. Representative images of LARP6C fused at its C-terminus with a tagRFP reporter are shown in Supplemental Figure S5A. (B) Confocal observation of mature pollen grains that stably co-express the LARP6C-tRFP fusion and the H2B-GFP fusion, the GFP-GEX2 fusion, the YFP-DCP1 fusion or the PAB5-GFP fusion. Except for the H2B-GFP marker, which is expressed from the tomato *LAT52* promoter, all marker genes are expressed from their own upstream genomic sequences. Scale bars correspond to 5 μ m. In (A) and (B), arrows indicate the position of the Nucleolus (No), Generative Cell Nucleus (GCN), Vegetative Nucleus (VCN), Sperm Cell Nucleus (SCN) and Cytoplasmic Connection (CC). (C) Confocal observation of *N. benthamiana* epidermis cells transiently expressing the LARP6C-tRFP fusion co-expressed with microtubule-binding GFP-AtTUB6 and two actin-binding GFP-FABD2 or LifeAct-GFP reporters. n = 20 cells from three independent infiltration repeats.

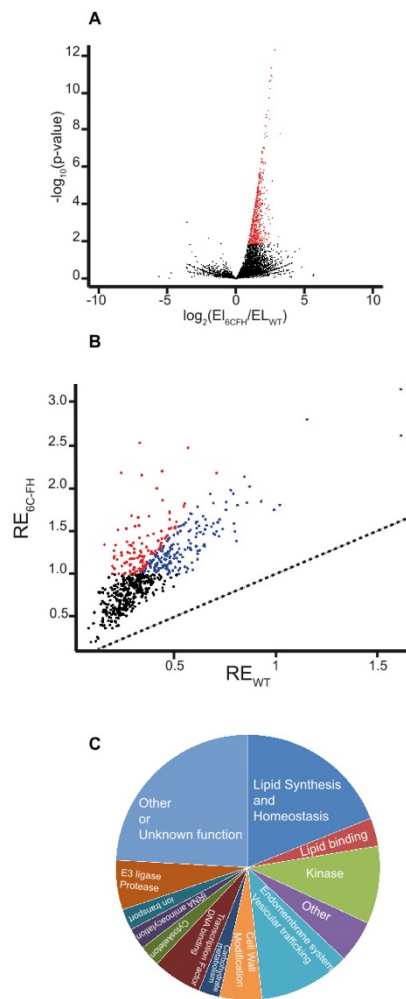


Figure 3: RIP-Seq identification of LARP6C mRNA targets. (A) Volcano plot repartition of the log₂ of fold changes between values in the eluate fractions of LARP6C-FH and wildtype for mRNAs found in the LARP6C-FH eluate fraction, according to their p-values obtained through the DESeq2 pipeline. Red dots represent mRNAs that are significantly more represented in LARP6C-FH eluates. A p-value ≤ 0.01 and FC ≥ 1 was used as significance criteria. (B) Plotting the RE (Eluate-RPM/Input-RPM) values in LARP6C-FH against the RE values in wild type for the 635 mRNAs highlighted in graph A. mRNAs with a $RE_{6c-FH} \geq 3RE_{WT}$ are labelled as blue dots. See Supplemental Figure S6C for a detailed description of the RIP-seq pipeline. (C) Pie chart representation of the number of LARP6C targets within the various functional categories identified.

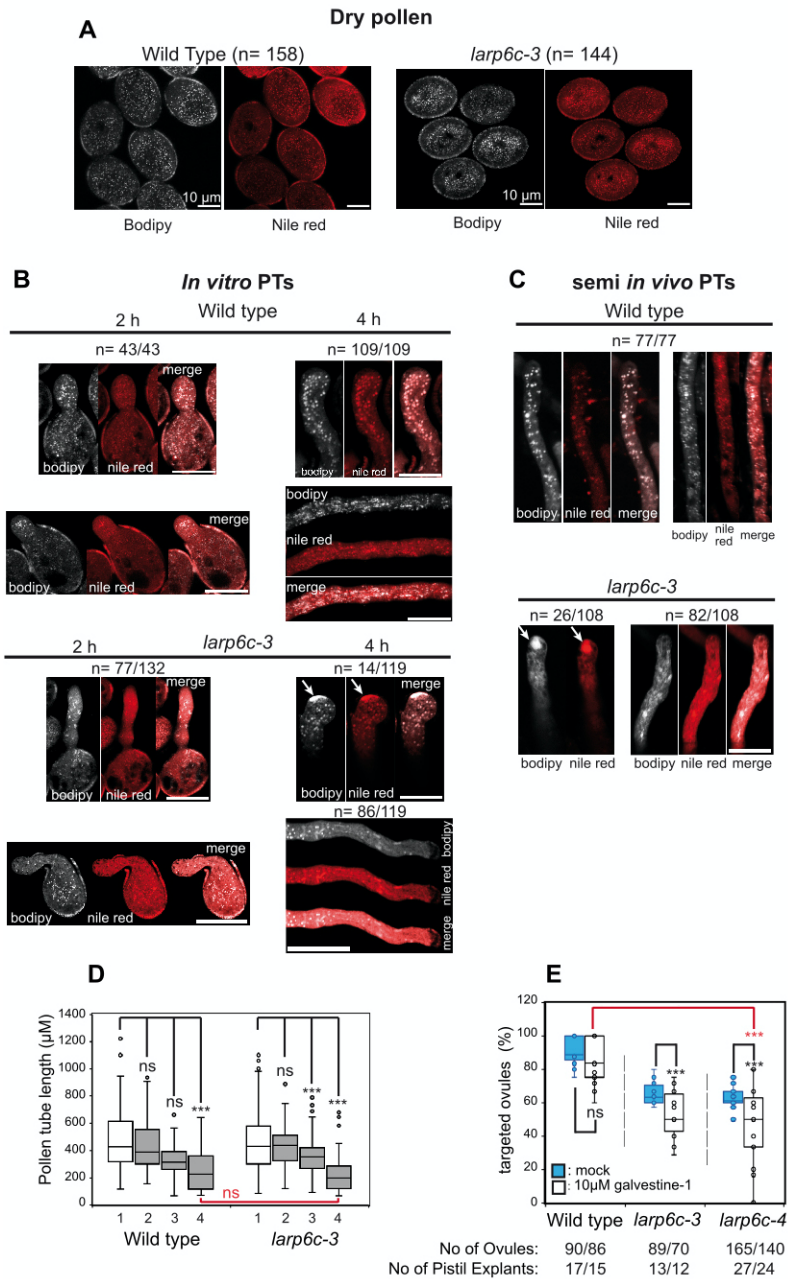


Figure 4: Loss of LARP6C function affects lipid homeostasis in pollen tubes. Wild-type and *larp6c-3* pollen grains were stained with Bodipy 505/515 and Nile red at the Mature Pollen Stage (MPG) (A) or in pollen tubes (PTs) (B, C). In (B) PTs were germinated and grown *in vitro*. PTs were collected at 2 h and 4 h after activation for staining. Representative images are shown. In (C) PTs grown semi *in vivo* were collected 7h following pollination (4 hap, pistils are cut at shoulder, placed on plate with ovules and further incubated 3 hours before scoring). n represents the number of pollen tubes with LDs distributed as on the presented image over the total number of observed pollen grains. Scale bars correspond to 10 μm in (A) and to 5 μm in (B, C). (D), Monitoring of pollen tube growth in the presence of galvestine-1. Whisker boxplot representation of the length of wild-type or *larp6c-3* pollen tubes grown *in vitro* for 4 hours in the presence or absence of galvestine-1. 1: untreated, 2: mock (1% DMSO), 3 and 4: 5 μM and 10 μM galvestine-1. (E) Semi *in vivo* pollen tube guidance assays. Assays were conducted either in the presence of 1% DMSO (untreated) or in the presence of 10 μM of galvestine-1. Results are represented as whisker boxplots. p-values were obtained through an unpaired Student t-test, ns: not significant, ***: p-value ≤ 0.001.

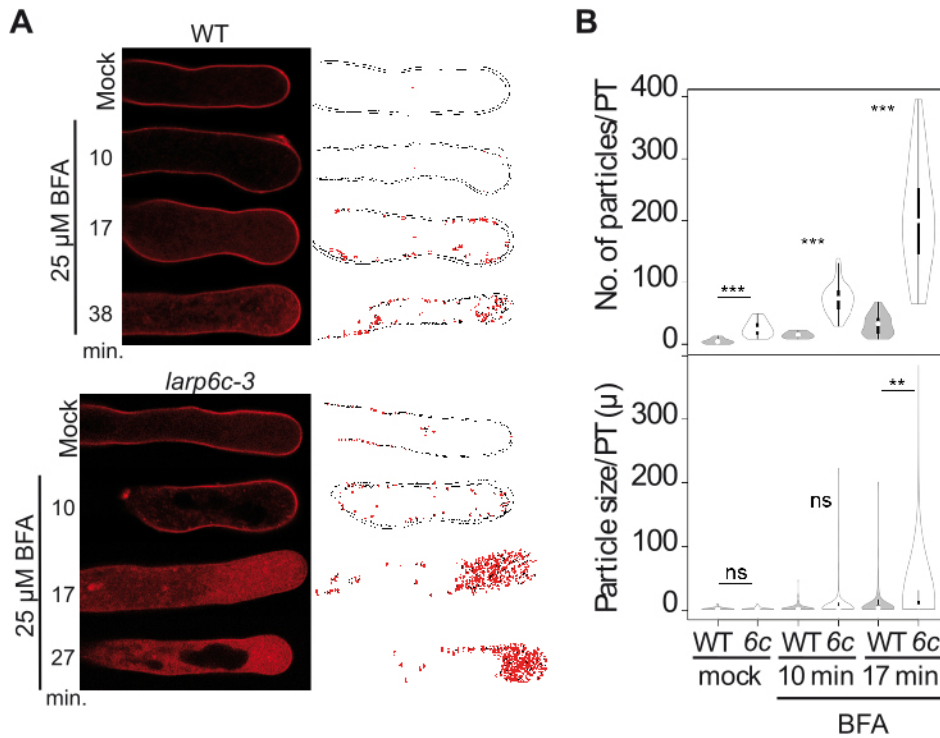


Figure 5: Pollen tubes deprived of LARP6C are hypersensitive to Brefeldin A (BFA). Pollen grains were germinated *in vitro* and after 1h activation on germination medium, pollen tubes were incubated with mock (DMSO) or 25 μ M BFA. **(A)** Representative images of FM4-64 staining captured at the respective times or wild type (WT) and *larp6c-3* PTs treated with mock or BFA. Sketched outline of the PTs with red dots (counts) describing the appearance of the particle frequency and size, as detected by the ImageJ particle analysis plug in. **(B)** Following FM 4-64 staining, the number (top panel) and size (bottom panel) of BFA bodies was scored over a time course and represented as violin plots. Number of PTs observed to score particle number: WT: mock: 23, 10 min: 14, 17 min: 30; *larp6c-3*: mock: 32, 10 min: 35, 17 min: 25. Number of PTs observed to score particle size: WT: mock: 59, 10 min: 62, 17 min: 95; *larp6c-3*: mock: 61, 10 min: 115, 17 min: 189. p-values were obtained with an unpaired Student t-test, ns: not significant, **: p-value \leq 0.01, ***: p-value \leq 0.001.

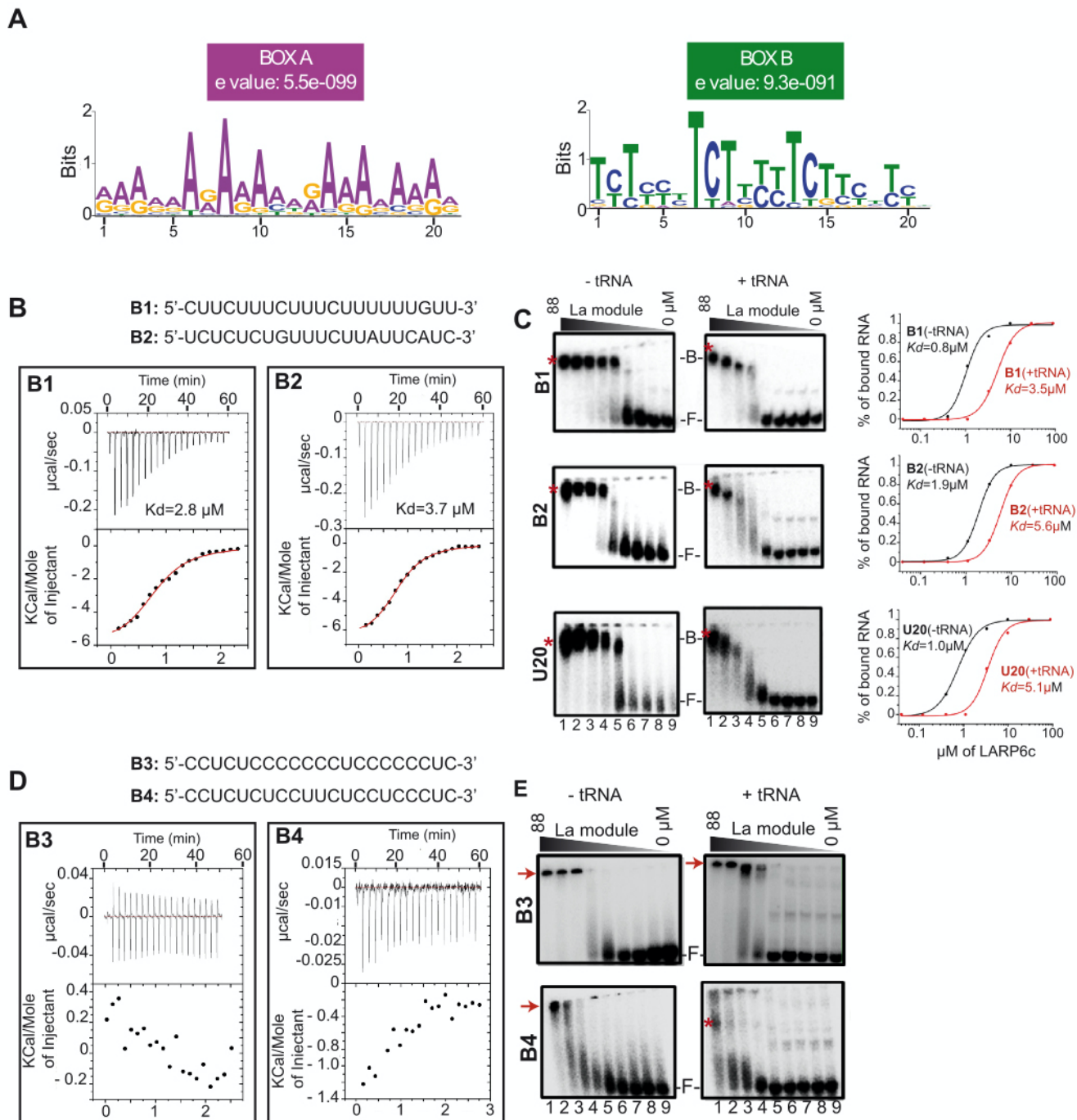


Figure 6: The LARP6C La-module binds to B-type RNA boxes. (A), Consensus sequences of the conserved motifs within the 5'-UTRs of LARP6C-bound mRNAs. Calorimetric (B, D) and EMSA (C, E) analyses of the interaction between the LARP6C La-module (encompassing residues 137-332) and oligos B1, B2 (B, C), U₂₀ (C), B3 and B4 (D, E). In (B) and (D): for each graph, the upper panel corresponds to the raw titration data showing the thermal effect of injecting an RNA oligo solution into a calorimetric cell containing the recombinant LARP6C La-module. The lower panels show the normalized heat per injection values obtained by integrating the raw data and subtracting the heat value of the RNA dilution. The red lines in the graphs for oligos B1 and B2 (B) represent the best fit derived by a non-linear best-square procedure based on an independent binding site model. The dissociation constants (K_d) are indicated for the B1 and B2 oligos; the thermodynamic parameters are shown in Supplemental Table S1. (C, E), EMSAs of LARP6C La-module binding to: B1, B2 or oligo U₂₀ (C), B3 or B4 (E). Decreasing concentrations (μM) (88 (lane 1), 29.3 (lane 2), 9.8 (lane 3), 3.3 (lane 4), 1.1 (lane 5), 0.4 (lane 6), 0.12 (lane 7), 0.04 (lane 8) and 0 (lane 9)) of the recombinant LARP6C La-module were mixed with 3nM of 5'-labelled oligos. B stands for Bound, F for Free, red asterisks mark the RNA-protein complex, and the red arrows on panels E shows samples retained into the gel wells. Experiments were conducted in the absence (-tRNA) or presence (+tRNA) of unlabelled competitor (tRNAmix of *E. coli* MRE 600 at 0.01 mg/mL concentration). Graphs in panel C show the quantification of the bound RNA fraction versus the protein concentration in the absence (black lines) or presence (red lines) of tRNA competitor. The values of the dissociation constants are reported. K_d values reported for the EMSA experiments were calculated out of three independent replicates with the following standard deviations: LARP6C-B1 (-tRNA): 0.8 +/- 0.1; LARP6C-B1 (+tRNA): 3.5 +/- 0.3; LARP6C-B2 (-tRNA): 1.9 +/- 0.3; LARP6C-B2 (+tRNA): 5.6 +/- 0.2.

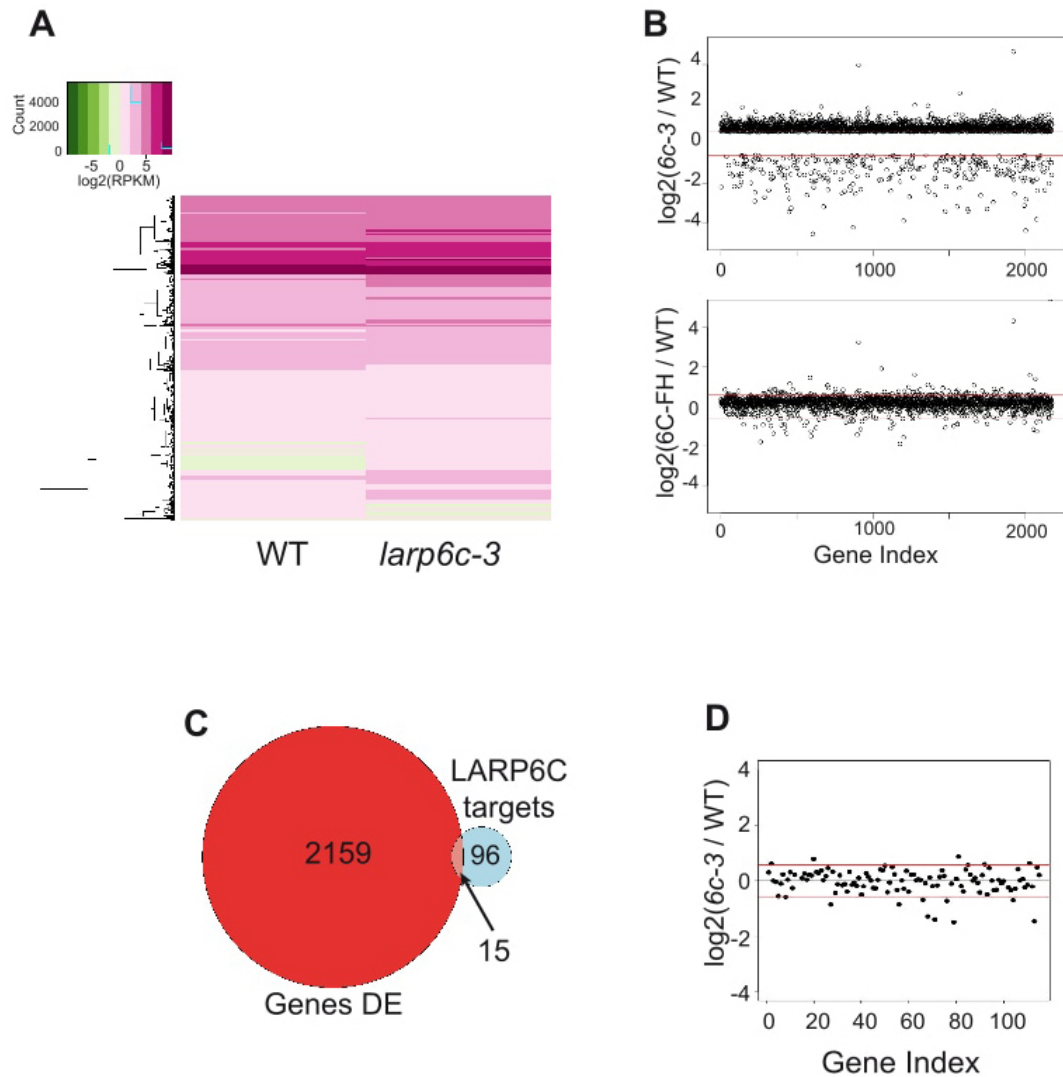


Figure 7: *larp6c* loss-of-function does not affect the steady-state transcript levels of its target in dry pollen. (A), Heat map representation of the log₂(RPKM) values of genes that are differentially expressed between wild type (WT) and *larp6c-3* plants. The heat map was built from the list of DE genes with log₂(RPKM) values between -2 and +10 (2142 genes: 98.5% of the DE genes). (B), Plot representation of the log₂ values of the ratios: (*larp6c-3*/wild type) (upper panel) and log₂(6C-FH/wild type) (lower panel) for the 2174 genes found to be differentially expressed in *larp6c-3* mutant pollen. Red lines mark the cut off value (log₂(1.5) and log₂(1/1.5)). (C) Venn diagram representation of the number of transcripts that are DE in *larp6c-3* and/or immunoprecipitated by 6C-FH. Note that of the 115 RIP targets, 19 were not present in the transcriptomic data from RNA-seq. (D) plot representation of the log₂(*larp6c-3*/WT) for mRNAs identified by RIP-seq. Red lines mark the cut off value (log₂(1.5) and log₂(1/1.5)).

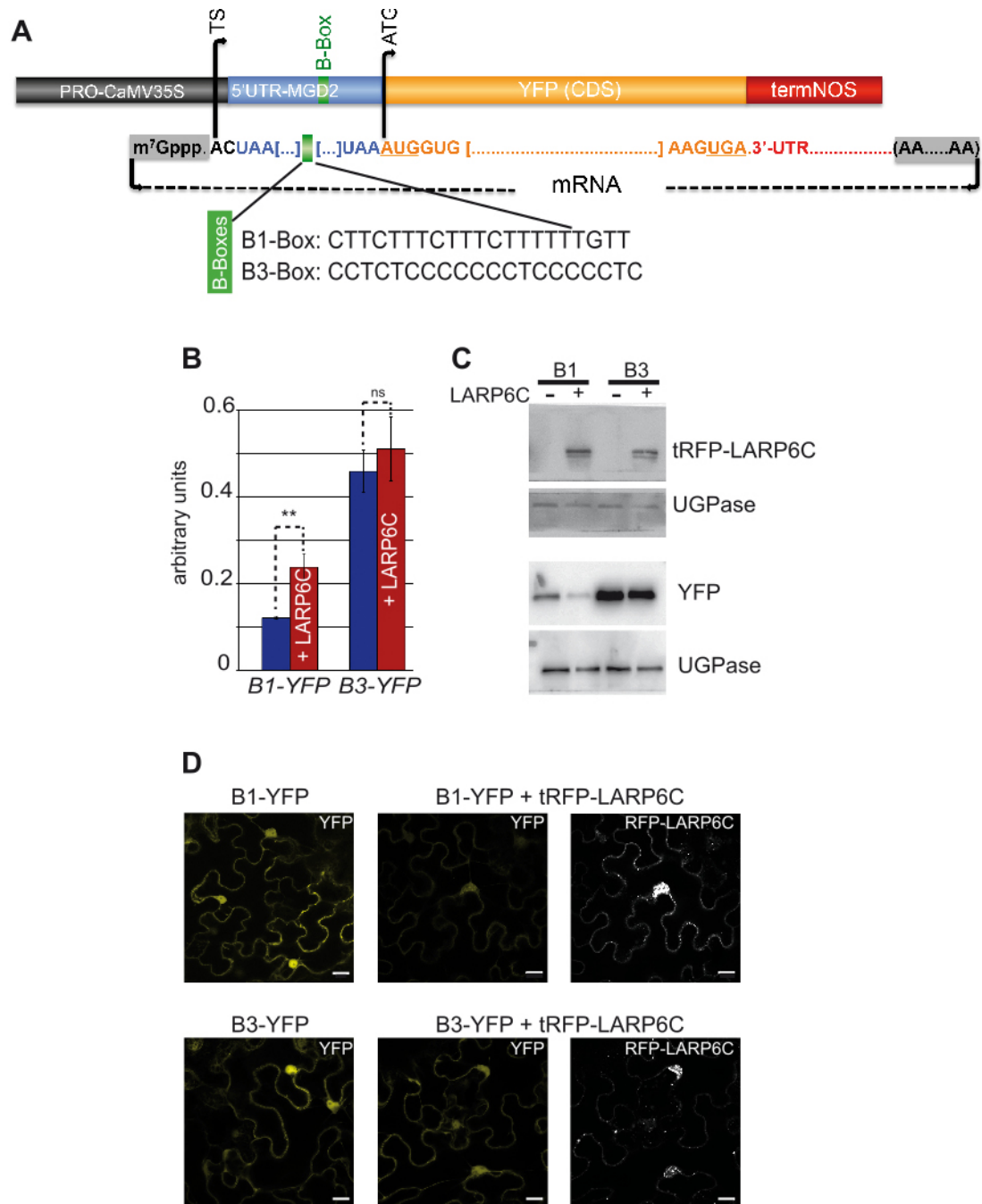


Figure 8: LARP6C binding at the 5'UTR of a reporter construct reduces protein and increases mRNA levels. (A) Schematic representation of the YFP reporter constructs, **(B)** RT-qPCR monitoring of *YFP* mRNA levels. To normalize *YFP* mRNA levels to transformation efficiency, we used the levels of *HPTII* mRNA encoded by the *HPTII* gene carried by the YFP binary plasmid but not the tRFP-LARP6C one. SDs were calculated from three biological replicates. p-value were obtained using a Student-t test. **P < 0.005, ns: not significant. **(C)** Immunoblot analysis of tRFP-LARP6C and YFP protein levels. Two immunoblots were prepared and respectively hybridized with anti-LARP6C or GFP antibodies. Levels of UGPase were used as a loading control. Representative images of three replicates are shown. **(D)** Confocal imaging of YFP from leaves not transformed with tRFP-LARP6C (left panels) and of YFP and tRFP-LARP6C distribution (right panels). Scale bars represent 20 μ m. Leaves that were observed are different from those used to prepare total RNA and protein extracts. Representative images of three biological replicates are shown.

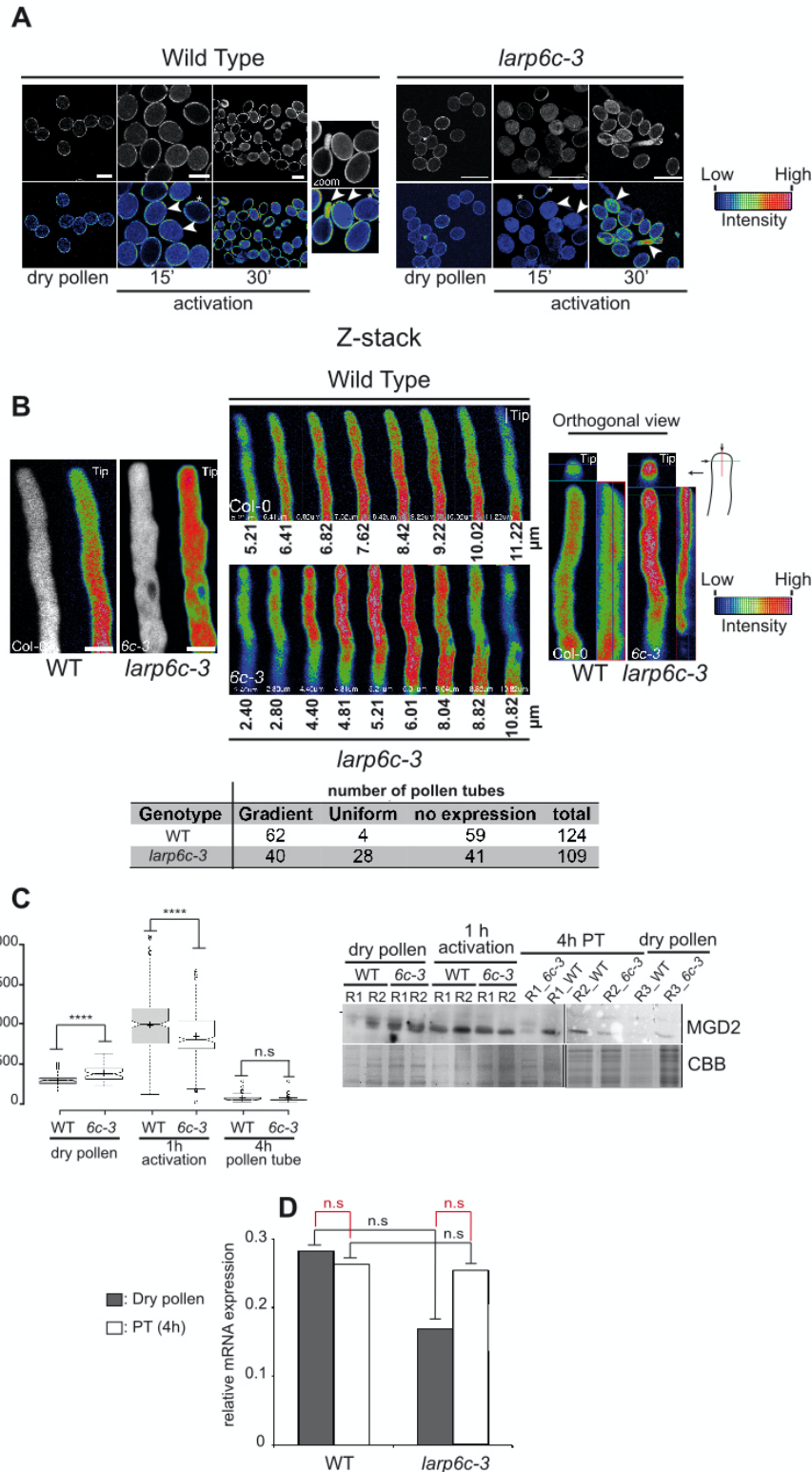
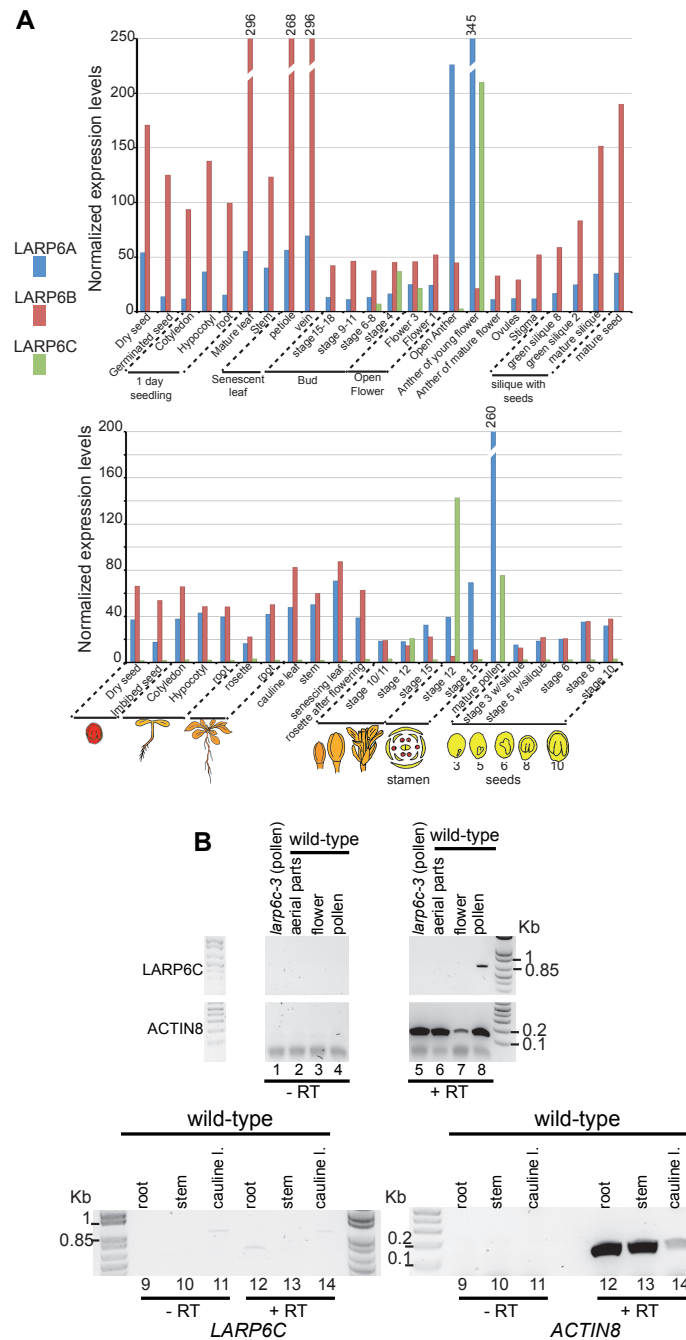
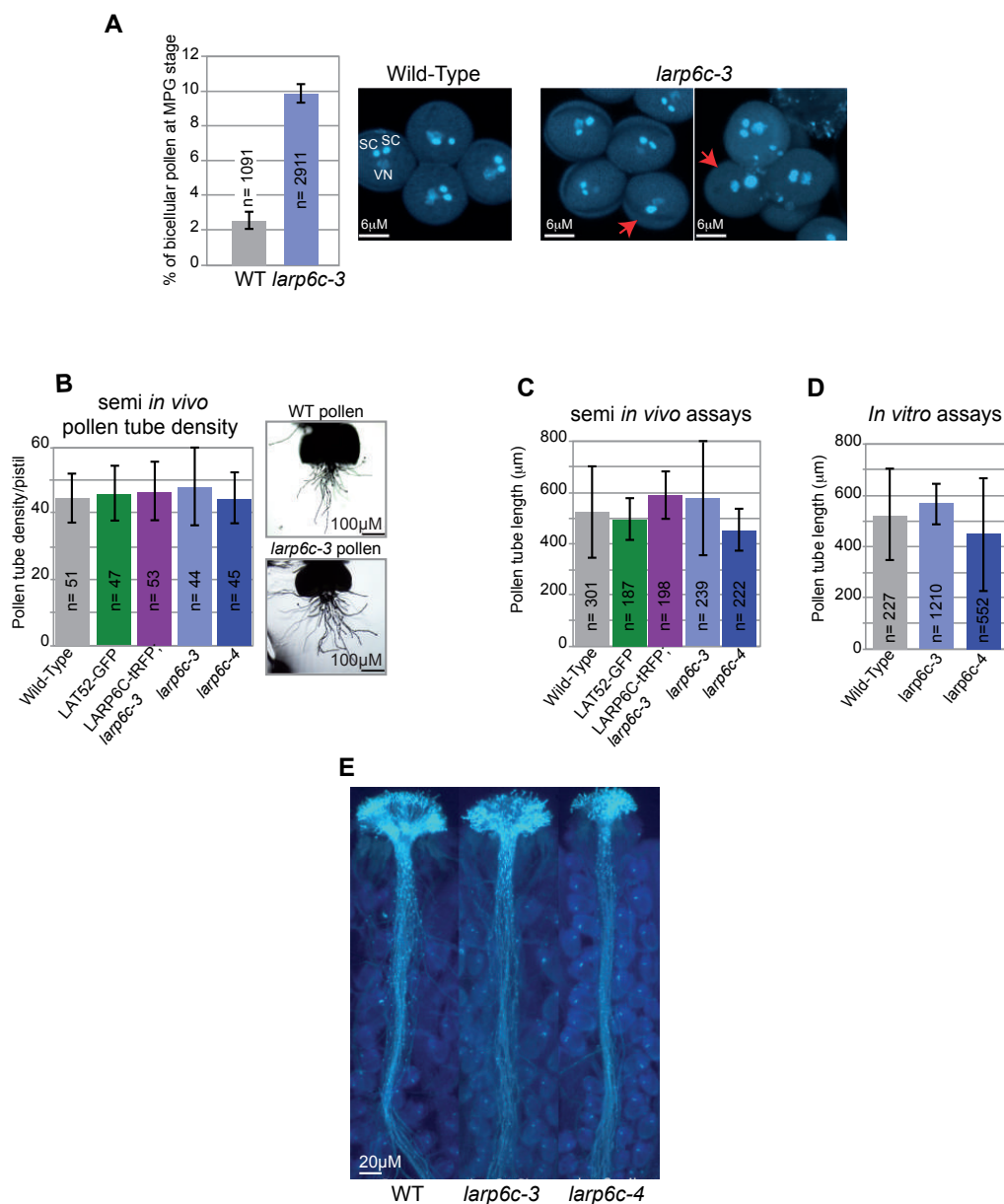


Figure 9: LARP6C is involved in the dynamic fine-tuning of MGD2 protein accumulation *in vivo*. Monitoring of the levels of MGD2-YFP fusion protein expressed from the *MGD2* native promoter (*PRO_{MGD2}:MGD2-YFP*) and endogenous MGD2 in wild type (WT) and *larp6c-3* plants. **(A)** Representative images of YFP signal in heterozygous mature pollen grains at activation: 0, 15 and 30 min after incubation on *in vitro* germination medium. Bottom panels show images in pseudo color with the associated scale bar representing the intensity of the YFP signal. White arrows and asterisks respectively point to segregation pollen grains expressing or not expressing the translational fusion. **(B)** Live cell imaging of MGD2-YFP distribution in pollen tubes. The numbers of pollen tubes with gradient MGD2 distribution toward the tip, uniform (lost gradient), or no expression of MGD2-YFP are reported in the table below. Scale bars correspond to 10 μ m. **(C)** Left panel: fluorescence quantification of MGD2-YFP in wild type (WT) and *larp6c-3* (*6c-3*) pollen and during the progamic phase (1 and 4h). $n=3$ biological replicates at each time point, a Student t-test for two independent samples/two-tailed test was conducted, with ns: not significant, **** p -value ≤ 0.0001 . Right panel: immunoblot analysis of endogenous levels of MGD2 in pollen and during progamic phase in wild type and *larp6c-3*. Experiments were conducted in two or three independent replicates labelled R1, R2, and R3. **(D)** RT-qPCR analysis of *MGD2* mRNA levels originating from the *MGD2-YFP* transgene and endogenous *MGD2* gene in dry pollen and 4h pollen tubes. Experiments were conducted in three independent replicates, and *TUBULIN8* mRNA was used as a control. An unpaired Student t-test was conducted, with n.s.: not significant. Both wild type and *larp6c-3* express MGD2-YFP from the same primary transformant (line 6). In A and B, the MGD2-YFP transgene is in the heterozygous state and the *larp6c-3* allele is homozygous. In C and D, wild type and *larp6c-3* carry the MGD2-YFP transgene in the homozygous state.

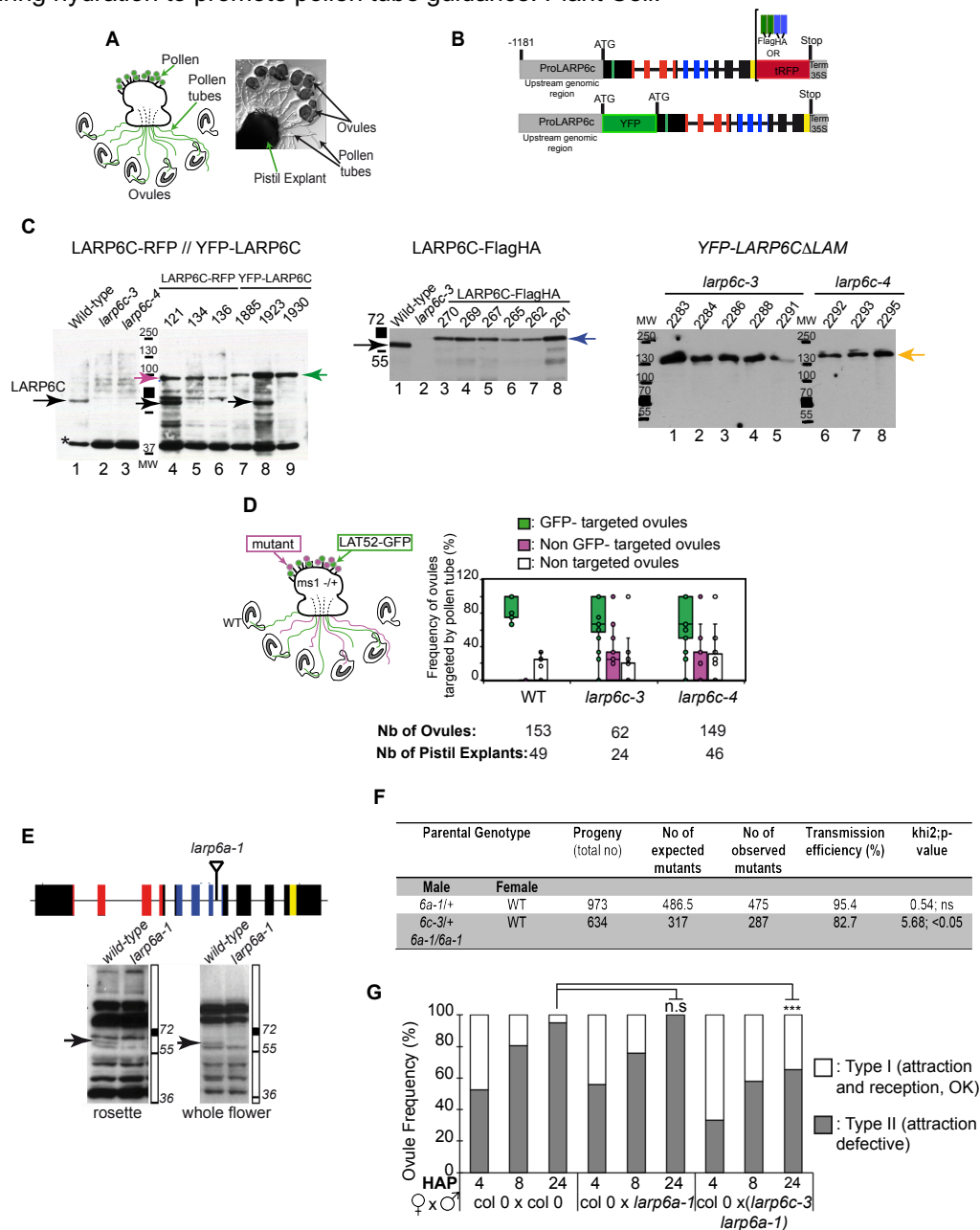
Supplemental data. Billey, Hafidh et al. (2021). LARP6C orchestrates post-transcriptional reprogramming of gene expression during hydration to promote pollen tube guidance. Plant Cell.



Supplemental Figure S1: Expression profiles of LARP6A, 6B and 6C mRNAs across development. (Supports Figure 1A). (A), Expression profiles of the *LARP6A* (AT5g46250), *6B* (AT2g43970) and *6C* (AT3g19090) mRNA across Arabidopsis development. Data were retrieved from the TraVa database of gene expression profiles monitored by RNA-seq (<http://travadb.org/>) (Klepikova et al., 2015) (upper graph) and from the Arabidopsis eFP Browser from the Bio-Analytic Resources for plant biology (<http://bar.utoronto.ca/>) (Winter et al., 2007) and are represented as histograms. The normalized expression values are arbitrary units. (B) RT-PCR analysis of steady-state *LARP6C* mRNA levels in various tissues from wild-type plants. Specificity of the PCR reactions was verified by omitting the reverse transcription step (no RT, lanes 1-4; 9-11). RNAs from *larp6c-3* pollen grains were utilized as negative controls (lanes 1 and 5). RNAs extracted from: seedling aerial parts (lanes 2, 6), whole flower (lanes 3, 7), mature pollen grains (lanes 4, 8), seedling roots (lanes 9, 12), stem (lanes 10, 13) and cauline leaves (lanes 11, 14) were tested. The *ACTIN8* transcript was used as a positive control.



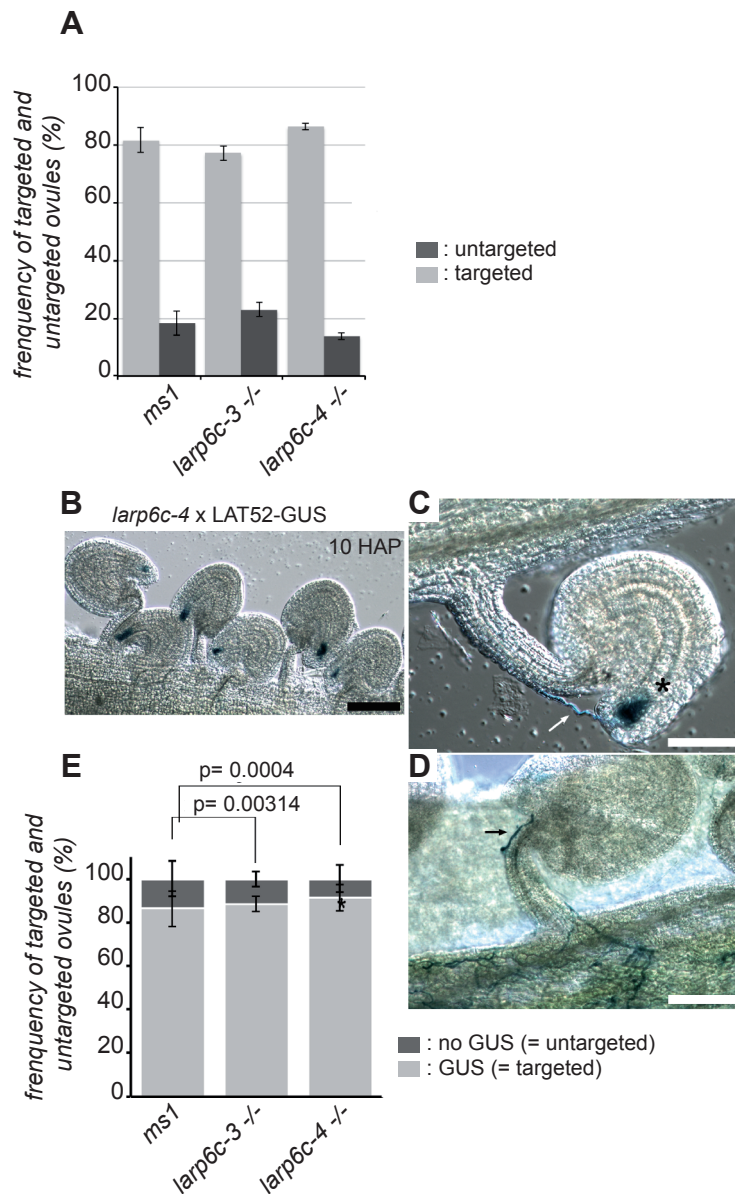
Supplemental Figure S2: Pollen maturation, germination, and pollen tube growth of *larp6c* loss-of-function mutants. (Supports Figure 1). **(A)**, *larp6c* loss-of-function induces a slight pollen maturation deficiency. Mature Pollen Grain (MPG) from wild type (WT) or *larp6c-3* homozygous in quartet (*qrt-/-*) mutant plants were collected and observed following DAPI staining. The number of bicellular pollen grains was scored over the total number of observed MPGs. The results are presented as histograms and correspond to mean values of three replicates \pm SD and "n" is a total number of pollen grains examined. On the right are representative fluorescence micrographs of wild-type and *larp6c-3* pollen grains stained with DAPI. Red arrows point to mature pollen grains in which the generative cell remained undivided and appeared as binucleate. Scale bars correspond to 6 μ m. **(B)**, Mean germination rates (\pm SD) of pollen tubes emerged per pistil in a semi *in vivo* assay. The total number of observed pistils is reported as "n" from three biological replicates. Transgenic LAT52-GFP pollen grains were used as a control. **(C)**, Pollen tube length derived from the semi *in vivo* assay. No significant difference was observed between wild-type and mutant pollen tubes (Student *t* test $p > 0.05$) calculated from pooled replicates. **(D)**, *In vitro* pollen tube length measurements. The total number of pollen tubes measured is reported on the histogram as "n". **(E)** *In vivo* aniline blue staining of pollen tubes after fertilization with wild-type (WT), *larp6c-3* or *larp6c-4* pollen. $n = 10$, 16 and 21 pistils respectively. In the semi *in vivo* assays, scoring was conducted 7 hours after pollination (hap) (4 hap pistils were cut at the shoulder, placed on a plate, and further incubated 3 hours before scoring). In the *in vitro* assays, scoring was conducted 4 hours after activation on germination medium. In the *in vivo* assays, scoring was performed 24 hap.



Supplemental Figure S3: Schematic representation of LARP6C transgenes and immunoblotting analyses of their accumulation. Semi *in vivo* pollen tube guidance competition assays. Analysis of LARP6A function in male fertilization. (Supports Figures 1 to 3). **(A)** Representation of the setting of a semi *in vivo* guidance assay. **(B)** Schematic representation of the transgenes utilized to stably express tagged versions of LARP6C protein in mature pollen. The drawing and color codes are as in Figure 1B. **(C)** Immunoblot analysis of the expression of tagged LARP6C transgenic proteins. Total proteins were extracted from whole flowers, and blots were probed with anti-LARP6C antibodies. Left panel: expression levels of LARP6C-tRFP and YFP-LARP6C in the wild type (lanes 4 and 8), *larp6c-3* (lanes 5, 6, 9) and/or *larp6c-4* (lane 7) backgrounds. Confocal analyses presented in Figure 2 were conducted with pollen from: lines 1885 (UNM), 1930 (BCP and TCP), 1923 (MPG) and 136 (pollen tubes). Line 134 was used to co-express the various markers presented in Figure 3. Lines 134 and 1930 were used as complemented lines for pollen experiments reported in Figures 1D and E and Supplemental Figure 2. Black arrows point to endogenous LARP6C, red arrows to LARP6C-tRFP, green arrows to YFP-LARP6C and black asterisk to non-specific signal. Middle panel: steady-state levels of the LARP6C-FlagHA (6C-FH) fusion from six distinct transformants (lanes 3 to 8). 6C-FH was expressed in *larp6c-3* knockout plants. Mature pollen from line number 267 (lane 5) was used for the RIP-seq experiment. Right Panel: expression levels of YFP-LARP6C-ΔLAM expressed in the *larp6c-3* (lanes 1-5) or *larp6c-4* (lanes 6-8) backgrounds. Complementation assays presented in Figure 1F were conducted with lines 2291 (lane 5) and 2293 (lane 7). **(D)** Semi *in vivo* pollen tube guidance competition assays. On the left, a cartoon representation of the pollen tube guidance assay. Unfertilized wild-type ovules were arranged around an *ms1* pistil pollinated with both mutant *larp6c* and LAT52-GFP pollen. A limited pollination was performed with pollen from wild-type plants homozygous for LAT52-GFP reporter (hmLAT52-GFP) (labeled "WT"), with hmLAT52-GFP and *larp6c-3* pollen (labeled "*larp6c-3*") or with hmLAT52-GFP and *larp6c-4* pollen (labeled "*larp6c-4*"). Ovules were scored as: GFP positive (targeted by LAT52-GFP pollen), non-GFP ovules (targeted by mutant pollen) or non-targeted. The results are presented as whisker boxplots. **(E)** Top panel: Schematic representation of the LARP6A genomic locus; the color code is identical to that of Figure 1B. The position of *larp6a-1* (SK39668) T-DNA is reported. Bottom panel: immunoblot analysis of LARP6A steady-state levels in the wild-type and *larp6a-1* backgrounds. **(F)** Male transmission efficiencies of *larp6a-1* and (*larp6c-3*+/; *larp6a-1*) mutants. Transmission Efficiency (TE) was calculated as: (([No of mutant] / [No of wild type]) x 100). ns: the number

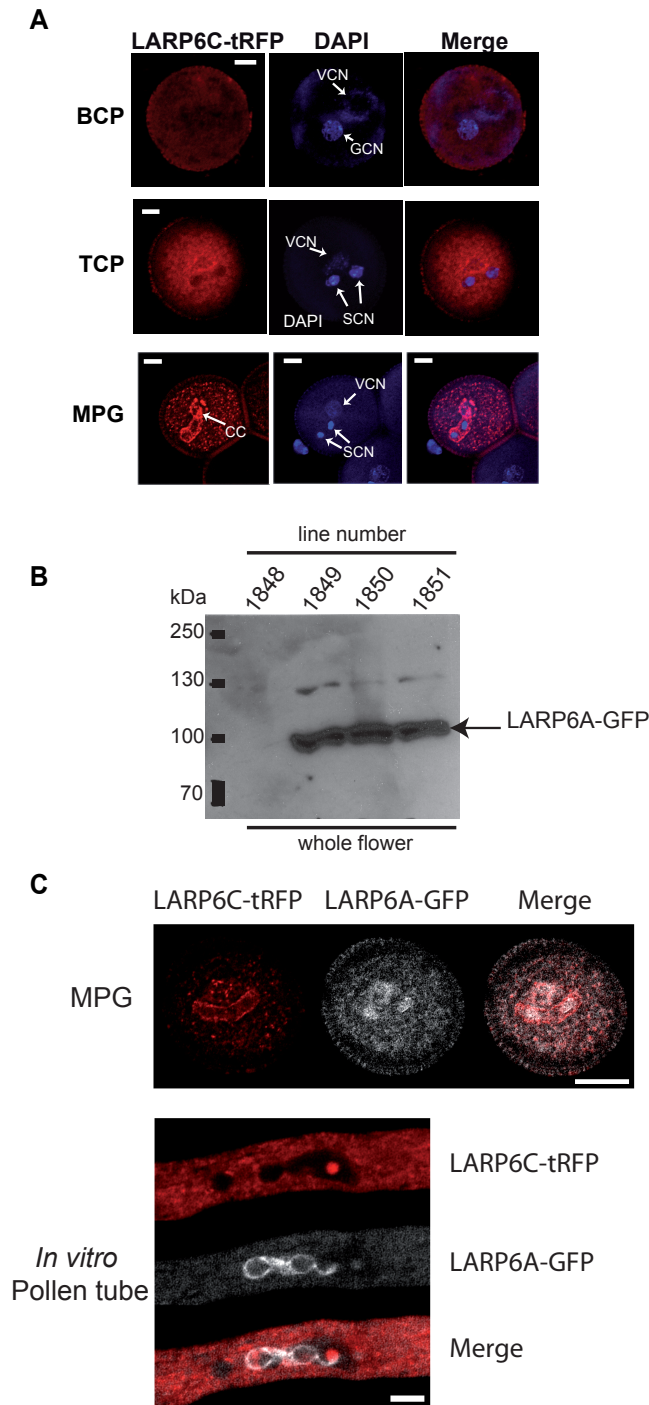
Supplemental data. Billey, Hafidh et al. (2021). LARP6C orchestrates post-transcriptional reprogramming of gene expression during hydration to promote pollen tube guidance. *Plant Cell*.

of mutant seedlings in the progeny is not significantly different from the expected number of mutant seedlings. **(G)** *In vivo* scoring of pollen tube behaviors. Wild-type pistils were pollinated *in planta* with pollen from various homozygous genotypes and the behavior of pollen tubes monitored and scored over a time course: 4h, 8h and 24h after pollination (HAP). Type I (white bars): targeting and reception are normal, Type II (grey bars): targeting is defective (see Supplemental Figure S3D). The numbers of scored ovules are reported as "n" in the table below the graphs. p-values were calculated with a t-test, unpaired, ns: non significant, ***, p-value <0.001.

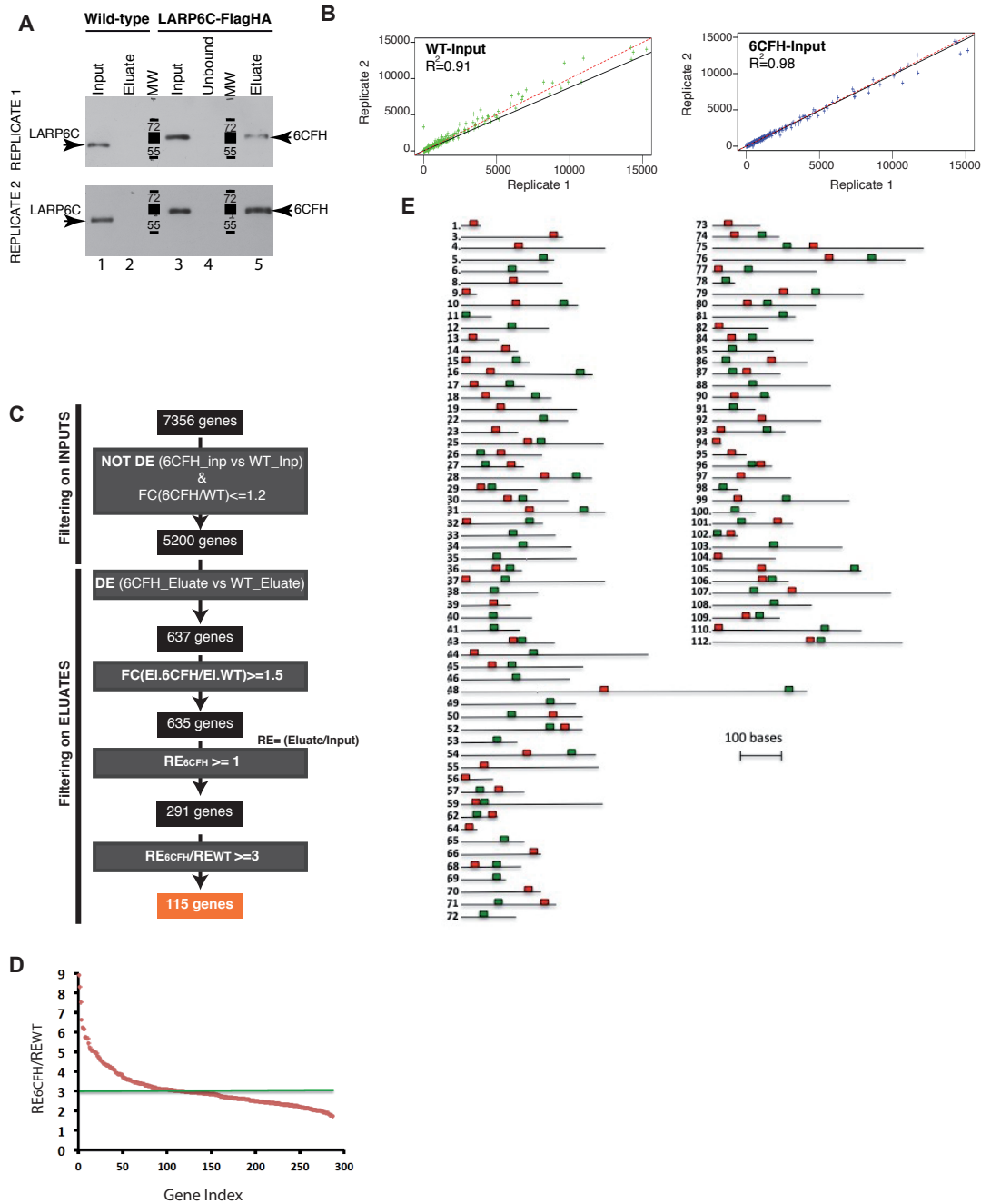


Supplemental Figure S4: Pollen attraction competence of *larp6c-3* and *6c4* ovules. (Supports Figure 1C-F). **(A)**, Semi *in vivo* assays using wild-type (WT) (Col 0 ecotype) or *larp6c* (from *larp6c-3* or *larp6c-4* homozygous plants) mutant ovules for wild-type (WT) pollen tube attraction. The histograms report the frequency of targeted/untargeted ovules for each ovule genotype. Error bars are standard deviations calculated from 2 biological replicates with $n = 150$ ovules (contained in 25 pistil explants) tested for each replicate and each genotype. **(B-E)**, *In vivo* ovule attraction competence assays. Pollen tube targeting events were scored as successful attraction. *ms1*, *larp6c-3* or *larp6c-4* homozygous pistils were pollinated with pollen grains expressing the GUS transgene under the control of the *LAT52* promoter. Ovules showing positive GUS staining were scored as competent. **(B-D)**, representative micrographs of pollinated *larp6c-4* mutant ovules. Arrows point to pollen tubes (C, D) and asterisks to pollen tube penetration and burst (C). Scale bars correspond to 20 μm . **(E)**, Histogram representation of ovule attraction frequency. The minus GUS (dark grey) corresponds to frequency of untargeted ovules and the plus GUS (light grey) to the frequency of targeted ovules. Error bars are standard deviations calculated from 2 biological replicates. The total number of ovules scored in replicate 1 (n_1) and 2 (n_2) are: *ms1* ($n_1=802$ from 24 pistils; $n_2= 975$ from 29 pistils), *larp6c-3* ($n_1= 1063$ from 31 pistils; $n_2= 869$ from 28 pistils) and *larp6c-4* ($n_1=860$ from 26 pistils, $n_2= 912$ from 29 pistils).

Supplemental data. Billey, Hafidh et al. (2021). LARP6C orchestrates post-transcriptional reprogramming of gene expression during hydration to promote pollen tube guidance. *Plant Cell*.



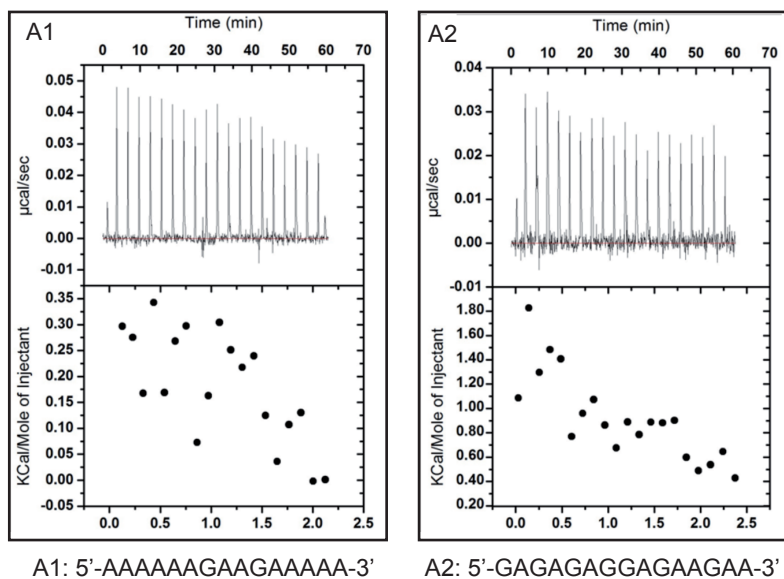
Supplemental Figure S5: Confocal analyses of LARP6C-tRFP and/or LARP6A-GFP in pollen. (Supports Figure 2). **(A)** Confocal analyses of LARP6C-tRFP distribution in bicellular pollen (BCP), tricellular pollen (TCP), and mature pollen grain (MPG). Line 134 was used to monitor LARP6C-tRFP subcellular distribution. White arrows point to the cytoplasmic connexion (CC), the generative and vegetative cell nuclei (GCN and VCN), and the sperm cell nuclei (SCN). Scale bars correspond to 5µm. **(B)** Immunoblot analysis of LARP6A-GFP expression in four independent transgenic lines. The *LARP6A* whole genomic region (including promoter and introns) was fused at its C-terminus with the GFP CDS and expressed in the wild-type background. Line 1850 was crossed with line 134 (LARP6C-tRFP) to monitor LARP6A and 6C co-localization. **(C)** Confocal analysis of LARP6A-GFP and LARP6C-tRFP localization in mature pollen grain (MPG) and *in vitro* grown pollen tubes. Scale bars correspond to 10 µm.



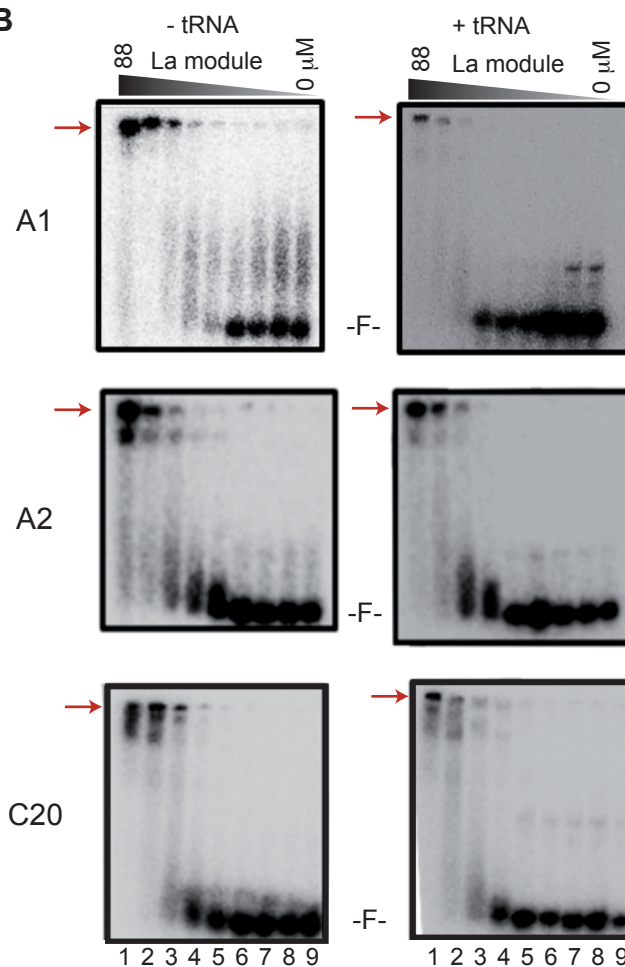
Supplemental Figure S6: Reproducibility of the RIP-seq data, RIP-seq filtering workflow, representation of the position of A and/or B boxes on the 5'-UTRs of LARP6C targets. (Supports Figure 3). **(A)**, Immunoblot analysis of the input (lanes 1, 3), unbound (lane 4), and eluate fractions (lanes 2, 5) of the RIP samples. 0.3% (15 μ L) of the input and unbound and 3% (7.5 μ L) of the eluate fractions were analyzed. The blots were probed with the anti-LARP6C antibody. **(B)**, Comparison of the two biological replicates for the inputs of the RIP-Seq analysis. Correlation of expression levels between replicates of the inputs from wild-type (Col 0) (left panel) or complemented *larp6c-3* ((LARP6C-FlagHA; *larp6c-3*), labelled 6C-FH) (right panel) lines. The X and Y axes correspond to read counts in RPKM respectively for replicates 1 and 2. The expected correlation line for a correlation coefficient of 1 is represented by a red dotted line and the actual correlation line is in black. Correlation coefficients are reported as R^2 on each graph. **(C)**, Representation of the workflow utilized to identify the putative mRNA targets of the LARP6C protein in mature pollen grains. The filtering process was conducted with the weighted average values calculated between replicates, and with the list of genes that displayed at least 1 RPKM value in one of the four conditions (inputs, wild type and 6C-FH and eluates, wild type, and 6C-FH) (see Supplemental Data Set S1). To identify Differentially Expressed (DE) genes between wild type and 6C-FH, respectively, in the input and eluate fractions, we used the Cuffdiff suite. The first filtering step consisted of the elimination of all DE genes in the input. To increase stringency, in the first step, we also filtered out genes non-DE but having Fold Change (FC) values over 1.2, calculated as the ratios between 6C-FH and WT inputs. The second filtering step selects DE genes between the eluate fractions that present a FC of 1.5 or more, calculated as the ratios between 6C-FH and WT eluates. The third filtering step is based on the Enrichment Ratio (RE) calculated as the ratio between eluate and input values and initially selected genes with a $RE_{6CFH} \geq 1$. We then calculated the ratio between RE_{6CFH} and RE_{WT} values, whose distribution is represented in **D** and retained genes with a ratio ≥ 3 . The target gene list is shown in Supplemental Data Set S1. **(E)**, Schematic representation of the 5'-UTRs of Box A and/or Box B containing mRNAs identified as putative LARP6C baits. The positions of the A (red boxes) and B (green boxes) motifs are shown. Correspondence between numbers on the left hand-side and gene accession numbers are reported in Supplemental Data Set S1.

Supplemental data. Billey, Hafidh et al. (2021). LARP6C orchestrates post-transcriptional reprogramming of gene expression during hydration to promote pollen tube guidance. *Plant Cell*.

A



B



Supplemental Figure S7: ITC and EMSA assessment of LARP6C La-module binding to A type oligos. (Supports Figure 4). **(A)**, Calorimetric analysis of the interaction between the LARP6C La-module (encompassing residues 137-332) and two A-type oligos (A1 and A2) whose sequences are reported below the graphs. For each graph, the upper panel corresponds to the raw titration data showing the thermal effect of injecting an RNA oligos solution into a calorimetric cell containing the recombinant LARP6C La-module. The lower panels show the normalized heat value for the titrations obtained by integrating the raw data and subtracting the heat value of the RNA dilution. **(B)**, EMSAs of the LARP6C La-module binding to A1, A2, or C20 oligos. Decreasing concentrations (μM) 88 (lane 1), 29.3 (lane 2), 9.8 (lane 3), 3.3 (lane 4), 1.1 (lane 5), 0.4 (lane 6), 0.12 (lane 7), 0.04 (lane 8) and 0 (lane 9) of the recombinant La-module were mixed with 3 nM of 5'-labelled oligos. F stands for Free RNA and the red arrows show samples that were retained in the wells of the gel. Experiments were conducted in the absence (-tRNA) or presence (+tRNA) of unlabelled competitor (tRNAmix of *E. coli* MRE 600 at 0.01 mg/mL concentration).

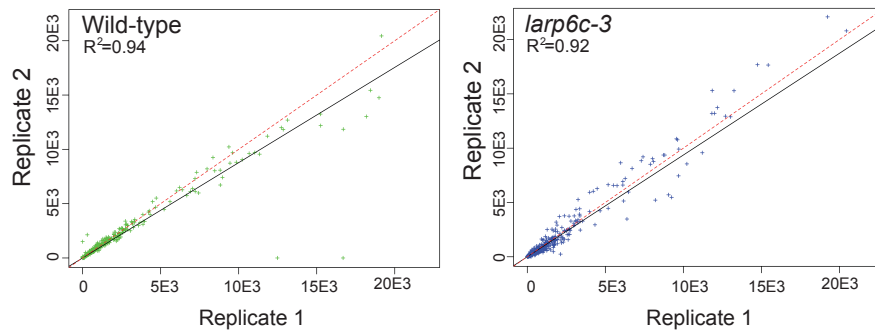
Supplemental data. Billey, Hafidh et al. (2021). LARP6C orchestrates post-transcriptional reprogramming of gene expression during hydration to promote pollen tube guidance. *Plant Cell*.

Experiment Syringe: Cell	n	K_b M ⁻¹	K_d μM	ΔH kcal/mol	$-T\Delta S$ kcal/mol	ΔG kcal/mol
B1:La module 6C	0.8 +/- 0.01	(2.8 +/-0.4)xE ⁵	3.5+/-0.5	-6.6+/-0.1	-1.3+/-0.1	-7.4+/-0.1
B2:La module 6C	0.9 +/- 0.1	(3.7 +/-0.9)xE ⁵	2.8+/-0.4	-6.6+/-0.3	-1.0+/-0.3	-7.6+/-0.1
B3:La module 6C	na	na	na	na	na	na
B4:La module 6C	na	na	na	na	na	na
U₂₀:La module 6C*	1.1 +/- 0.1	(5.8 +/-0.3)xE ⁵	1.7+/-0.1	-3.1+/-0.1	-4.7+/-0.7	-7.8+/-1.0
A1:La module 6C	na	na	na	na	na	na
A2:La module 6C	na	na	na	na	na	na
C₂₀:La module 6C	na	na	na	na	na	na

Every value is averaged over three experiments and the errors are obtained as the standard deviation from the mean value. *: The values for oligo(U₂₀) are those previously reported in (Merret et al. *RNA*, 2013). na: not attributed.

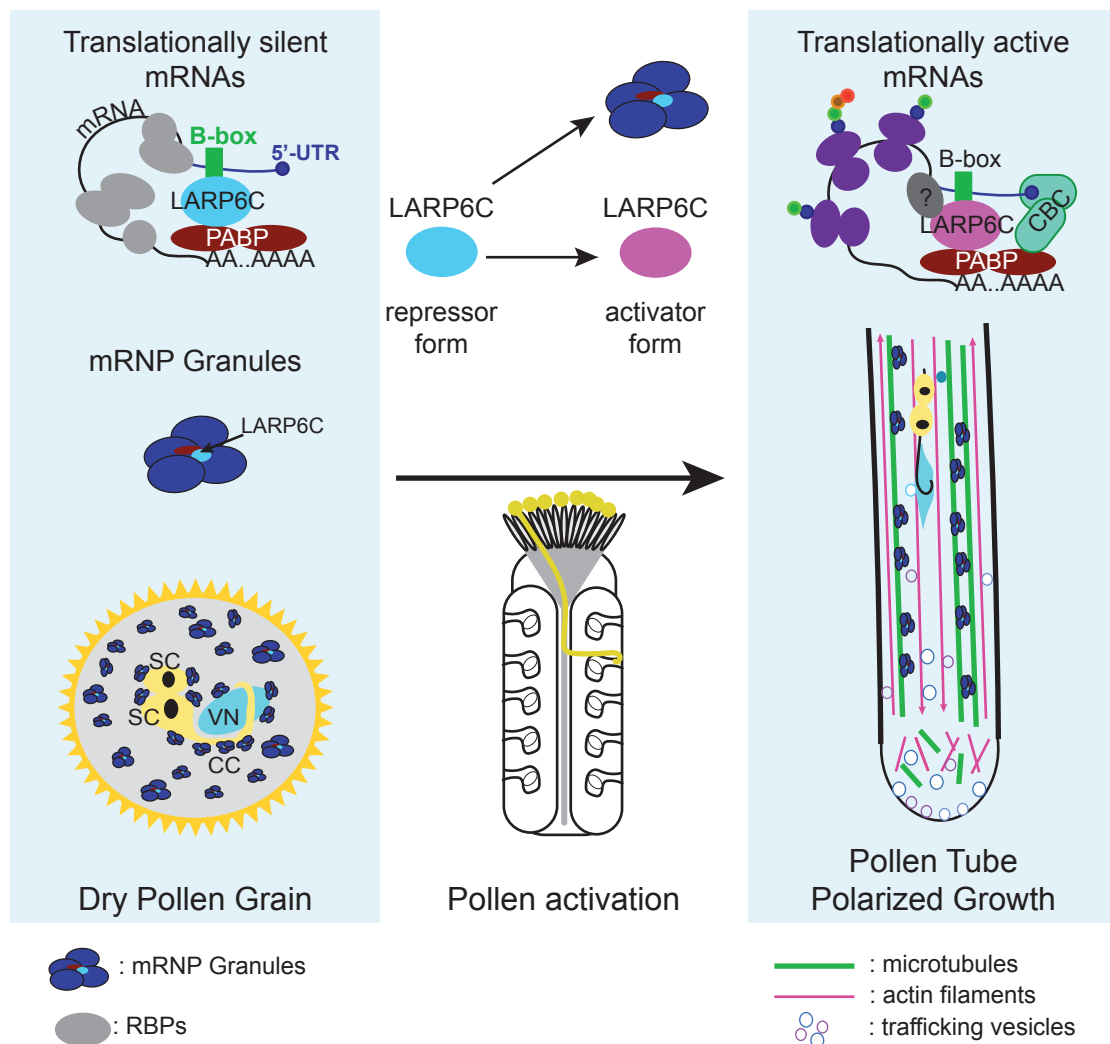
Supplemental Table S1: Thermodynamic parameters of the calorimetric analyses shown in Figure 4B, 4D and Supplemental Figure 6A.

Supplemental data. Billey, Hafidh et al. (2021). LARP6C orchestrates post-transcriptional reprogramming of gene expression during hydration to promote pollen tube guidance. Plant Cell.



Supplemental Figure S8: Reproducibility of the RNA-seq data. (Supports Figure 7) Comparison of the two biological replicates used for the RNA-seq analyses. Correlation of expression levels between replicates of the RNA-seq data from wild-type (Col 0) (left panel) or from *larp6c-3* (right panel) lines. The X and Y axes correspond to read counts in RPKM respectively for replicates 1 and 2. The expected correlation line for a correlation coefficient of 1 is represented by a red dotted line and the actual correlation line is in black. Correlation coefficients are reported as R^2 on each graph.

Supplemental data. Billey, Hafidh et al. (2021). LARP6C orchestrates post-transcriptional reprogramming of gene expression during hydration to promote pollen tube guidance. *Plant Cell*.



Supplemental Figure S9: Model of the molecular functions of LARP6C in male fertilization. In mature dry pollen grain, LARP6C is part of mRNP granules and acts as a repressor of translation of its target transcripts. During pollen hydration and along the progamic phase, LARP6C shifts from a repressor to an activator of translation. In growing pollen tubes, we postulate that LARP6C could also participate in the transport of at least some of its target transcripts, navigating them along the cytoskeleton as translationally silent to their site of translation.

Supplemental data. Billey, Hafidh et al. (2021). LARP6C orchestrates post-transcriptional reprogramming of gene expression during hydration to promote pollen tube guidance. Plant Cell.

qPCR PRIMERS						
Primer Name	Gene	5'-3' sequence	Primer Tm (°C)	Amplicon Tm (°C)	Amplicon length (nt)	Primer pair Efficiency (%)
YFP-F	YFP	TAAACGGCCACAAGTTCAGC	59.05	86.91	87	99.85
YFP-R		CGGTGGTGCAGATGAACTTC	59.20			
Hyg-F	Hygromycin	CGTGGTTGGCTTGTATGGAG	58.91	86.91	156	97.9
Hyg-R		CCCAAGCTGCATCATCGAAA	58.90			
MGD2-F	YFP-MGD2 & MGD2	TGTGACTGCATCATCACAAAAG				
MGDR		GGCTGAGCTAGTTTACGTGCAT				
TUBULIN 8-R	TUBULIN 8	CTTCGTATTGGTCAATCCGGTGC				
TUBULIN 8-F		GAACATGGCTGAGGCTGTCAAGTA				

Cloning & Genotyping Primers		
Primer Name	5'-3' sequence	Purpose
31	CACCTcacactttttcaagtctcatt	MGD2 genomic region cloning (-579 to last nt before stop codon)
32	AACTAAACTGGCAAAAGAAGAG	
543	CCCCGGTACCCTGCTTTCTGATTTAAGAGAGGCAAAGGA	LARP6C genomic region (-1181 to Stop codon) cloning
544	CCCCGCTAGCGAGATTGTTAGGTGAGAGTGAGATGGAA	
974	CCCCGAGCTCGTGCTTTCTGATTTAAGAGAGGCAAAGGA	ProLARP6C genomic region (-1181 to -1) cloning
975	CCCCGGTACCTTTCTCTCACTACTCTGAAAAAATCTCTAAC	
976	CCCCACTAGTATGGCGCAGATGCAGCGAGAAG	Cloning of genomic LARP6C from ATG to STOP codon
977	CCCCGATATCTTAGAGATTGTTAGGTGAGAGTGAGATGG	
eb3	CCCCTCTAGACTCGAGCTAGAAAGAGAACCAGGGACTTCT	Cloning of genomic PAB5 from ATG to STOP codon
eb4	CCCCGGATCCCTCGGATGAGGATAGAGCAAACCTGGTCATC	
1197	GCAGGCTGCGGCCGCTCTAG	Construction of LARP6CDLAM CDS (underlined sequence is complementary to the 20 first nt of pcr product 2, obtained with primers 1198 and 1200)
1198	<u>GCAATTCCTCTCTGTCTCTCTTCGACGAAGAAGACGAGTTCTGA</u>	

Supplemental data. Billey, Hafidh et al. (2021). LARP6C orchestrates post-transcriptional reprogramming of gene expression during hydration to promote pollen tube guidance. Plant Cell.

1199	AGAGACAGAGAGGAATTGCA	Construction of LARP6CDLAM CDS
1200	TATCGATAAGCTTGATATCGA	
1201	GCTCTAGAATGGCGCAGAT	
488	GAAGTAGAGTCCGTCACGACG	<i>larp6c-3</i> LP primer
489	TTTCTTGCCGTCTTCACTCAC	<i>larp6c-3</i> RP primer
491	TAGCATCTGAATTTTCATAACCAATCTCGATACAC	SAIL-LB2
999	GTTCAAATTCAACGCTCAAGC	<i>larp6c-4</i> LP primer
1000	AATTCTCTGCAACGACAGTCC	<i>larp6c-4</i> RP primer
483	AACGTCCGCAATGTGTTATTAAGTTGTC	DsLox-p745-LB
475	AAGCTGGAAGGTAGGCTATGG	<i>larp6a-1</i> RP primer
476	GACGCTTTGAGACCTCAACAG	<i>larp6a-1</i> LP primer
474	ATACGACGGATCGTAATTTGTCTG	<i>Saskatoon-3</i>

Supplemental table S2: List and sequences of primers used for qPCR analyses, genotyping and cloning.

Supplemental data. Billey, Hafidh et al. (2021). LARP6C orchestrates post-transcriptional reprogramming of gene expression during hydration to promote pollen tube guidance. *Plant Cell*.

SUPPLEMENTAL METHODS

Plant material and plasmid construction

The *larp6a-1* (SK39668) line from the Saskatoon Arabidopsis T-DNA population collection (Robinson et al., 2009) was obtained from the NASC stock center. Genotyping primer sequences are listed in Supplemental Table S2. To determine whether this insertion line was loss-of-function, we ordered a custom-made antibody through immunization of rabbits with peptide "EESEKGGKKNFIRTR" (Agro-Bio (La Ferté St Aubin, France)). Anti-LARP6A antibodies were used at 1/5,000 dilution. To obtain the LARP6A-GFP fusion, we PCR amplified the whole genomic locus *AT5G46250* from position -1498 up to the last nucleotide before the stop codon with primers 959 and 960 and inserted the DNA fragment following *KpnI*-*SacI* digestion upstream of the *GFP*, into a pCAMBIA1300-based plant binary vector expressing the *HPTII* (hygromycin) resistance gene, giving rise to plasmid p791. A stable transgenic line was prepared through agroinfiltration of plasmid p791 into wild-type Col-0. To monitor co-localization of LARP6A and LARP6C, we transferred the LARP6A-GFP transgene (line 1850) into a LARP6C-tRFP expressing line (line 134) through crossing.

Growth conditions and pollen collection technique for RNA-Seq and RIP-Seq assays

Mature pollen materials for RNA-seq and RIP-seq were obtained from plants sown, grown and harvested under the exact same conditions. Wild type (Col-0), *larp6c-3* and (*larp6c-3*; PRO_{6C}-LARP6CFLAGHA) (abbreviated as 6C-FH) were sown on 1/2 MS - 0.8% agar in duplicate and cultivated for 15 days *in vitro* at 20°C, with 24 h light (50-60 mE⁻¹m⁻²-s⁻¹). Seedlings were then transferred to soil treated with the nematode *Steinernema feltiae* (at 5000 / soil Liter) and cultivated in a greenhouse with approximately 16 h day at 22°C night and day (greenhouse conditions, July 2013 Gif/Yvette France) for 5 weeks. Wild type Col-0, *larp6c-3* and 6C-FH (transformant number 267 (see Supplemental Figure S3C for an immunoblot analysis of LARP6C-FLAGHA protein accumulation)) plants were grown together in the same compartment of the greenhouse in large plates, each containing 96 plants. Two sets (Col-0, *larp6c-3*, 6C-FH) of plants were grown to produce two replicates. For each replicate, 15 Col-0, 3 *larp6c-3* and 15 6C-FH plates were prepared. The plates of each replicate were respectively installed on two distinct growth shelves inside a same compartment and each genotype interspersed inside each replicate. To avoid the effects of cooling air efflux and temperature gradients and to obtain homogeneous growth between genotypes inside each replicate, the plates were rotated along their respective shelf every 2 weeks. Mature pollen grains were collected using a homemade pollen collector as described in (Johnson-Brousseau and McCormick, 2004). Briefly, mature pollen was collected by aspiration with a vacuum cleaner equipped with three successive filters

Supplemental data. Billey, Hafidh et al. (2021). LARP6C orchestrates post-transcriptional reprogramming of gene expression during hydration to promote pollen tube guidance. *Plant Cell*.

of 140, 60 and 10 μm diameter. Pollen grains were scraped from the 10 μm filter into an Eppendorf tube, weighed, flash frozen in liquid nitrogen, and stored at -80°C .

RNA sequencing

Total RNAs were extracted from 5 mg of wild-type and *larp6c-3* mature pollen grains as described in the Methods section of the main text. RNA quality was verified by gel electrophoresis and staining with Gel-red (Biotium). DNase treatment was conducted as for RT-PCR assays. The reaction was stopped and DNase extracted with phenol/chloroform/IAA before RNA was precipitated and resuspended in RNase-free water. The quality of DNase-treated RNA was assessed with a Bio-Analyser. Library preparation (with a True seq Stranded mRNA kit from Illumina) and sequencing were subcontracted to Fasteris (Switzerland). Single-end (101bp read length) sequencing was performed on the HiSeq 2000 platform with a depth of 31 to 60 M reads. Experiments were conducted in duplicate for each genotype.

RNA Immunoprecipitation and sequencing (RIP-Seq)

After pollen collection, crude extracts (Inputs) were prepared from identical amounts of wild-type and 6C-FH expressing pollen grains. Twenty-five mg of mature pollen was resuspended in 250 volumes of extraction buffer (50 mM Tris HCl pH 7.4, 10% glycerol, 100 mM NaCl, 5 mM MgCl_2 , 80 units / ml RNasin® Plus RNase Inhibitor (Promega), 1X mg132, 1% protease inhibitor cocktail for plant extract (Sigma)) and ground using a Silamat S6 before extracts were cleared by centrifugation (4°C , 14.000 g for 10 min). 700 and 40 μL of Input fraction were saved to purify total RNA (Input RNA) and total protein (Input Protein) to respectively conduct RNA-sequencing and immunoblotting. For each sample (Col0-Replicate 1, Col0-Replicate 2, 6C-FH-Replicate 1 and 6C-FH-Replicate 2), the immunoprecipitation step was conducted with 5 mL of crude extract. For each sample, 250 μL of Anti-Flag M2 (Sigma) magnetic beads were thoroughly washed with 10 volumes of extraction buffer and evenly divided between the 5 tubes. After removing the supernatant, 1 mL of crude extract (approximately 300 μg of total protein) were added to each tube and rotated for 1 h at 4°C on a wheel at 10 rpms. The unbound fractions were collected, pooled, and 700 and 60 μL stored for RNA and protein analyses. The beads were washed once with 5 vol of washing buffer (50 mM Tris HCl pH 7.4, 10 % Glycerol, 150 mM NaCl, 3 mM MgCl_2 , 80 units / ml RNasin® Plus RNase Inhibitor (Promega), 1X Mg132, 1% protease inhibitor cocktail for plant extract (Sigma), 0.1% Triton™ (Sigma)) before being transferred to a new tube, pooled, and washed twice more in 2 vol of washing buffer. The elution step was conducted as follow: 6% of the beads (15 μL) were resuspended in 1X Laemmli buffer, heated for 10 min at 100°C , and

Supplemental data. Billey, Hafidh et al. (2021). LARP6C orchestrates post-transcriptional reprogramming of gene expression during hydration to promote pollen tube guidance. *Plant Cell*.

the supernatant used to run immunoblot analysis to monitor the efficiency of immunoprecipitation of the 6C-FH protein. The remaining 94% of the beads were resuspended into 400 μ L of guanidium hydrochloride buffer, incubated for 10 min at RT, the supernatant collected and separated from proteins with two phenol/chloroform/IAA extractions before the RNA was precipitated in the presence of 80 μ g of glycogen and resuspended into 10 μ L of RNase-free water. RNAs in the eluate fractions were quantified with a NanoDrop and their quality verified with a Bio-Analyzer system. The library preparation and sequencing (Input RNA and Eluate RNA) were subcontracted to Fasteris (Switzerland). The libraries constructed with the input RNAs were prepared from poly(A) purified RNAs using a True seq Stranded mRNA kit from Illumina and the libraries prepared from the eluate fractions were constructed from unpurified RNAs. Sequencing was performed as single-end 101 bp and with a depth of 42 to 64 M reads for the inputs and 25 to 40 M reads for the eluates.

Bioinformatics

For each RNA-seq and RIP-seq sample and replicate, read quality was first verified with FastQC software (<http://www.bioinformatics.babraham.ac.uk/projects/fastqc>) and clusters with a Qscore below 30 filtered out. 95-96% of the RNA-seq clusters and 92-94% of the RIP-seq clusters had a Qscore of at least 30 (please see Supplemental Data Set S1 and S2 for the sequencing depth and quality scores of each sample). In the second step, non-nuclear genomic and ribosomal RNA sequences were filtered out against the TAIR10 database using Bowtie2 (Langmead and Salzberg, 2012) and the remaining clusters aligned against TAIR10 (TAIR10_genes_transposons.gtf) with TopHat2 (Kim et al., 2013). After filtering, more than 99% of the clusters were retained for the RNA-seq samples and inputs of the RIP-seq. For the eluates, 5% of the Col-0 clusters and 15% of the 6C-FH clusters were retained, because of the high contamination with ribosomal RNAs. For the RNA-seq and RIP-seq assays, genes that did not display at least 1 RPKM (read per kilobase per million mapped reads) value in one of the conditions were filtered out. Normalized mean values were attributed to each gene, and differentially expressed genes were identified with the Cufflinks, Cuffmerge and Cuffdiff suite (Trapnell et al., 2010) with an FDR of 0.05 for RNA-seq and 0.01 for RIP-seq and $|\log_2(\text{FC})| \leq 0.585$ as cut-off for total RNA-seq and $\log_2(\text{FC}) \geq 0.585$ for eluate values of RIP-Seq. To search for a motif shared by putative targets of LARP6C, we looked at the Araport database (<https://www.araport.org/>) for their 5' and 3'-UTR sequences and retrieved sequences for 112 out of 115 putative targets. We then ran MEME searches (at the MEME suite portal (

Supplemental data. Billey, Hafidh et al. (2021). LARP6C orchestrates post-transcriptional reprogramming of gene expression during hydration to promote pollen tube guidance. *Plant Cell*.

suite.org/)) using, as control sequences, a set of 112 randomly chosen 5'- and 3'-UTR sequences from genes expressed in pollen according to our transcriptomic analysis.

Pollen phenotyping: pollen maturation, pollen tube germination and growth

To monitor pollen maturation defects, mature pollen grains were collected from wild-type and *larp6c* homozygous plants, deposited on a DAPI solution (1X PBS pH7, 0.5% Triton, 1 μ g/mL 4',6-diamidino-2-phenylindole (DAPI)) and the number of mutant pollen grains with undivided generative cells determined using confocal microscopy. Pollen tube germination and growth defects were monitored *in vitro* or through semi *in vivo* assays. To grow pollen tubes *in vitro*, we used a modified version of the protocol from (Boavida and McCormick, 2007). Freshly prepared pollen tube growth medium (0.01% boric acid, 5 mM CaCl₂, 5 mM KCl, 1 mM MgSO₄, 10% sucrose, pH 7.5 (KOH), 1.5% Phytigel) was directly poured onto a microscope slide. Mature pollen was deposited on the solid medium and slides incubated for 8 h in a humid chamber at 20-22°C in the dark. Pollen tubes were photographed (with a Hamamatsu camera (Sunayama-cho, Shizuoka, Japan)) and pollen tube lengths measured with NIS-element software from Nikon (Nikon Instruments, Melville, NY USA). Pollen tube density and length were also determined through semi *in vivo* analyses. Following hand pollination with wild-type or *larp6c* homozygous mutant pollen, the pistils were excised at the shoulder and incubated for 16 h on a plate containing pollen tube solid growth medium. Pistil explants and pollen tubes were photographed and images analyzed with the plugin Bio-format (Open microscopy environment) from Image J software (Rasband, W.S. ImageJ, NIH, Bethesda USA) (Abràmoff et al., 2004) to determine pollen tube length and density per pistil.

Ovule attraction assays

larp6c-3 or *larp6c-4* pistils were emasculated at stage 12C and left to mature for 2 days. Limited pollination was performed on day 3 using LAT52-GUS homozygous pollen grains in the *qrt-/-* background alongside *ms1-/-* pistils as the control. Eighteen hours after pollination, pollinated pistils were collected and gently dissected with a 25G needle to expose fertilized ovules. Dissected pistils were stained for GUS activity in GUS staining buffer (50 mM PBS, pH7, 0.2% Triton-X100, 10 mM potassium ferrocyanide and 1 mM X-Glu). Pistils were vacuum infiltrated for 10 min and stained o/n at 37°C. For microscopy analyses, stained pistils were cleared using an ethanol series (70%-30%), mounted on 30% glycerol, and analyzed with a Nikon TE2000 equipped with DIC modulation contrast and NIS-element software. Images were processed with ImageJ.

Supplemental data. Billey, Hafidh et al. (2021). LARP6C orchestrates post-transcriptional reprogramming of gene expression during hydration to promote pollen tube guidance. *Plant Cell*.

SUPPLEMENTAL REFERENCES

- Abràmoff, M., Magalhaes, P., and Ram, S.** (2004). Image processing with ImageJ. *Biophotonics Int.* **11**: 36–41.
- Boavida, L.C. and McCormick, S.** (2007). TECHNICAL ADVANCE: Temperature as a determinant factor for increased and reproducible in vitro pollen germination in *Arabidopsis thaliana*. *Plant J.* **52**: 570–582.
- Johnson-Brousseau, S.A. and McCormick, S.** (2004). A compendium of methods useful for characterizing *Arabidopsis* pollen mutants and gametophytically- expressed genes. *Plant J.* **39**: 761–775.
- Kim, D., Pertea, G., Trapnell, C., Pimentel, H., Kelley, R., and Salzberg, S.L.** (2013). TopHat2: accurate alignment of transcriptomes in the presence of insertions, deletions and gene fusions. *Genome Biol.* **14**: R36.
- Klepikova, A. V, Logacheva, M.D., Dmitriev, S.E., and Penin, A.A.** (2015). RNA-seq analysis of an apical meristem time series reveals a critical point in *Arabidopsis thaliana* flower initiation. *BMC Genomics* **16**: 466.
- Langmead, B. and Salzberg, S.L.** (2012). Fast gapped-read alignment with Bowtie 2. *Nat. Methods* **9**: 357–359.
- Robinson, S.J. et al.** (2009). An archived activation tagged population of *Arabidopsis thaliana* to facilitate forward genetics approaches. *BMC Plant Biol.* **9**: 101.
- Trapnell, C., Williams, B.A., Pertea, G., Mortazavi, A., Kwan, G., van Baren, M.J., Salzberg, S.L., Wold, B.J., and Pachter, L.** (2010). Transcript assembly and quantification by RNA-Seq reveals unannotated transcripts and isoform switching during cell differentiation. *Nat. Biotechnol.* **28**: 511–515.
- Winter, D., Vinegar, B., Nahal, H., Ammar, R., Wilson, G. V., and Provart, N.J.** (2007). An “Electronic Fluorescent Pictograph” Browser for Exploring and Analyzing Large-Scale Biological Data Sets. *PLoS One* **2**: e718.